5-1-1998

A Study of aircraft lateral dynamics & ground stability

Howard Brott

A Study of Aircraft Lateral Dynamics & Ground Stability

by

Howard W. Brott Jr

A Thesis Submitted
in
Partial Fulfillment
of the
Requirements for the

MASTER OF SCIENCE
in

Mechanical Engineering

Approved by:

Professor _____
Dr. Kevin Kochersberger
Thesis Advisor

Professor _____
Dr. Alan Nye

Professor _____
Dr. Michael Hennessey

Professor _____
Dr. Charles Haines
Department Head

DEPARTMENT OF MECHANICAL ENGINEERING
COLLEGE OF ENGINEERING
ROCHESTER INSTITUTE OF TECHNOLOGY

MAY 1998

Disclosure Statement

Permission Granted

I, Howard W. Brott Jr., hereby grant permission to the Wallace Memorial Library of Rochester Institute of Technology to reproduce my thesis entitled: A Study of Aircraft Ground Stability and Lateral Dynamics, in whole or in part. Any reproduction will not be for commercial use or profit.

May 21, 1998

_____

Howard W. Brott Jr.

Abstract

The stability of an aircraft on the runway is dependent on many factors. In this thesis, a mathematical model is developed that allows the ground stability and lateral dynamics of an aircraft to be analyzed while it is in the process of taking off or landing. Only two degrees-of-freedom will be considered: lateral displacement and angular rotation. Equations of motion for the model are developed using Newtonian mechanics. The major components of the aircraft that are included in the model are the main landing gear, the vertical tail, and the tail wheel. The model is developed into both linear and non-linear forms.

Comparisons are made between a tricycle gear aircraft and a taildragger. Simulations for both the linear and non-linear model are performed to better understand stability. The results of these simulations are used to comment on the applicability of the linear model.

Table of Contents

List of Tables

List of Figures

List of Symbols*

$\overline{\alpha}$	Front tire normalized slip angle
$\overline{F}_y$	Normalized tire lateral force
$\overline{\theta}$	Magic Formula intermediate variable
$\overline{\psi}$	Magic Formula intermediate variable
Ω	Angular velocity of aircraft-fixed coordinate system [rad/sec]
α	Front tire slip angle [deg or rad]
β	Aircraft sideslip angle [deg or rad]
δ	Difference between peaks in responses
γ	Angle of incidence on vertical tail [deg or rad]
μ_y	Tire lateral friction coefficient
ρ	Density of air [kg/m^3]
ζ	Damping ratio
Ω_Z	Angular velocity of aircraft-fixed coordinate system about z-axis [rad/sec]
$\dot{\Omega}_Z$	Time derivative of angular velocity
a	Distance from mass center to main landing gear [m]
$\boldsymbol{a}_o$	Acceleration of the origin of the vehicle-fixed coordinate system

*By convention, scalar variables are italicized and vectors are boldfaced

A_p	Planform area of vertical tail [m^2]
a_y	Acceleration of vehicle mass center in y-direction [m/sec^2]
b	Distance from mass center to aerodynamic center of vertical tail [m]
B_1	Magic Formula curve fit parameter
B_3	Tire cornering coefficient intercept
B_5	Tire lateral friction coefficient intercept
C_1	Magic Formula curve fit parameter
C_3	Tire cornering coefficient slope
C_5	Tire lateral friction coefficient slope
C_c	Tire cornering coefficient
C_f	Front tire cornering stiffness – two tires [N/rad]
$C_{f\text{-}tail}$	Tail wheel cornering stiffness [N/rad]
$C_{L\gamma}$	Coefficient of lift of the vertical tail [1/deg]
C_α	Tire cornering stiffness [N/rad]
D_1	Magic Formula curve fit parameter
E_1	Magic Formula curve fit parameter
f	fraction of weight on main landing gear
F	External force [N]
F_y	Tire lateral force [N]
$F_{y\_disturbance}$	Side force disturbance [N]
$F_{y\_front\text{-}tire}$	Front tire lateral force – two tires [N]
F_{y_tail}	Vertical tail aerodynamic force [N]

$F_{y\_tail\text{-}wheel}$	Tail wheel lateral force [N]
F_z	Tire vertical load [N]
g	Acceleration due to gravity [m/sec^2]
$\boldsymbol{G}$	Linear momentum
$\boldsymbol{H}$	Angular momentum (about mass center)
$\boldsymbol{i}$	Unit vector in x-direction of aircraft-fixed coordinate system
I_{zz}	Total aircraft yaw mass moment of intertia [kg-m^2]
$\boldsymbol{j}$	Unit vector in y-direction of aircraft-fixed coordinate system
$\boldsymbol{k}$	Unit vector in z-direction of aircraft-fixed coordinate system
L	Wheel base [m]
$\boldsymbol{M}$	External moment (about mass center)
m	Total aircraft mass [kg]
M_z	Moment about z-axis of aircraft fixed coordinate system
r	Yaw velocity [rad/sec]
$\boldsymbol{R}_f$	Position vector from aircraft mass center to main landing gear [m]
$\boldsymbol{R}_r$	Position vector from aircraft mass center to tail wheel [m]
u	Forward velocity [m/sec]
$\dot{u}$	Time derivative of forward velocity [m/sec^2]
v	Lateral velocity [m/sec]
$\dot{v}$	Time derivative of lateral velocity [m/sec^2]
V	Magnitude of aircraft velocity [m/sec]
$\boldsymbol{V}_f$	Velocity of front tire [m/sec]

$\boldsymbol{V_o}$	Velocity of aircraft fixed-coordinate system [m/sec]
$\boldsymbol{V_{tail}}$	Velocity of vertical tail [m/sec]
V_x	Component of velocity in x-direction [m/sec]
V_y	Component of velocity in x-direction [m/sec]

1 Introduction

In 1903, the Wright brothers built their first airplane, which they named the *Flyer*. It was a biplane (two-wing plane) with a 12-horsepower (9-kilowatt) gasoline engine. The wings, which measured 40 feet 4 inches (12.29 meters) from tip to tip, were wooden frames covered with cotton cloth. The pilot lay in the middle of the lower wing. The engine, which was mounted to the pilot's right, turned two wooden propellers located behind the wings. The plane had wooden runners that were guided by rails during take-off and used to skid across the ground during a successful landing. The Brother's had very little control of the airplane while in flight. As a result, they crashed many times before they were able to perfect their flying technique. Throughout their attempts to build a flying machine they considered many different designs. They knew that certain components were necessary to fly, and the details of these components were important to maintaining controlled flight.[1]

There have been many significant improvements in aviation and aircraft construction since the days of cloth covered wings and wooden runners. Most aircraft are now very well designed and pilot friendly. Maintaining control while in flight is hardly a concern any more, except in extreme conditions. Pilots can even take their hands off of the wheel or stick and still maintain stable flight. Today, the hardest part about flying is taking off and landing. The interaction between the wheels of the landing gears and the runway produces forces that act simultaneously with the aerodynamic lift and drag forces that an aircraft generates. In fact, during the take-off, landing, and taxiing portions of

flight an aircraft is essentially a cross between a ground vehicle and a flying machine. Like any type of vehicle, it is desirable to maintain control at all times.

This thesis focuses on aircraft stability. However, unlike most studies involving aircraft, this is a study of the aircraft while it is still on the runway and when it is just beginning to take-off or just starting to land, rather than when it is in the air. The dynamics of the aircraft are looked at from the point of view of a ground vehicle. Since the goal of an aircraft is to fly, there has been little concern with the dynamic behavior of the aircraft while it is still on the runway. Nonetheless, there are safety concerns linked to maneuvering an aircraft while it is still on the ground. Thus, it is important to fully understand aircraft ground stability in an effort to maintain control and prevent accidents from occurring. Directly related to this issue are the landing gears. The location of the landing gears influence aircraft stability. Yet despite this, determination of landing gear location is governed by the geometry of the aircraft rather than the stability.

An aircraft on the runway has three basic modes of performance. Vertical dynamics refers to the vertical response of the aircraft to runway disturbances such as slopes or bumps. Longitudinal dynamics is concerned with the straight-line motion of the aircraft. Factors such as acceleration, braking, and drag play a role in this type of performance. Finally, lateral dynamics is the study of the turning or sideslipping behavior of the aircraft. Tire and aerodynamic forces are the major items of interest in lateral dynamics. Although each of these modes is important, this thesis will only focus on the lateral dynamics of the aircraft since this is the major concern of pilots. It is an undesirable effect to have the aircraft moving left or right and yawing when a pilot is

taking off or landing. The goal of this thesis is to maximize the lateral performance of the aircraft by minimizing these unwanted effects.

The major influence on lateral dynamics is the configuration of the aircraft. Is the aircraft a taildragger, which has the main landing gear in front of the center of gravity and tail wheel behind the CG? Or is the aircraft a tricycle gear design, where the main landing gear is behind the CG and a nose wheel is present? Recent aircraft designs provide increased reliability, comfort, and are easier to fly than their predecessors. In terms of many design enhancements, the tricycle landing gear is perhaps the most noteworthy. During the landing exercise, the pilot can make a number of mistakes when manipulating the controls. A tricycle gear aircraft is more forgiving to the pilot. That is, they are easier to steer on the ground. When one learns to fly in a taildragger, it is a challenge just to taxi it. The pilot constantly has to be "on the rudder," attempting to make the airplane go where he wants it to go. Add a little crosswind, and the exercise sometimes became an adventure. If the nose of the aircraft starts to deviate from the desired path (yaw), the pilot has to respond with opposite rudder. This does not happen when one learns to fly in an airplane equipped with a tricycle gear. An airplane with a tricycle landing gear has an inherent tendency to "go straight" when being taxied. Additionally, most training aircraft today have a wheel-control, not unlike that of an automobile. Consequently, one may have a natural tendency to attempt to "drive" the airplane. Needless to say, this simply does not work, particularly during gusty, crosswind landings. It is not uncommon to see a pilot attempt during a landing exercise to correct for a "gust-induced" yaw with opposite aileron. Not only does this not work, but also the

drag created by the down-aileron exacerbates the yaw while at the same time raising the wind and, thereby, removing or reducing any required crosswind correction (sideslip). Although one may get away with this when landing a tricycle gear aircraft, with a taildragger, a landing incident or accident is highly probable. Most likely, a ground loop will occur. A ground loop is a directional stability problem where the tail of the aircraft swings to the front of the plane.

All of these problems are caused in the same basic way. It has to do with the place where the side loads are reacted out against the ground, and where that is with respect to the center of gravity and the center of lateral area of the aircraft. Tail wheel aircraft are not quite as forgiving about sloppy landings as nose wheel aircraft. Part of the reason for this has to do with the tendency of an irregular object that is passing rapidly through the air to align itself with the heavy end in front. As a result, the center of gravity will do its best to get in front of any resistance to the aircraft's motion that is encountered. There are also some inertial effects here. These tell us that if something is stopped, it tends to stay stopped, and if something is moving, it prefers to keep moving in the same direction. It seems apparent then that in order to solve the problem of stability and ground looping, one must design the aircraft in such a way as to correct itself during maneuvering, as a tricycle gear aircraft does. If one really wants to fly a taildragger aircraft, then some parameters must be specified to determine a method for the best landing gear placement.

Since it is difficult, time consuming, and costly to experiment with these effects on an actual aircraft, this is going to be a paper study. Mathematical modeling is an

effective way for engineers to design and develop aircraft that meet performance goals. This type of study will allow the effects of design changes to be evaluated immediately to see if they meet the required goals. Furthermore, computer simulation will be effective in characterizing the model in a controlled, repeatable environment. In addition, simulation is used to prevent the aircraft and pilot from entering into dangerous situations where safety is a key concern. In many ways, this study mirrors those that are done when evaluating aircraft flight characteristics.

As one might expect, the complexity of the mathematical model can vary. For instance, a model might consider only one mode of performance, be it vertical, longitudinal, or lateral, or it can be any combination of these modes. For this study of just the lateral dynamics of the aircraft, a simple two degree-of-freedom model, known as the bicycle model, is used. Regardless of its simplicity, the two degree-of-freedom model can be very useful in demonstrating the interaction of the major parameters such as tire properties and center of gravity location.

Chapter 2 is a review of the literature that is available on aircraft stability and vehicle dynamics, since this study is a combination of both.

Chapter 3 aims to describe the behavior of the tires and the forces they produce. Also in this chapter are descriptions of the two tire models used in this thesis. Both a linear tire model and a non-linear tire model are used in this study. The non-linear model is based on a method called tire data non-dimensionalization, which was developed by Hugo Radt.

Chapter 4 deals with the two degree-of-freedom aircraft model. The bicycle model is described in detail and several simplifying assumptions are made. The equations of motion are then developed for the entire model. At this point, the model is broken into pieces to study the effects of each component of the aircraft such as its main landing gear, vertical tail, and tail wheel. Once the results have been established and verified, the model is developed in two forms: linear and non-linear. Simulation is performed for each model for a variety of aircraft component configurations. Furthermore, these simulations are expanded to include modeling of the aircraft when the wheels are not entirely in contact with the runway, as during take-off or landing. The results are then compared and conclusions are made regarding the suitability and quality of the linear model. Attempts are also made to stabilize the aircraft given certain parameters, and suggestions for future designs are given.

2 Literature Review

Aircraft have been studied extensively since those first days when the Wright Brothers flew. Since then, they have been studied in every possible way to improve their performance and handling characteristics while in flight. Many mathematical simulations have been done as well as experimental testing in wind tunnels and actual flight. The interaction between the aircraft and the surrounding air in conjunction with the control surfaces is usually the main focus of these studies. As of yet, there has been little concern with the ground handling capability and performance of aircraft. The interaction between the runway and the tires along with the control surfaces is not as well known as the interaction in flight. Performance on the ground is just not as important as performance in the air. After all, aircraft spend only a small percentage of their time on a runway. As such, the topic of this thesis is a relatively new concept.

Because there is no direct literature on the ground handling capability of aircraft, three different topics were researched and brought together to create this study. The first topic is aircraft flight stability. Some aspects of the aircraft's performance in flight can be carried over to ground performance. The second topic of interest is vehicle dynamics. An aircraft on the runway exhibits behaviors that are in some ways similar to ground vehicles such as cars or trucks. The final topic of interest deals with tire forces and modeling of tire behavior.

One of the problems that was beyond the grasp of aeronautical engineers in the early 20^{th} century was the lack of understanding of the relationship between stability and control, as well as the influence of the pilot on the pilot-machine system. It was not

uncommon for experiments to be done with uncontrolled hand-launched gliders. Through these experiments, investigators discovered that a glider had to be inherently stable to fly successfully. A few of the early pioneers that contributed to the stability theory were Albert Zahm from the United States, Alphonse Penaud from France, and Frederick Lanchester from England. Zahm presented a paper in 1893 that correctly outlined the requirements for static stability. He studied an airplane descending at constant speed to analyze the conditions necessary for obtaining a stable equilibrium. Zahm's conclusion was that the center of gravity had to be in front of the aerodynamic force.[2]

Otto Lilienthal of Germany, and Octave Chanute and Samuel Pierpont Langley of the United States made other significant contributions to aircraft performance. Lilienthal was known for his work on human-carrying gliders. He mainly dealt with the properties of camber in wings. His designs were statically stable but had very little control capability. As a result, Lilienthal died in a glider crash. Octave Chanute experimented with biplane and multiplane wings. He also incorporated a vertical tail for steering and controls to adjust the wings to maintain equilibrium. Langley, a secretary at the Smithsonian Institution, was the first one to experiment with heavier-than-air powered flight. His initial work consisted of collecting and examining aerodynamic data.[2]

Finally, the Wright Brothers made history in 1903. These earlier aviators influenced much of the Wright's work. The Wright's designs, on the other hand, were statically unstable but very maneuverable. Their work was mostly directed towards improving control.

Aircraft stability is a rapidly growing field of study. The introduction of new control surfaces, automatic controls, and radical geometry makes it difficult to get a complete picture of exactly what transpires in the air. However, there are sources that allow the reader to get a general understanding of flight stability. One such book was written by a professor from the University of Notre Dame's Department of Aerospace and Mechanical Engineering. *Flight Stability and Automatic Control,*[2] by Dr. Robert C. Nelson, was originally written in 1989 and has since been revised. Nelson's work covers static stability, aircraft equations of motion, dynamic stability, flying or handling qualities, and automatic control theory. Another good source for analysis of aircraft is *Airplane Flight Dynamics and Automatic Flight Controls* by Jan Roskam.[3] Roskam develops the mathematical models for the aerodynamic and thrust forces and moments that act on an airplane. He also reviews the properties of lifting surfaces before developing the steady state equations of motion of airplanes. Finally, the perturbed equations of motion are discussed.

Several other books have been written that cover the subject of aircraft stability. Among these are *Airplane Stability and Control: A History of the Technologies That Made Aviation Possible* (Abzug, 1997),[4] *Aircraft Dynamic Stability and Response* (Babister, 1986),[5] *Dynamics of Flight: Stability and Control* (Etkin, 1996),[6] *Flight Stability and Control* (Hacker, 1970),[7] *Performance and Stability of Aircraft* (Russell, 1996),[8] and *Introduction to Aircraft Flight Dynamics* (Schmidt, 1998).[9]

Vehicle dynamics research has been going on since the early 1900's. William Lanchester wrote one of the first papers concerning road vehicle lateral dynamics in

1908.[10] Another early pioneer in this field was Maurice Olley. His paper "Suspension and Handling" covers the research of vehicle dynamics up to 1937.[11] During the early 1960's, Olley summarized his vast knowledge of suspension systems and handling in a series of papers now known as "Olley's Notes".[12, 13]

The Millikens, William and Douglas, did some more recent work in the field of vehicle dynamics. In their book, *Race Car Vehicle Dynamics,*[14] they cover everything from tire behavior to suspensions in regards to vehicle stability and control. They even state in the preface that aircraft engineering has been the key to understanding vehicle dynamics.

The Society of Automotive Engineers published a number of papers in *Car Suspension Systems and Vehicle Dynamics (SP-878),*[15] that cover suspension designs and steering systems. They also discuss analysis techniques and effective test methods.

Another good reference for both tire behavior and vehicle dynamics is J.Y. Wong's *Theory of Ground Vehicles.*[16] Wong discusses the mechanics of pneumatic tires and some practical methods for predicting tire behavior. He also deals with the analysis and prediction of road vehicle performance.

Other references covering the subject of vehicle dynamics include *Vehicle Dynamics* (Ellis, 1969),[17] *Fundamentals of Vehicle Dynamics* (Gillespie, 1992),[18] *Modeling of Road Vehicle Lateral Dynamics* (Keifer, 1996),[19] *Fundamentals of Vehicle Dynamics* (Mola, 1969),[20] and *Analysis of Tire Lateral Force and Interpretation of Experimental Tire Data* (Nordeen, 1967).[21]

3 Tire Model

3.1 Introduction

Tires play an important role in determining aircraft behavior while it is on the ground. The tires are the primary source of the forces and torques that provide the control and stability or handling of the aircraft (handling commonly refers to the directional stability and controllability of a vehicle). The forces developed by the tire will affect the aircraft in a number of ways. Clearly, the tires support the aircraft weight in addition to any other vertical forces that develop such as those due to road banking. The interaction between the tires and the ground supply the tractive, braking, and cornering forces for maneuvering. The tires also provide the forces used for controlling and stabilizing the aircraft and for resisting external disturbances. All of the forces acting on an aircraft are applied through its tires, with the exception of aerodynamic and gravitational forces. Therefore, to accurately model the dynamics of an aircraft on the ground, it is necessary to have an appropriate depiction of tire behavior. This chapter deals with the function of tires in producing lateral forces.

In this thesis, two tire models are used. A simple linear model is used to lay the foundation for understanding tire behavior, and then a more precise non-linear model is used for better accuracy. The non-linear model is also developed because it supports a wide variety of applications. The requirements of a typical tire model will vary depending on which aspects of vehicle performance are being modeled and the accuracy required. In general, there are three force components (longitudinal, lateral, and vertical)

and three moment components (pitching, yawing, and rolling) acting on a tire due to its interaction with the ground. If a complete model of aircraft ground dynamics is required, then all six of these components must be included to accurately model the effect of the tires on the dynamics of the aircraft. This thesis is only concerned with the lateral dynamics of the aircraft. Therefore, it will only discuss lateral and rotational degrees of freedom in the horizontal plane. This will reduce to only forces in the lateral direction and moments about the vertical axis of the aircraft.

3.2 Lateral Force

According to SAE J670, "Vehicle Dynamics Terminology",[22] a lateral tire force originates at the "center" of tire contact with the road, lies in the horizontal plane, and is perpendicular to the direction in which the wheel is headed if no inclination or camber exists. Strictly speaking, the center of tire contact is the origin of the SAE Tire Axis System, which is the intersection of the wheel center plane with the ground plane and a point directly below the center of the upright wheel. The mechanics of the lateral force generation is an elaborate process; so elaborate that a complete discussion of this process is beyond the scope of this thesis. However, many thorough explanations of the mechanics of lateral force generation can be found in literature.[14,16,18] The lateral force, F_y, generated by a pneumatic tire depends on many variables such as road surface conditions, tire carcass construction, tread design, rubber compound, size, pressure, temperature, speed, vertical load, longitudinal slip, inclination angle, and slip angle. The two variables that have the biggest impact on a given tire for dry, unchanging runway

surface conditions are vertical load and slip angle. Thus, these variables are the main focus of this chapter and this thesis.

The vertical load acting on the tires of an aircraft is a function of the aircraft weight, the slope of the runway and the lift generated by the airplane. The tire slip angle is defined by SAE as "the angle between the X' axis and the direction of travel of the center of tire contact".[22] Simply put, the slip angle is the angle between the direction the wheel is pointing and the direction it is traveling at any given instant. The tire slip angle is represented by the symbol α. This definition corresponds to the SAE tire axis system.[29] As stated earlier, the origin of this system is at the center of the tire contact patch. The X' axis is the intersection of the plane of the wheel and the plane of the ground and is positive in the forward direction. The Z' axis is perpendicular to the plane of the road and is positive in the downward direction. The Y' axis is in the plane of the road and positive to the right in order to form the right-hand Cartesian coordinate system. The tire slip angle, lateral force, and tire axis system are shown in Figure 3.1, with a positive slip angle and lateral force shown.

The lateral force produced by a tire is a non-linear function of vertical load and slip angle, as well as other variables. Figure 3.2 shows a typical lateral force versus slip angle curve for a single vertical load. As you can see, at low slip angles the curve is approximately linear. In this region the lateral forced generated depends primarily on the tire construction, tread design, and tire pressure. There is little sliding occurring between the tire and the ground within the contact patch. Lateral force is mainly developed as a result of deformation of the tire.

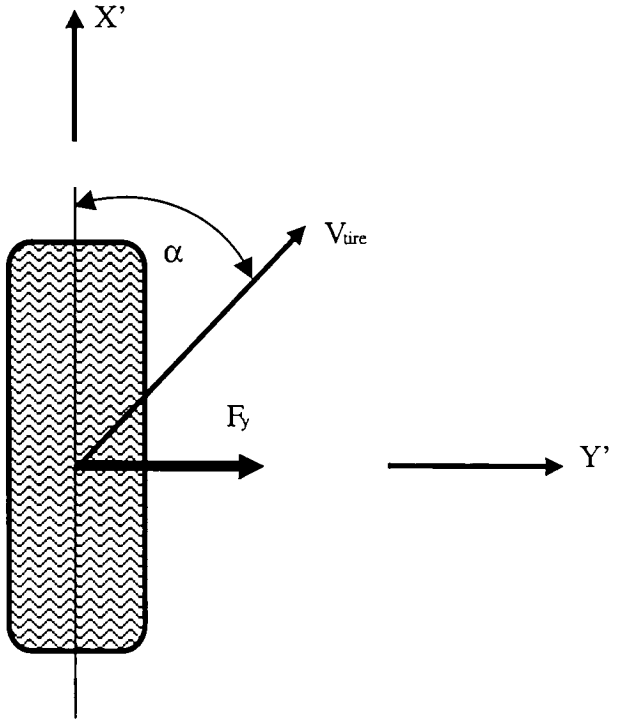

Figure 3.1: Tire Slip Angle

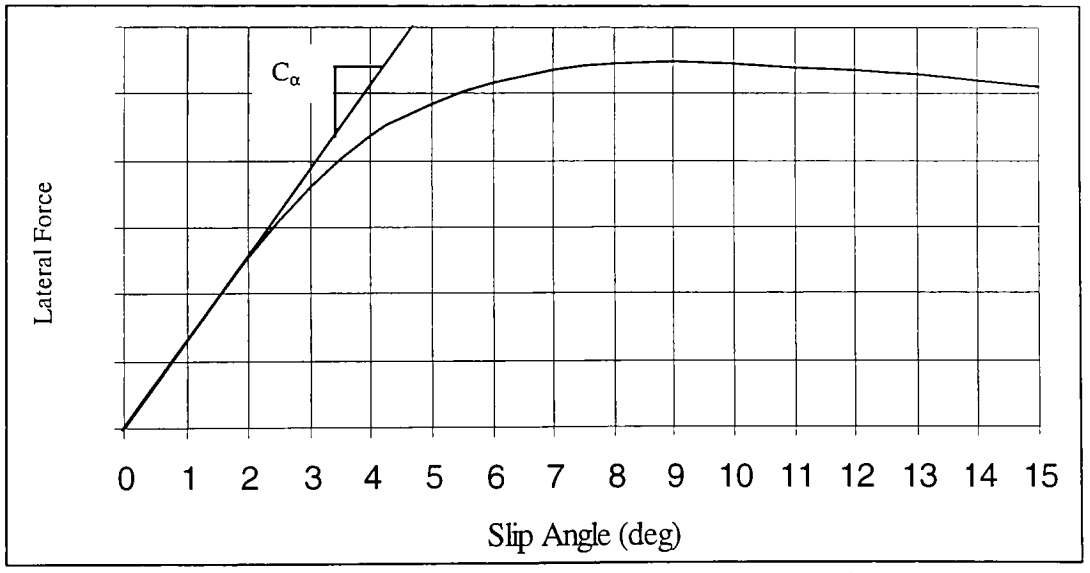

Figure 3.2: Tire Lateral Force versus Slip Angle

The initial slope of this lateral force versus slip angle curve is called the cornering stiffness of the tire and denoted by the symbol C_α. The cornering stiffness is often used as a linear approximation for the relationship between lateral force and slip angle, as you will see later in this chapter. If the cornering stiffness is normalized by dividing by the vertical load, a quantity known as the cornering coefficient, C_c, is found. As expected, both the cornering stiffness and the cornering coefficient are proportional to the vertical load. In general, the cornering stiffness increases with the vertical load, while the cornering coefficient decreases. These parameters will be needed as the tire model is further developed.

As the slip angle increases, the slope of the lateral force curve decreases until the lateral force reaches a maximum. The maximum lateral force is used to find the tire lateral friction coefficient, μ_y. Dividing the maximum value by the vertical load does this. Beyond this maximum value, the lateral force itself begins to decrease. In this section of the curve a larger portion of the contact patch is sliding than at low slip angles. Here the lateral force produced depends largely upon the road surface, tire rubber compound, and the interface between the two.

The lateral force versus slip angle curve shown in Figure 3.2 represents steady-state tire lateral force characteristics. Due to the elasticity and damping within a pneumatic tire it is actually a dynamic system within itself. When a change in slip angle occurs, the change in lateral force lags behind. Although the effects of tire dynamics can be modeled by including an additional differential equation in the vehicle model for each

tire, the effects are generally small for low input frequencies. Tire dynamics are neglected in this model as they are typically used when simulating extreme situations.

3.3 Linear Tire Model for Main Landing Gear

As stated in the previous section, the initial slope of the lateral force versus slip angle curve for a single vertical load is the cornering stiffness, C_α. This constant can be used as a reasonable representation of tire behavior under certain conditions. Inspection of Figure 3.2 reveals that at small slip angles the lateral force is nearly linear. Thus, at sufficiently small slip angles the lateral force produced by a tire can be approximated by

$$F_y = C_\alpha \alpha \tag{3.1}$$

When this linear approximation is combined with other assumptions regarding the aircraft, the lateral force versus slip angle relationship allows the aircraft to be modeled as a linear system. This is very beneficial to the user because some very well developed analysis techniques exist that allow us to study a linear model and learn a great deal about aircraft lateral dynamics. The range of applicability of the linear tire model is examined by comparison to the non-linear model in the next chapter.

3.4 Non-Linear Tire Model for Main Landing Gear

As you saw in Figure 3.2, the lateral force versus slip angle curve is no longer linear at high slip angles, and thus will not accurately predict the tire lateral force. If we try to use the linear model to predict the lateral force at these high slip angles, we will get

a force that is greater than the actual tire force. Therefore, it is necessary to develop a non-linear tire model that will correctly determine the tire lateral force at high slip angles.

Several approaches to modeling tire behavior exist. Some models are purely empirical, based upon curve fitting of experimentally measured tire data. Other models are primarily theoretical, with some parameters determined experimentally, such as the stiffness of the tire. Each type of model has its advantages and disadvantages. Since experimentally measured aircraft tire data exists for a variety of tires, we will use the first method to develop the model.

The tire model chosen for this study is called tire data non-dimensionalization, and was originated by Hugo Radt.[14,23,24] This technique is able to predict tire aligning moment, longitudinal force, and lateral force for combined lateral slip, camber, and longitudinal slip. However, only the lateral force due to lateral slip will be used in this study. The effects of camber on lateral force are being neglected. Also, if we assume the aircraft has a constant forward velocity then it is not necessary to consider longitudinal force. Although tire-aligning moments are present, they are considered to have a negligible effect on the overall dynamics of the aircraft.

The technique you are about to see consists of two main steps. The first step deals with preprocessing the experimental tire data to determine the parameters for the tire model. The second step uses these results to calculate the tire lateral force for a given vertical load and slip angle. In a vehicle dynamics simulation, the first step is typically done before running the simulation. The second step is then done at each time step during the simulation based on instantaneous values of tire vertical load and slip angle.

The tire data used in developing this model was obtained from the Goodyear Tire & Rubber Company for a standard aircraft tire, model 6.00-6 6PR at 42 psi. The tire data is given in Table 3.1 and shown in Figure 3.3. Lateral force versus slip angle curves are available for vertical loads of 1779 N, 2669 N, 3559 N, 4448 N, and 5338 N. The slip angle for each of these loads varies from 0° to 20°. Typically, the lateral force at 0° slip angle is not zero as might be expected. This is due to conicity and/or ply steer in the tire. Conicity results from asymmetries in tire construction, while ply steer results from errors in the angles of the belt cords in the tire. Both of these effects are random in nature and vary from tire to tire. These effects are not important to this model, and the manufacturer has adjusted the data accordingly.

Preprocessing the experimental data is done by normalizing the data and then curve fitting the normalized data. The first step in normalizing the data is to determine the tire cornering coefficient, C_c, at each load. As previously stated, the cornering stiffness is the initial slope of the lateral force versus slip angle curve. The cornering coefficient is then equal to the cornering stiffness divided by the vertical load, which can be approximated at each load by dividing the lateral force at 1° slip angle by the corresponding vertical load. Thus, the cornering coefficient at any load is

$$C_c = \frac{F_y\big|_{\alpha=1^\circ}}{F_z} \tag{3.2}$$

Table 3.1: Experimental Tire Data

Slip Angle (deg)	Lateral Force @ Vertical Load (N)				
	1779	2669	3559	4448	5338
0	0	0	0	0	0
1	302	414	454	485	489
2	534	734	823	899	912
3	707	988	1125	1246	1281
4	841	1179	1370	1535	1601
5	939	1334	1575	1784	1882
6	1014	1450	1739	1993	2122
7	1072	1544	1877	2166	2335
8	1112	1615	1988	2313	2518
9	1143	1673	2077	2438	2678
10	1170	1717	2153	2544	2816
11	1188	1748	2215	2633	2936
12	1201	1775	2264	2709	3038
13	1214	1797	2304	2771	3132
14	1219	1810	2340	2825	3212
15	1228	1824	2366	2869	3278
16	1232	1833	2389	2909	3341
17	1237	1842	2406	2940	3390
18	1237	1846	2424	2967	3434
19	1241	1850	2433	2989	3474
20	1241	1855	2447	3011	3510

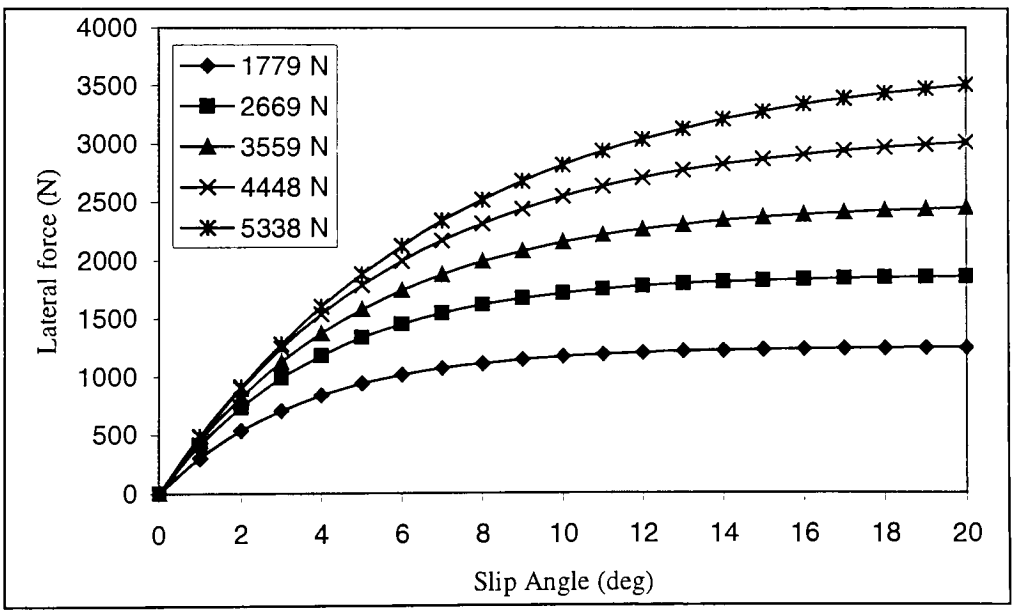

Figure 3.3: Experimental Tire Data

Figure 3.4 shows the tire cornering coefficient for each load. As you can see, the relationship between cornering coefficient and vertical load is approximately linear. For this tire, the cornering coefficient as a function of vertical load can be represented as

$$C_c = B_3 + C_3 F_z \tag{3.3}$$

Values of the constants B_3 and C_3 are given in Table 3.2. The resulting expression can be used to predict the cornering coefficient for an arbitrary load during a simulation.

The next step is to find the lateral friction coefficient, μ_y, at each load. Dividing the maximum lateral force for a given vertical load by the vertical load itself does this. Thus, for a single vertical load the lateral friction coefficient is

$$\mu_y = \frac{F_y\big|_{\max}}{F_z} \tag{3.4}$$

The lateral friction coefficients for each load are plotted in Figure 3.5. As with the cornering coefficients, the relationship between the lateral friction coefficient and the vertical load is approximately linear for this tire. The lateral friction coefficient can then be expressed as

$$\mu_y = B_5 + C_5 F_z \tag{3.5}$$

Values of the constants B_5 and C_5 are given in Table 3.2. This expression can also be used during simulation to predict the lateral force coefficient for an arbitrary vertical load.

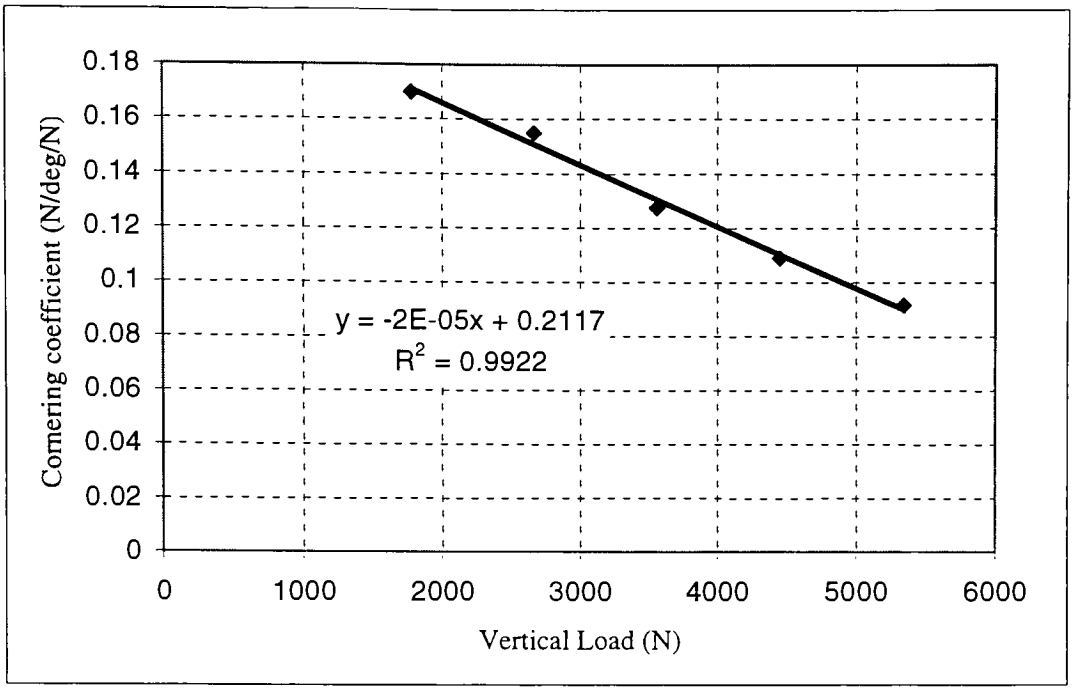

Figure 3.4: Tire Cornering Coefficient

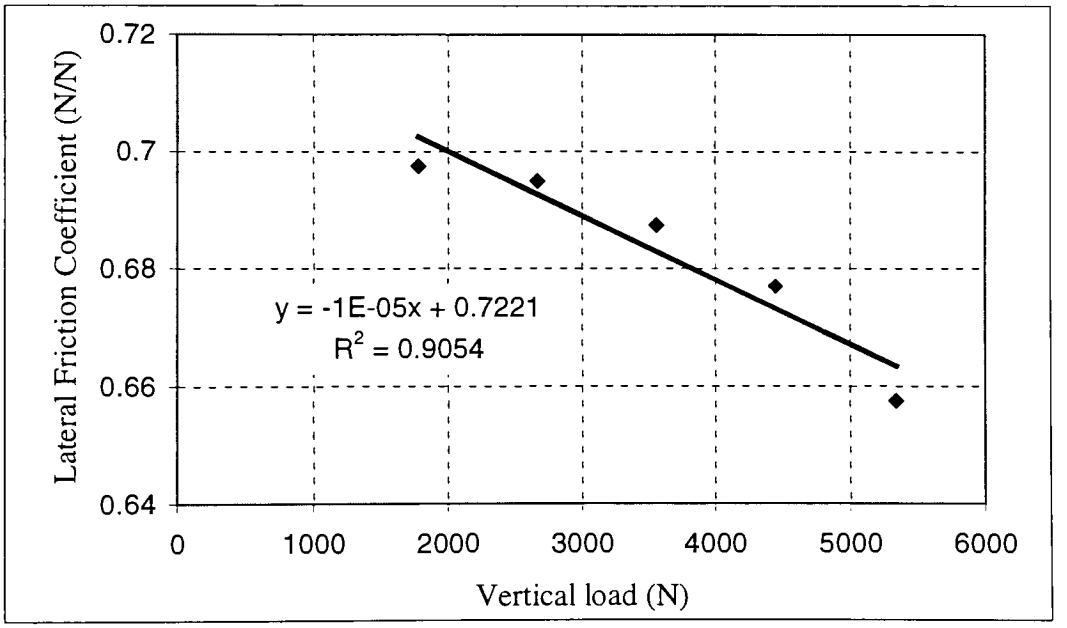

Figure 3.5: Tire Lateral Friction Coefficient

Table 3.2: Non-Linear Tire Model Parameters

Parameter	Symbol	Value
Tire cornering coefficient intercept	B_3	0.2117
Tire cornering coefficient slope	C_3	-2.2918×10^{-5}
Tire lateral friction coefficient intercept	B_5	0.7221
Tire lateral friction coefficient slope	C_5	-8.81055×10^{-6}
Magic Formula curve fit parameter	B_1	0.7947
Magic Formula curve fit parameter	C_1	0.1901
Magic Formula curve fit parameter	D_1	6.1197
Magic Formula curve fit parameter	E_1	1.0637

Now that the cornering coefficient and lateral friction coefficient are known at each load, the normalized slip angle, $\overline{\alpha}$, can be calculated at each data point from the formula

$$\overline{\alpha} = \frac{C_c tan(\alpha)}{\mu_y} \tag{3.6}$$

Similarly, the normalized lateral force, $\overline{F}_y$, at each data point is

$$\overline{F}_y = \frac{F_y}{\mu_y F_z} \tag{3.7}$$

When the normalized lateral force is plotted against the normalized slip angle for each vertical load, the results lie on a single curve as shown in Figure 3.6. This normalized data is then curve fit. There are a number of methods used to fit this data. This model uses a popular function known as the "magic formula".[25] The magic formula, as you will see, is a combination of trigonometric functions and has the capability to accurately fit tire data curves of various shapes such as lateral force, longitudinal force, and aligning moment.

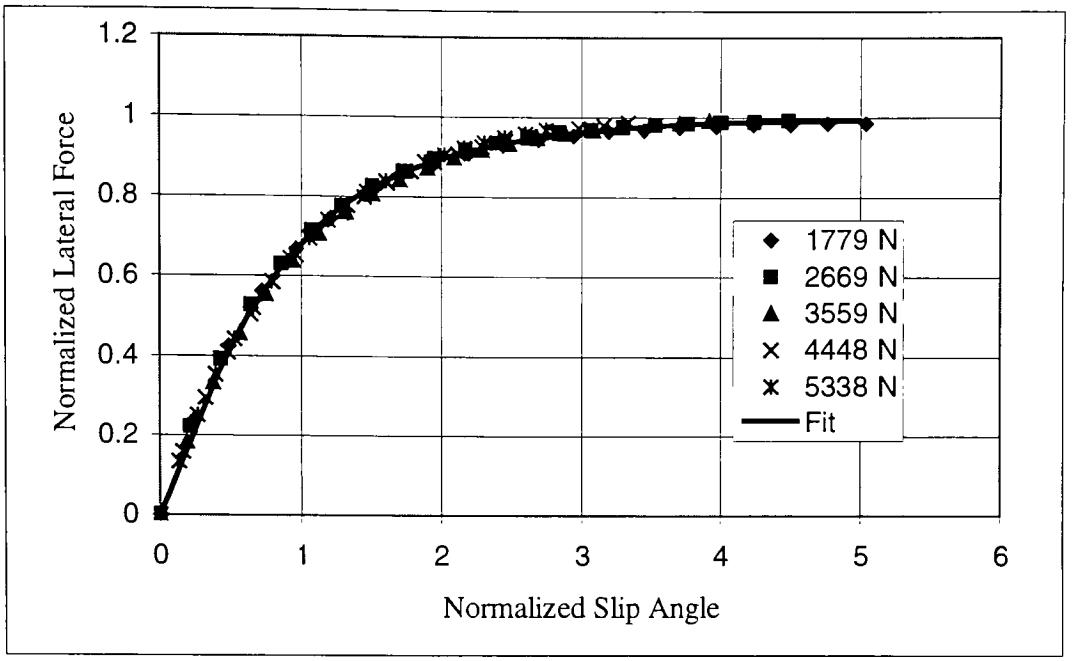

Figure 3.6: Tire Normalized Lateral Force

The normalized lateral force is fit to the function

$$\bar{F}_y = D_1 \sin\left(\bar{\theta}\right) \tag{3.8}$$

where

$$\bar{\theta} = C_1 \operatorname{atan}\left(B_1 \bar{\psi}\right) \tag{3.9}$$

and

$$\bar{\psi} = \left(1 - E_1\right)\bar{\alpha} + \frac{E_1 \operatorname{atan}\left(B_1 \bar{\alpha}\right)}{B_1} \tag{3.10}$$

The parameters B_1, C_1, D_1, and E_1 must be determined to provide the best fit to the normalized experimental data. The curve fitting is implemented in the MATLAB script *MAGICFIT.m*. This script reads the normalized lateral force versus slip angle data from a

file and uses the MATLAB Optimization Toolbox function *LEASTSQ* to do a non-linear least squares fit. The *LEASTSQ* function calls the function *MAGICERROR.m* that computes the errors between each data point and the curve fit function. The parameters B_1, C_1, D_1, and E_1 are found to minimize the sum of the squares of these errors. The files *MAGICFIT.m* and *MAGICERROR.m* were developed by Joseph Kiefer for use in *Modeling of Road Vehicle Lateral Dynamics*.[19] They are listed in Appendix A.1 and Appendix A.2, respectively. Values for the curve fit parameters are given in Table 3.2, and the function is plotted in Figure 3.6 along with the normalized data. As you can clearly see from the plot, an excellent fit to the data had been obtained.

Now that a function for the normalized lateral force in terms of normalized slip angle is available, the tire lateral force can be calculated for any combination of vertical load and slip angle. First, the cornering coefficient and lateral friction coefficient are calculated from the vertical load using Eq. (3.3) and (3.5). Second, the normalized slip angle is calculated from the slip angle, the cornering coefficient, and the lateral friction coefficient using Eq. (3.6). Next, the normalized lateral force is calculated from the normalized slip angle using Eq. (3.10), (3.9), and (3.8) in this order. Finally, the tire lateral force can then be found from the normalized lateral force, the lateral friction coefficient, and the vertical load as

$$F_y = \overline{F}_y \mu_y F_z \tag{3.11}$$

This procedure is implemented in the MATLAB function *NLTIRE.m* that is listed in Appendix A.3. The function takes the tire vertical load and slip angle as inputs and

outputs the lateral force. Plots of lateral force versus slip angle from this function for vertical loads of 1779 N, 2669N, 3559 N, 4448 N, and 5338 N are shown in Figure 3.7 as solid lines along with the experimental data points.

The non-linear tire model implemented in this section accurately reproduces the experimentally determined lateral force versus slip angle relationship of the tire used in this study. This model is capable of predicting the lateral force produced by the tire at high slip angles. Thus, the tire model is suitable for inclusion in a model of aircraft lateral dynamics where high tire slip angles are obtained. While this tire model only determined lateral force due to slip angle, it can be extended to predict aligning moment due to slip angle, lateral force and aligning moment due to camber, and longitudinal force due to longitudinal slip.

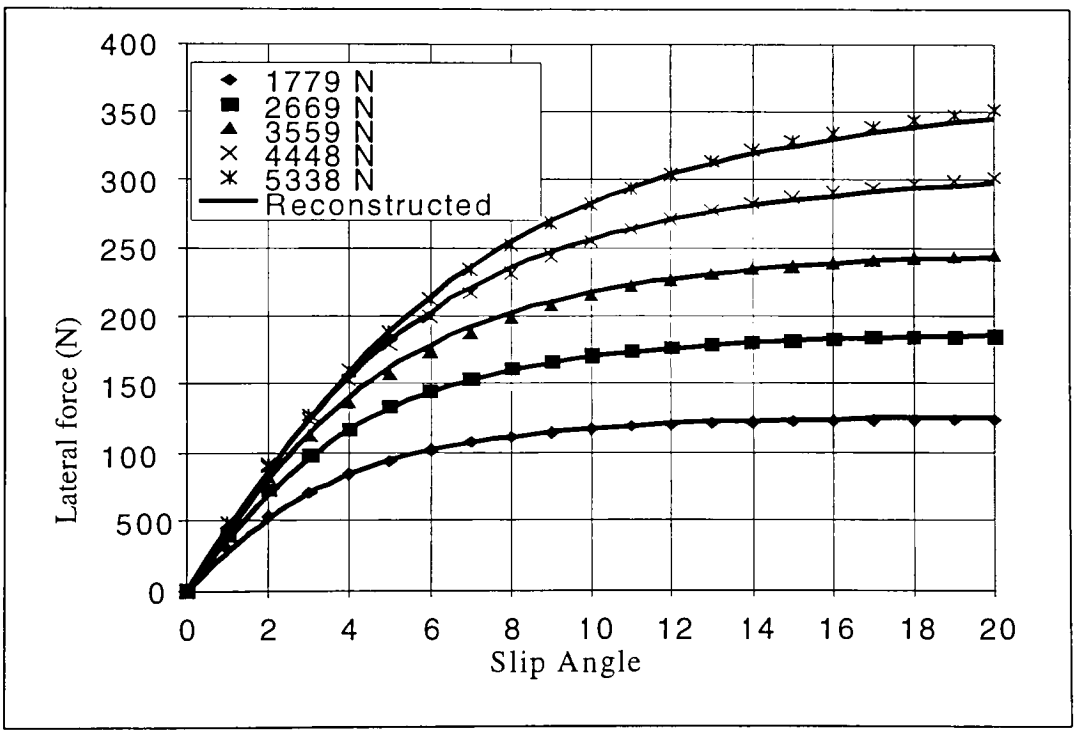

Figure 3.7: Reconstructed Tire Lateral Force

3.5 Tire Model for Tail Wheel

The tail wheel for this study was chosen to be an 8-½ inch outer diameter by 3-inch width tire. The inflation pressure is 40 psi. This model was also created from data provided by Goodyear Tire & Rubber Company. Using the dimensions of the tire, they were able to calculate the cornering stiffness for a specified load. The data points were then plotted and a curve fit was applied using the *MICROSOFT EXCEL* function *TRENDLINE.* This function calculates a least squares fit through the data points. A fourth order polynomial was fit to the data points as shown in Figure 3.8. The equation *EXCEL* used to fit the data points is displayed in the figure. Also shown is the R-Squared value. The R-Squared value can be interpreted as the proportion of the variance in y attributable to the variance in x. This function returns the Pearson product moment correlation coefficient, r, which is a dimensionless index that ranges from -1.0 to 1.0 inclusive and reflects the extent of a linear relationship between two data sets. As you can see, the R-Squared value for this curve fit is exactly 1. Therefore, the equation shown represents the best possible fit to the data. The tail wheel model is used in Chapter 4 when calculating tail wheel cornering stiffness based on the fraction of weight on the tail wheel.

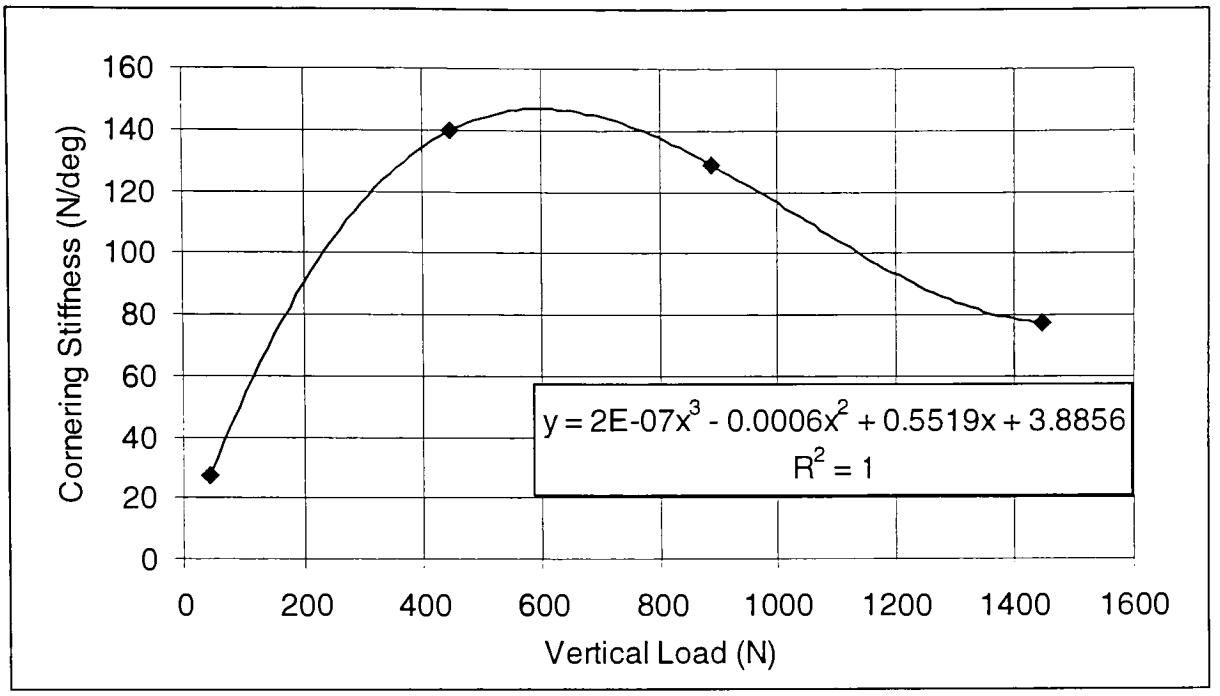

Figure 3.8: Tail Wheel Cornering Stiffness

4 Two Degree-of-Freedom Aircraft Model

4.1 Introduction

In this chapter, we will be looking at a simplified mathematical model of an aircraft. By using a computer generated model we will be able to vary all aspects of the aircraft. This is extremely useful for this study in which we need to explore the difference between a tricycle gear aircraft and a taildragger aircraft. This model will ultimately allow us to develop the basic concepts that govern the response of the aircraft and control the stability. From these concepts we will be able to predict the motion of the aircraft as it moves along the runway regardless of its configuration, as well as examine the stability of the aircraft as it is in the process of taking off or landing.

This simplified representation of the aircraft, referred to as the "bicycle" model, is a two degree-of-freedom model that is often used to examine the lateral response of road vehicles.[14] The model is altered slightly to reflect the geometry of the aircraft used in this study. The model is developed in a general form for a taildragger aircraft. Later in this chapter, you will see that only minor changes to the model are needed to make it into a tricycle gear aircraft. As you will see, this model greatly simplifies an aircraft. However, through its use we can investigate the effects of major design and operational parameters on the yawing and sideslipping motions that determine the path and attitude of the aircraft. Such parameters include tire properties, inertia properties, center of gravity location along the wheelbase, and main landing gear location, among others.

This chapter aims to describe the two degree-of-freedom model in detail. To accomplish this, each vital component of the aircraft will be studied until the model is complete. First, we will start with just the main landing gear to see how its location affects stability. After these results have been established, the vertical tail will be added on to the model and the change in the response will be examined. Finally, the study will conclude with the addition of the tail wheel to the model. At this point, we should understand enough about the effects of each component to be able to make reasonable suggestions to improve the stability of a taildragger aircraft.

4.2 Description of Model

The two degree-of-freedom model for the taildragger aircraft used in this study is shown in Figure 4.1. As its name suggests, the model is only concerned with two types of variable motion: lateral velocity, v, and yawing velocity, r. The forward velocity, u, is assumed to be constant and shall be chosen by the user. The single tire shown represents the pair of tires forward of the center of gravity for an aircraft with a taildragger configuration. The tail wheel shown is allowed to swivel. However, it can be locked into place to create some stiffness that will result in a lateral tire force. The vertical tail shown will have a significant contribution to the motion of the aircraft. The longitudinal alignment of the components of the aircraft show why this is called a "bicycle" model.

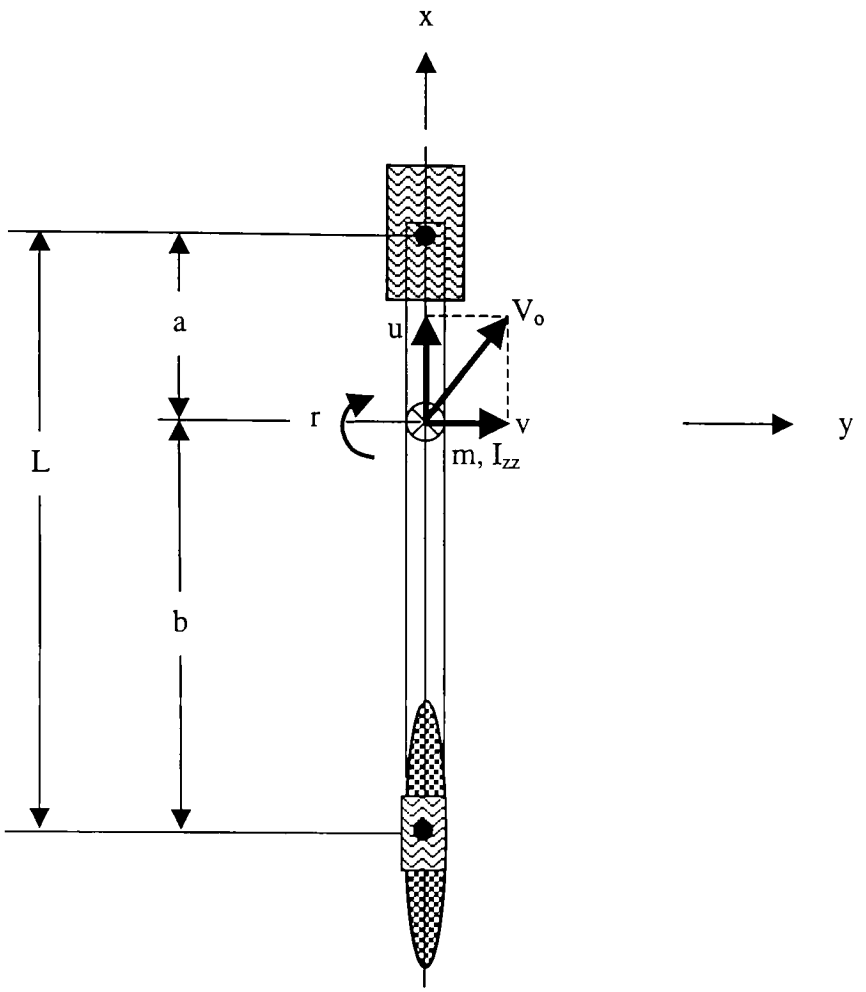

Figure 4.1: Bicycle Model for a Taildragger Aircraft

On a typical vehicle, the distance from the center of the front tires to the center of the rear tires is termed the wheelbase, *L*. This is also the case with an aircraft. For this particular model of aircraft, the tail wheel is located almost directly below the aerodynamic center of the vertical tail. Assuming that they are both in the same location will simplify the model even further. Thus, the distance from the front tires to the aerodynamic center of the vertical tail is also *L*. The aircraft has a mass, *m*, and a yaw

mass moment of inertia, I_{zz}, with its center of gravity located a distance a from the center of the front tire and a distance b from the tail wheel and the aerodynamic center of the vertical tail.

Notice that the front tires on an aircraft are not capable of rotating about the z-axis as on a car or truck. Therefore, they cannot be considered as control inputs. Again, this greatly simplifies the model, as we need not concern ourselves with steer angles.

The coordinate system used to describe the motion of the aircraft is the standard SAE vehicle-fixed x-y-z coordinate system, which translates and rotates with the aircraft.[22] The x-axis is positive in the forward direction, the y-axis is positive to the right, and the z-axis is positive down into the page as specified by the right-hand rule. The origin of the coordinate system is at the center of gravity (CG) of the aircraft. Motion is only permitted in the x-y plane.

4.2.1 Assumptions

The representation of the aircraft as a "bicycle" model takes into account several simplifying assumptions in addition to those previously mentioned. They are:

- Constant aircraft parameters (m, I_{zz}, a, b, L)
- Constant aircraft forward velocity, u
- Motion in x-y plane only (ignore vertical, rolling and pitching motions)
- Aircraft is rigid
- Aircraft is symmetrical about x-z plane

- Runway surface is smooth
- Ignore lateral gravity effects (ignore runway slope in lateral direction)
- Ignore longitudinal gravity effects (ignore runway slope in longitudinal direction)
- Ignore all longitudinal forces (tire driving/braking forces, tire rolling resistance, aerodynamic drag)
- Ignore front landing gear suspension system kinematics and dynamics
- Ignore tire slip angles resulting from lateral tire scrub
- Ignore lateral and longitudinal load transfer (vertical tire forces remain constant)
- Tire properties are independent of time and forward velocity
- Ignore tire lateral forces due to camber, conicity, and ply steer
- Ignore tire aligning moments
- Ignore effects of longitudinal slip on tire lateral force
- Ignore tire dynamics (no delay in lateral force generation)
- Ignore tire deflections

4.2.2 Aircraft Parameters

The nominal values of the aircraft parameters used for the two degree-of-freedom model in this study are given in Table 4.1. All parameters were obtained through direct measurements on the aircraft, except for the mass and the CG location, which can be found on the aircraft type certificate. For most aircraft, the CG location is referenced from a specified datum and is usually in the form of a range. The CG range for this plane

is 13.6-16.8 inches from the datum. As a point of reference for the reader, the forward most CG position of 13.6 inches from the datum was chosen to measure the center of gravity parameters, a and b, given in Table 4.1. These distances can then be used to calculate the fraction of weight on the front axle, f. The SI system of units is used for all calculations. The unit of length is the meter (m), and the unit of time is the second (s). Force is measured in the derived unit Newton (N). These parameters are representative of a production aircraft.

Table 4.1: Vehicle Parameters

Parameter	**Symbol**	**Value**
Aircraft Mass	m	748 kg
Yaw Moment of Inertia	I_{zz}	1760 kg-m^2
Wheelbase	L	4.52 m
Distance from CG to Front Landing Gear	a	0.599 m
Distance from CG to Aerodynamic Center of Vertical Tail & Tail Wheel	b	3.92 m
Front Landing Gear Weight Fraction	f	0.867
CG Limits	CG	13.6-16.8 in
Vertical Tail Area	A_p	0.693 m^2
Coefficient of Lift on Vertical Tail	C_{L_γ}	0.100/deg

4.2.3 Free Body Diagram

Due to the simplifying assumptions in Section 4.2.1, there are four types of external forces acting on the aircraft in the x-y plane that are considered in this model: front tire lateral force, tail wheel lateral force, vertical tail force, and a disturbance input. The front tire lateral force, $F_{y\_front\text{-}tire}$, occurs due to tire slip angles as does the tail wheel lateral force, $F_{y\_tail\text{-}wheel}$. The vertical tail force, F_{y_tail}, is a function of the relative air speed squared, the side force coefficient, and a reference area. The disturbance force,

$F_{y\_disturbance}$, is an input that acts at the aerodynamic center of the vertical tail, as does the tail force. The most common disturbance input is a crosswind encountered on the runway. These forces are shown acting on the vehicle in Figure 4.2 and are considered positive when acting in the positive y-direction.

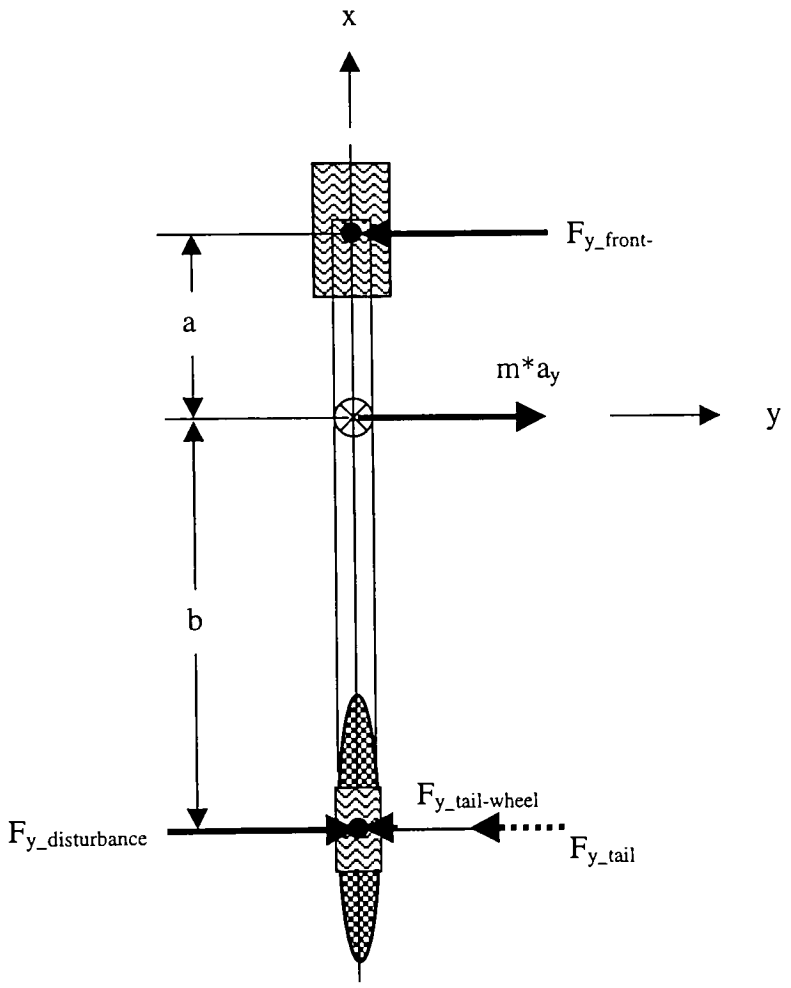

Figure 4.2: Free Body Diagram

4.3 Derivation of Equations of Motion

The equations of motion will be developed for the "bicycle" model. To do this we use basic principles of Newtonian mechanics for rigid body motion relative to translating and rotating coordinate systems.[26] This is a linear model with two degrees-of-freedom which enables the calculation of the motion variables as a function of the forces and moments acting on the aircraft. Referring to Figure 4.1, the motion variables of interest are forward velocity, u, lateral velocity, v, and yaw rate, r. Yaw rate, r, is the angular velocity of the aircraft around a vertical axis passing through the CG. The vector sum of u and v is the path velocity, V. The x-axis of the aircraft is at a body slip angle, β, with V For straight-ahead motion $\beta = 0$. The total side force is Y and the yawing moment about the CG is N.

The reference axis system (aircraft axis system) is fixed on the aircraft with the origin at the aircraft CG (refer to section 4.2). The fundamental features of this system are that changes in the dependent variables are measured relative to inertial space and the moments and products of inertia are constant. If the actual path of the vehicle relative to the ground is required, an additional earth-fixed reference system is required.

The rigid body equations are obtained from Newton's Second Law. This states that the summation of all external forces acting on a body is equal to the time rate of change of the momentum of the body. Furthermore, the summation of the external moments acting on the body is equal to the time rate of change of the moment of momentum (angular momentum). The time rates of change of linear and angular

momentum are referred to an absolute or inertial reference frame. Newton's Second Law can be expressed in the following vector equations:

$$\begin{aligned} \sum \boldsymbol{F} &= \frac{d}{dt}\boldsymbol{G} \\ \sum \boldsymbol{M} &= \frac{d}{dt}\boldsymbol{H} \end{aligned} \tag{4.1}$$

where $\boldsymbol{F}$ and $\boldsymbol{M}$ are the external forces and moments (in vector form) acting about the center of gravity, and $\boldsymbol{G}$ and $\boldsymbol{H}$ are the linear and angular momenta of the body (also in vector form). The assumptions of the model allow us to reduce Eq. (4.1) since only motion in the x-y plane is considered and all longitudinal (x-direction) forces are neglected. Thus, we are left with

$$\begin{aligned} \sum F_y &= ma_y \\ \sum M_z &= I_{zz}\dot{\Omega}_z \end{aligned} \tag{4.2}$$

Since the x-y-z coordinate system is fixed to the aircraft with its origin at the aircraft center of gravity, the translational velocity of the aircraft mass center and rotational velocity of the aircraft are identical to those of the x-y-z system. From Figure 4.1, the velocity, $\mathbf{V_o}$, of the origin of the x-y-z system is

$$\mathbf{V}_o = u\mathbf{i} + v\mathbf{j} \tag{4.3}$$

and the angular velocity, Ω, is

$$\Omega = r\mathbf{k} \tag{4.4}$$

Since the x-y-z system is also rotating, the unit vectors are changing with time. Thus, the acceleration, $\mathbf{a_o}$, of the origin expressed in an inertial reference frame coincident with the x-y-z system is

$$\begin{aligned}\mathbf{a}_o &= \left.\frac{d\mathbf{V}_o}{dt}\right|_{xyz} + \Omega \times \mathbf{V}_o \\ &= (\dot{u} - vr)\mathbf{i} + (\dot{v} + ur)\mathbf{j}\end{aligned} \tag{4.5}$$

Likewise, the angular acceleration of the x-y-z system relative to an inertial reference frame is

$$\begin{aligned}\dot{\Omega} &= \left.\frac{d\Omega}{dt}\right|_{xyz} + \Omega \times \Omega \\ &= \dot{r}\mathbf{k}\end{aligned} \tag{4.6}$$

Thus, because we are only concerned with lateral motion, the acceleration values of interest are

$$\begin{aligned}a_y &= \dot{v} + ur \\ \dot{\Omega}_z &= \dot{r}\end{aligned} \tag{4.7}$$

These values apply to both the aircraft-fixed x-y-z system and to the aircraft center of gravity.

The external forces acting on the vehicle are shown in Figure 4.2. The sum of the forces in the y-direction and the sum of the moments about the z-axis can then be written as

$$\begin{aligned}\sum F_y &= -F_{y\_front-tire} + F_{y\_disturbance} - F_{y\_tail} - F_{y\_tail-wheel} \\ \sum M_z &= -a * F_{y\_front-tire} - b * F_{y\_disturbance} + b * (F_{y\_tail} + F_{y\_tail-wheel})\end{aligned} \tag{4.8}$$

Substitution of Eq. (4.7) and Eq. (4.8) into Eq (4.2) yields the equations of motion for the two degree-of-freedom taildragger aircraft:

$$\begin{aligned} -F_{y\_front-tire} + F_{y\_disturbance} - F_{y\_tail} - F_{y\_tail-wheel} &= m(\dot{v} + ur) \\ -a * F_{y\_front-tire} - b * F_{y\_disturbance} + b * (F_{y\_tail} + F_{y\_tail-wheel}) &= I_{zz}\dot{r} \end{aligned} \tag{4.9}$$

Here u is the vehicle forward velocity and is constant. The state variables are the lateral velocity, v, and the yaw velocity, r. $F_{y\_front-tire}$ is the front tire lateral force, $F_{y\_disturbance}$ is the disturbance input, F_{y_tail} is the vertical tail force, and $F_{y\_tail-wheel}$ is the tail wheel lateral force.

As stated, the aircraft system derived in Eq. (4.9) is a two degree-of-freedom system. This is the minimum number of independent coordinates needed to describe the motion of the system. Furthermore, Eq. (4.9) is a constraint equation. A system in which the constraints are functions of the coordinates or coordinates and time is called holonomic. In many cases the constraint equations relate the velocities or the velocities and coordinates. If these equations can be integrated to yield relations involving coordinates and time only, the system is still holonomic.[27] However, the system may not be holonomic in the event of large displacements during integration. Since each integration step in this study is small, the system remains holonomic.

4.4 Derivation of Tire Slip Angles & Vertical Tail Angle

From Chapter 3, the lateral force produced by a tire depends upon the vertical load on the tire and the slip angle of the tire, among other things. In this model the vertical load remains constant. However, the front tire slip angle varies as a function of the lateral

velocity and angular velocity. For this reason, we must develop an expression for the front tire slip angle, α, in terms of v and r.

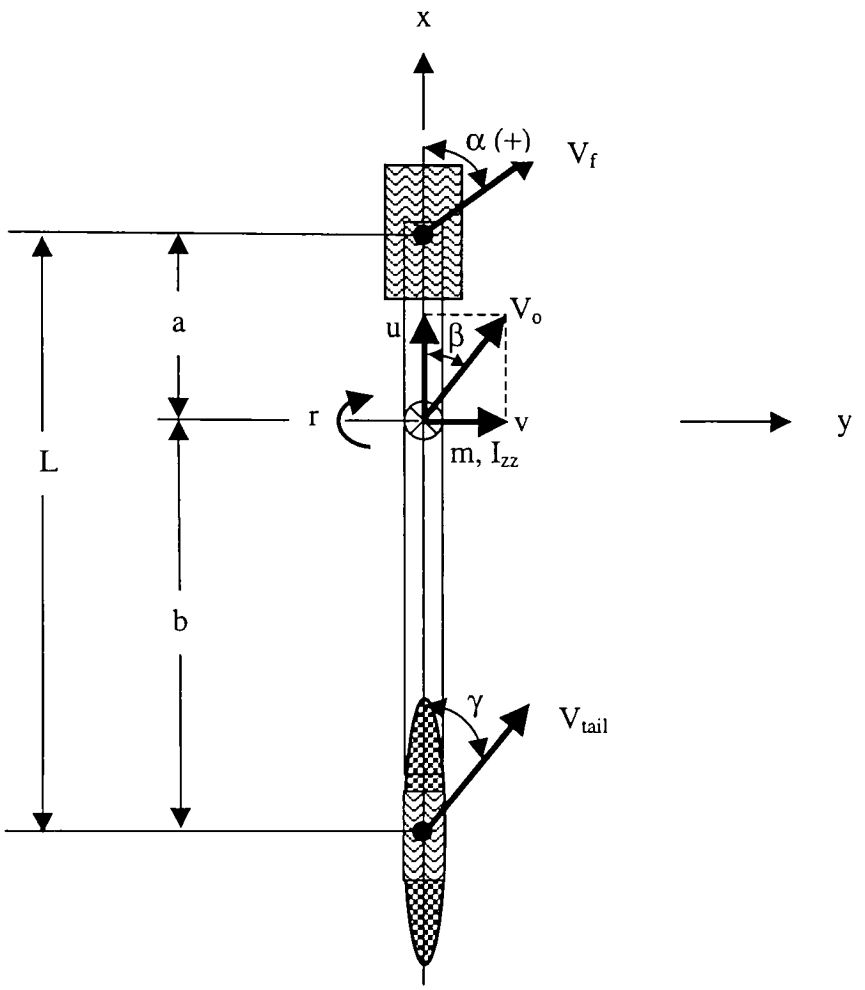

Figure 4.3: Kinematic Diagram

Figure 4.3 is a kinematic diagram of the vehicle showing the tire velocity vector and tire slip angle. The slip angle is shown in its positive sense as the angle between the tire and the tire velocity vector.

To determine these angles the velocities of the tire must be found first. Since the translational and rotational velocities of the aircraft-fixed *x*-*y*-*z* coordinate system are already known from Eq. (4.3) and Eq. (4.4), it is convenient to use the principle of relative motion to derive the front tire velocity, $\mathbf{V_f}$, as

$$\mathbf{V_f} = \mathbf{V_o} + \Omega \times \mathbf{R_f} \tag{4.10}$$

where $\mathbf{R_f}$ is the position vector from the vehicle center of gravity to the front tire:

$$\mathbf{R_f} = a\mathbf{i} \tag{4.11}$$

Thus, the front tire velocity is

$$\mathbf{V_f} = u\mathbf{i} + (v + ar)\mathbf{j} \tag{4.12}$$

In general, if the velocity of a tire is known, the respective angle is

$$\alpha = atan\left(\frac{V_{yi}}{V_{xi}}\right) \tag{4.13}$$

where V_{xi} and V_{yi} are the *x*- and *y*-components of the aircraft component under observation. Therefore, in its general non-linear form, the front tire slip angle is

$$\alpha = atan\left(\frac{v + ar}{u}\right) \tag{4.14}$$

In a similar manner, there is an angle of attack on the vertical tail that must be taken into consideration for this study. As with the front tire slip angle, we must first find the velocity of the tail using the same principles of relative motion. The velocity of the tail, $\mathbf{V_{tail}}$, is then

$$\mathbf{V_{tail}} = \mathbf{V_o} + \Omega \times \mathbf{R_r} \tag{4.15}$$

where $\mathbf{R_r}$ is the position vector from the vehicle center of gravity to the aerodynamic center of pressure of the tail:

$$\mathbf{R_r} = -b\mathbf{i} \tag{4.16}$$

Thus, the tail velocity is

$$\mathbf{V_{tail}} = u\mathbf{i} + (v - br)\mathbf{j} \tag{4.17}$$

Using the general form, the angle of attack on the tail is

$$\gamma = atan\left(\frac{V_{yi}}{V_{xi}}\right) \tag{4.18}$$

where, again, V_{xi} and V_{yi} are the x- and y-components of the aircraft component under observation. Therefore, in its general non-linear form, the vertical tail angle is

$$\gamma = atan\left(\frac{v - br}{u}\right) \tag{4.19}$$

As stated in section 4.2, the tail wheel is directly below the aerodynamic center of pressure of the vertical tail. Thus, the velocities of the tail and tail wheel are the same, which means the angle for the tail and the tail wheel are the same.

4.5 Linear Model

The equations developed in the previous section are in a general form. By using some additional assumptions to linearize the model at hand, analysis techniques for linear systems may be used to gain more insight into aircraft lateral dynamics. In this section, the tire slip angles, vertical tail angle of incidence, and lateral forces are assumed to be linear functions.

It is a common practice to use the vehicle sideslip angle, β, instead of the lateral velocity, v, to describe lateral motion when studying vehicle dynamics, particularly with the linear model. In this case, the aircraft sideslip angle, as shown in Figure 4.3 in its positive sense, is the angle between the aircraft-fixed x-axis and the aircraft vector, $\mathbf{V_o}$. Therefore,

$$\beta = atan\frac{v}{u} \tag{4.20}$$

Some additional assumptions are made for the linear two degree-of-freedom model in addition to those listed in Section 4.2.1. They are:

- Linear tire lateral force versus slip angle relationship
- Small tire slip angle, vehicle sideslip angle, and tail incidence angle

4.5.1 Aircraft Sideslip Angle

With the small angle assumption, Eq. (4.20), the aircraft sideslip angle, becomes

$$\beta = \frac{v}{u} \tag{4.21}$$

However, if the vehicle sideslip angle is small then

$$\cos(\beta) = \frac{v}{u} \approx 1$$

or (4.22)

$$u \approx \mathrm{V}$$

where V is the magnitude of the aircraft velocity, $\mathbf{V}_o$. Now, Eq. (4.21) becomes

$$\beta = \frac{v}{V} \tag{4.23}$$

4.5.2 Tire Slip Angle

With the small angle assumption, the tire slip angle becomes

$$\alpha = \frac{v + ar}{u} \tag{4.24}$$

Furthermore, if the aircraft sideslip angle is used in place of lateral velocity, then the tire slip angle can be expressed as

$$\alpha = \beta + \frac{a}{V} r \tag{4.25}$$

4.5.3 Tail Incidence Angle

With the small angle assumption, the tail incidence angle becomes

$$\gamma = \frac{v - br}{u} \tag{4.26}$$

Likewise, if aircraft sideslip angle is used in place of lateral velocity, then the tail incidence angle can be expressed as

$$\gamma = \beta - \frac{b}{V} r \tag{4.27}$$

4.5.4 External Forces and Moments

Referring back to the free-body diagram of the two degree-of-freedom model in Figure 4.2, we see that the external forces acting on the aircraft are the front tire lateral force, $F_{y\_front\text{-}tire}$, the disturbance force, $F_{y\_disturbance}$, the vertical tail force, F_{y_tail}, and the tail wheel lateral force, $F_{y\_tail\text{-}wheel}$.

Using the assumptions from Section 4.5, we would like to express the tire lateral force as a linear function. This was already done for the tire model described in Chapter 3. From Eq. (3.1) the tire lateral force is

$$F_{y\_front\text{-}tire} = C_f \alpha \tag{4.28}$$

where C_f is the front tire cornering stiffness and is the effective cornering stiffness of both tires on a main landing gear. Thus, for example, C_f is twice the cornering stiffness of a single front tire. As a result, $F_{y\_front\text{-}tire}$ is the sum of the tire lateral force of both tires on the main gear. The free body diagram in Figure 4.2 shows that this force is acting in the negative y-direction. Therefore, the cornering stiffness must be positive in order to produce the negative lateral force required by the sign convention. For further explanation of this tire model see Section 3.3. Values for the front tire cornering stiffness for the aircraft studied were obtained through Eq. (3.3) and are given in Table 4.2.

Table 4.2: Linear Tire Model Parameter

Parameter	**Symbol**	**Value**
Front tire cornering stiffness (two tires)	C_f	883 N/deg

As mentioned earlier in the chapter, the disturbance force, $F_{y\_disturbance}$, is used to simulate a crosswind. Airplanes often encounter strong breezes while they are moving

along the runway in an open field. For this study, we will assume that conditions are ideal and there is no crosswind ($F_{y\_disturbance} = 0$). However, this term is left in the equations should the reader wish to input a disturbance force. If this is done, the simulations shown later in this chapter will shift accordingly, but the stability of the aircraft will not be affected.

The vertical tail force, F_{y_tail}, is perhaps the most important external force acting on the aircraft in terms of stability. This force is a function of many variables including aircraft speed, vertical tail area, and the coefficient of lift of the tail.[2] This force is the same force that produces lift on the wings. However, in this case the orientation is vertical. As with the wings of an aircraft, the angle of attack on the vertical tail is an important factor in determining this tail force. The force on the vertical tail can be expressed as

$$F_{y\_tail} = (\tfrac{1}{2} \rho u^2 A_p C_{L_\gamma})\gamma \tag{4.29}$$

where ρ is the density of air at sea level, u is the forward velocity of the aircraft, A_p is the reference area, which in this case refers to the projected area of the vertical tail, and C_{L_γ} is the coefficient of lift of the vertical tail and is a property of the tail geometry. All of these factors are constants. The values for A_p and C_{L_γ} for the aircraft used in this study are given in Table 4.1. The force on the vertical tail is also a function of the angle of attack, γ, which is not a constant (see section 4.5.3). The angle of attack will change as the aircraft tries to regain stability. This force is linear as long as the tail incidence angle is linear.

The tail wheel lateral force, $F_{y\_tail\text{-}wheel}$, will be similar to that of the front tires in that there is some cornering stiffness, $C_{f\text{-}tail}$, which is a parameter of the type of tire and is a constant. The lateral force is then generated by this stiffness times the slip angle, which we determined to be γ. This force is already linear so there is no modification needed. It can be expressed as

$$F_{y\_tail\text{-}wheel} = C_{f\text{-}tail} * \gamma \tag{4.30}$$

4.5.5 Linearized Equations of Motion

Now that all of the external forces and angles have been linearized, we can substitute Eqs. (4.24), (4.26), (4.28), (4.29), and (4.30) into Eq. (4.9) to obtain the linearized equations of motion. In terms of the aircraft lateral velocity they are:

$$\begin{aligned} &-C_f\left(\frac{v+ar}{u}\right) + F_{y\_disturbance} - \left(\frac{1}{2}\rho u^2 A_p C_{L\gamma} + C_{f-tail}\right)\left(\frac{v-br}{u}\right) = m(\dot{v}+ur) \\ &-a*C_f\left(\frac{v+ar}{u}\right) - b*F_{y\_disturbance} + b*\left(\frac{1}{2}\rho u^2 A_p C_{L\gamma} + C_{f-tail}\right)\left(\frac{v-br}{u}\right) = I_{zz}\dot{r} \end{aligned} \tag{4.31}$$

As stated at the beginning of the chapter, the model in Figure 4.2 is going to be divided into the different components that act on the aircraft. This is done for the linear model so that we can get a very basic understanding of what the effects of these components will be. We will first start with just the main landing gear and its external force, $F_{y\_front\text{-}tire}$. To this we will add the vertical tail and its external force, F_{y_tail}. Finally, the model will be completed with the addition of the tail wheel lateral force,

$F_{y\_tail\text{-}wheel}$. Simulation will be performed at each step of the development so we can see how each component affects the stability of the aircraft for different configurations.

For this portion of the study, we will be comparing the tricycle gear configuration to the taildragger configuration. The main difference between these two types of aircraft is the location of the main landing gear. As you already saw in Figures 4.1, 4.2, and 4.3, the main landing gear on a taildragger is forward of the center of gravity. For a tricycle gear aircraft, the main landing gear is behind, or aft, of the center of gravity.

4.5.6 Simulation of Main Landing Gear Only

In this section, we will be examining the response of the aircraft to just the main landing gear external force, $F_{y\_front\text{-}tire}$. Therefore, Eq. (4.31) can be reduced to

$$\begin{aligned} -C_f\left(\frac{v+ar}{u}\right) &= m(\dot{v}+ur) \\ -a*C_f\left(\frac{v+ar}{u}\right) &= I_{zz}\dot{r} \end{aligned} \tag{4.32}$$

Previously we said that these equations were developed for a taildragger aircraft. In actuality, Eqs. (4.31) and (4.32) can be used for any aircraft configuration. As long as a, the distance from the CG to the main landing gear, is positive, then these equations represent a taildragger aircraft. This configuration is shown in Figure 4.2. However, once a becomes negative the CG moves forward of the main landing gear and we have a tricycle gear aircraft. By changing the sign, the velocity of the tires changes and so does

the yawing moment on the aircraft. The lateral force remains in the same direction. The tricycle gear configuration is shown in Figure 4.4.

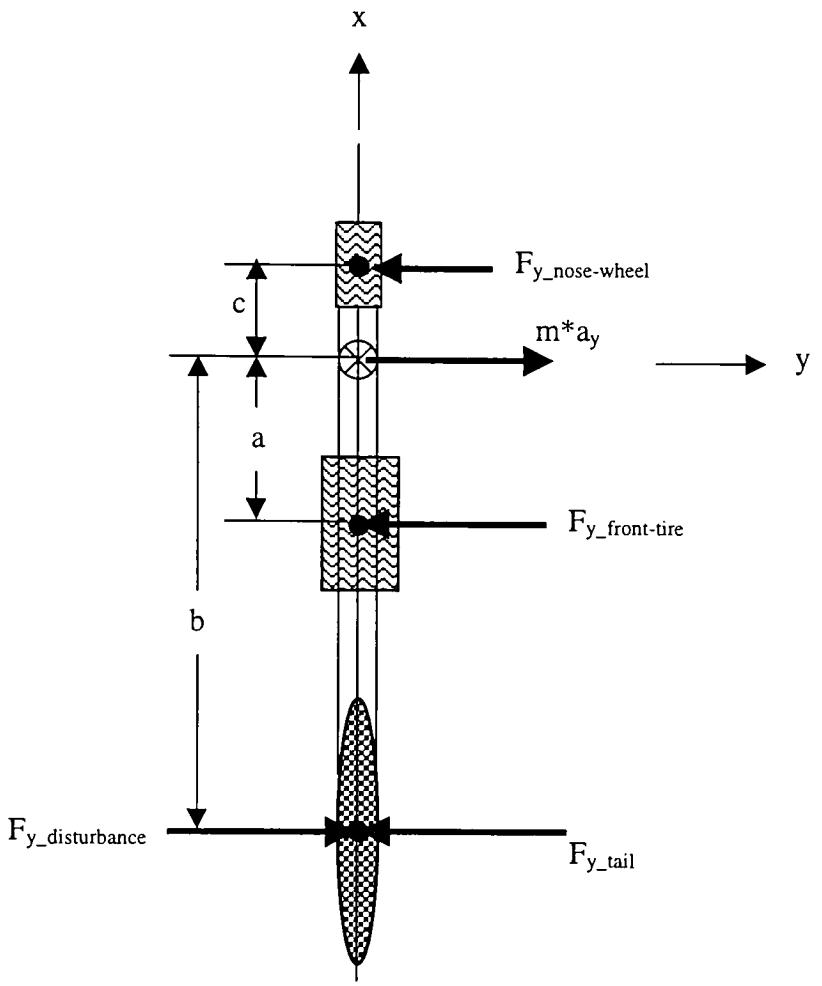

Figure 4.4: Tricycle Gear Configuration

Simulation of the model is performed by integrating the differential equations of motion with respect to time. The result is a graphical prediction of the motion of the aircraft over the specified time period. Some typical outputs of interest are lateral displacement and velocity, angular displacement and velocity, aircraft sideslip angle, tire

slip angle, tail incidence angle, and lateral acceleration. The parameters that are of most interest to a pilot while still on the runway are the lateral displacement response, how far the aircraft moves left or right, and the angular displacement response, which is the orientation of the aircraft with respect to the runway. The pilot ideally wants to be able to take his hands off the control stick or wheel, hands off condition, and have the plane travel straight down the runway with no yawing.

The simulation that follows was performed using the MATLAB software. Appendix A contains the files used to input the various aircraft parameters, do the integration, and output the responses of interest. These files will be referenced throughout this section.

The simulation is implemented in the script file *DOF2LSIM.m* that is listed in Appendix A.7. This file calls on the built-in MATLAB function *ODE23* to integrate differential equations of low order. *ODE23* integrates a system of ordinary differential equations using 2nd and 3rd order Runge-Kutta formulas.[28] The function returns the state variables v and r over the time interval specified for the simulation. The lateral and angular displacement, y and θ, can then be found by integrating v and r over the same time period.

At each time step the *ODE23* function refers to the file *DOF2LDE.m* which calculates the state derivatives $\dot{v}$ and $\dot{r}$ based upon the instantaneous values of the state variables v and r. *DOF2LDE.m* is listed in Appendix A.8. The state derivatives are found by solving Eq. (4.32) for $\dot{v}$ and $\dot{r}$ and resubstituting Eqs. (4.24), (4.26), (4.28), (4.29), and (4.30):

$$\dot{v} = \frac{-F_{y\_front-tire}}{m} - ur$$
$$\dot{r} = \frac{-a * F_{y\_front-tire}}{I_{zz}} \tag{4.33}$$

Prior to running the *ODE23* function, *DOF2LSIM.m* calls on three separate files to input the parameters for the simulation. The first file, *DOF2PARA.m* listed in Appendix A.5, loads in the mass, the yaw moment of inertia, the fraction of weight on the main landing gear (in this case all the weight is on the main gear), the wheelbase, the forward velocity, and the tire cornering stiffness' for the linear simulation. It also contains some parameters for the non-linear simulation that will be discussed later in the chapter. *DOF2CONT.m* then sets the time interval for the simulation and the tolerance accuracy for the outputs. *DOF2CONT.m* is listed in Appendix A.4. *DOF2DEPA.m*, listed in Appendix A.6, uses the file *DOF2PARA.m* to calculate the remaining aircraft parameters such as the distance from the front landing gear to the CG and the distance from the vertical tail aerodynamic center to the CG. This file will also calculate the front tire normal load based on the mass and the fraction of weight on the front landing gear that is used in the non-linear study. Finally, *DOF2LSIM.m* calculates the tire slip angle and tail incidence angle from Eq. (4.24) and (4.26) and the front tire lateral force from Eq. (4.28). Plots can then be generated for the lateral displacement and angular rotation to analyze stability.

The simulation of just the main landing gear is used to determine how its location affects stability. Therefore, two locations of the main gear will be examined: one directly at the CG and one in front of the CG. The location of the CG does not play a role in this

part of the simulation due to the absence of the tail wheel. This can be seen in Eq. (4.33). The only variable that is being changed in this equation is the distance from the main landing gear to the CG, which is a. Therefore, the CG can be placed at any location. The forward and aft limits of the CG only become critical when the distance from the tail wheel to the CG, b, is also in the equation. Then there is a direct relationship between a and b in which the forward and aft limits of the CG play a role.

Also of interest is the stability of the aircraft as it is taking off or landing. Changing the value of the front tire cornering stiffness can simulate this. Two different values for cornering stiffness are used. First, the full cornering stiffness for one tire, as shown in Table 4.2 for two tires, is used. This condition represents the full-static load. Then, this value is halved to represent the condition when only half of the tire may be touching the runway. This condition will be termed the half-static load. The configurations used in this section are given in Table 4.3. The model was simulated for an aircraft traveling at 100 km/hr.

Table 4.3: Main Landing Gear Simulation Configurations

Trial #	**Distance From Main Gear to CG, a (m)**	**Main Gear Cornering Stiffness, C_f (one tire) (N/deg)**
1	0	441.630
2	0	220.815
3	0.5	441.630
4	0.5	220.815

The results of the simulations are given numerically in Table 4.4 and shown graphically in Figure 4.5 through 4.8. Figures 4.5 and 4.6 show the lateral displacement and angular rotation, in aircraft coordinates, over the time period of 5 seconds for the case when the main gear is at the CG, Trial #1 and #2. The effect of decreasing the front tire cornering stiffness can also be seen in Figure 4.5. Inspection of the figure and the steady state results in Table 4.4 show that the response increased when the cornering stiffness was decreased.

There is no rotation of the aircraft, as seen in Figure 4.6, because the main gear is at the CG. Thus, there is no moment about the z-axis.

Trial #3and #4, on the other hand, show that the aircraft is unstable. Figure 4.7 shows that the displacement increases exponentially with time regardless of the cornering stiffness. The same is true of the rotation of the aircraft, as shown in Figure 4.8. This means that the aircraft will be unstable at all times during take-off and landing. It is interesting to note that when the aircraft is inherently unstable, as in Trial #3 and #4, reducing the cornering stiffness actually helps the response. As shown in Figures 4.7 and 4.8, the rate at which the aircraft goes out of control is slower for the lower cornering stiffness.

Table 4.4: Results of Linear Simulation of Main Gear Only

Trial #	Eigenvalues	Steady State Displacement (m)	Steady State Angle (deg)	Time Constant (sec)	Settling Time (sec)	Rise Time (sec)	Peak Overshoot (%)
1	-2.43, 0	0.041	0.000	0.411	1.23	0.907	N/A
2	-1.22, 0	0.082	0.000	0.822	2.46	1.81	N/A
3	-5.37, 2.67	N/A	N/A	N/A	N/A	N/A	N/A
4	-3.44, 2.09	N/A	N/A	N/A	N/A	N/A	N/A

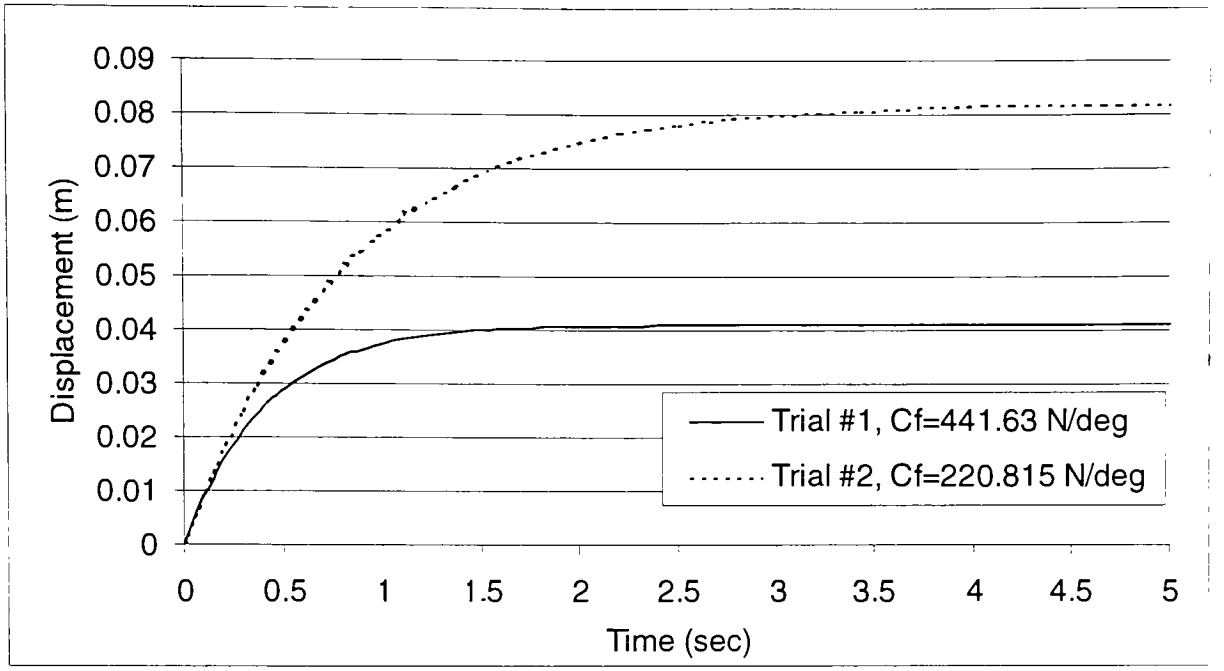

Figure 4.5: Linear Lateral Displacement Response for Main Gear at CG, Main Gear Only

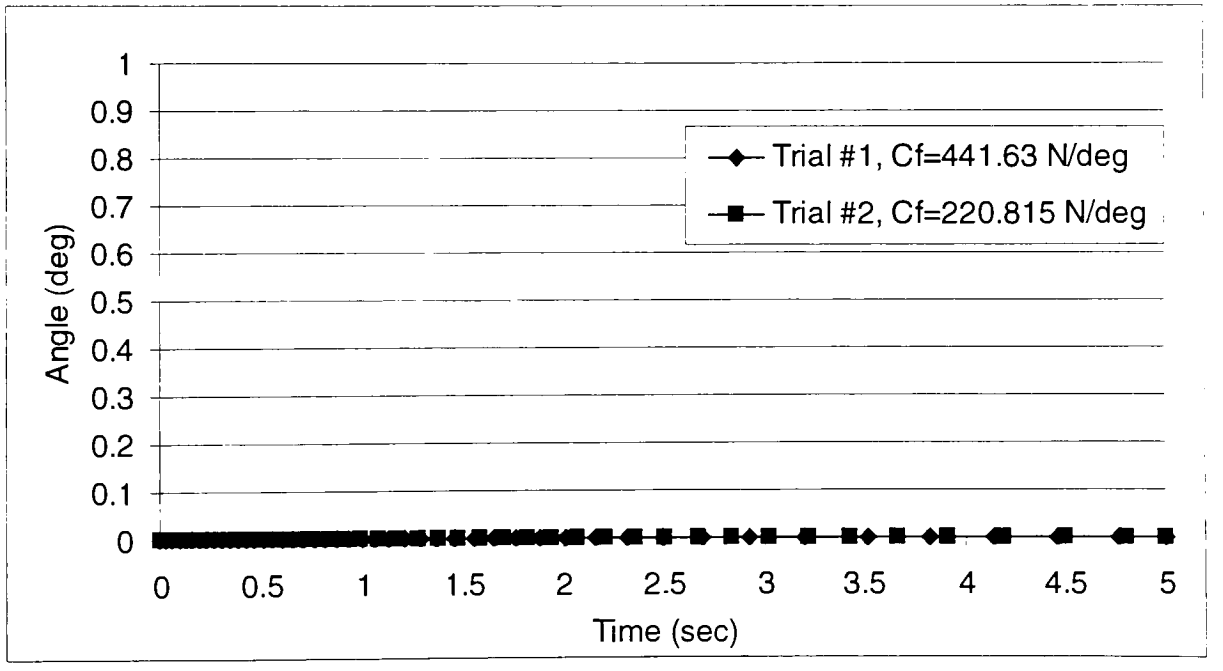

Figure 4.6: Linear Angular Rotation Response for Main Gear at CG, Main Gear Only

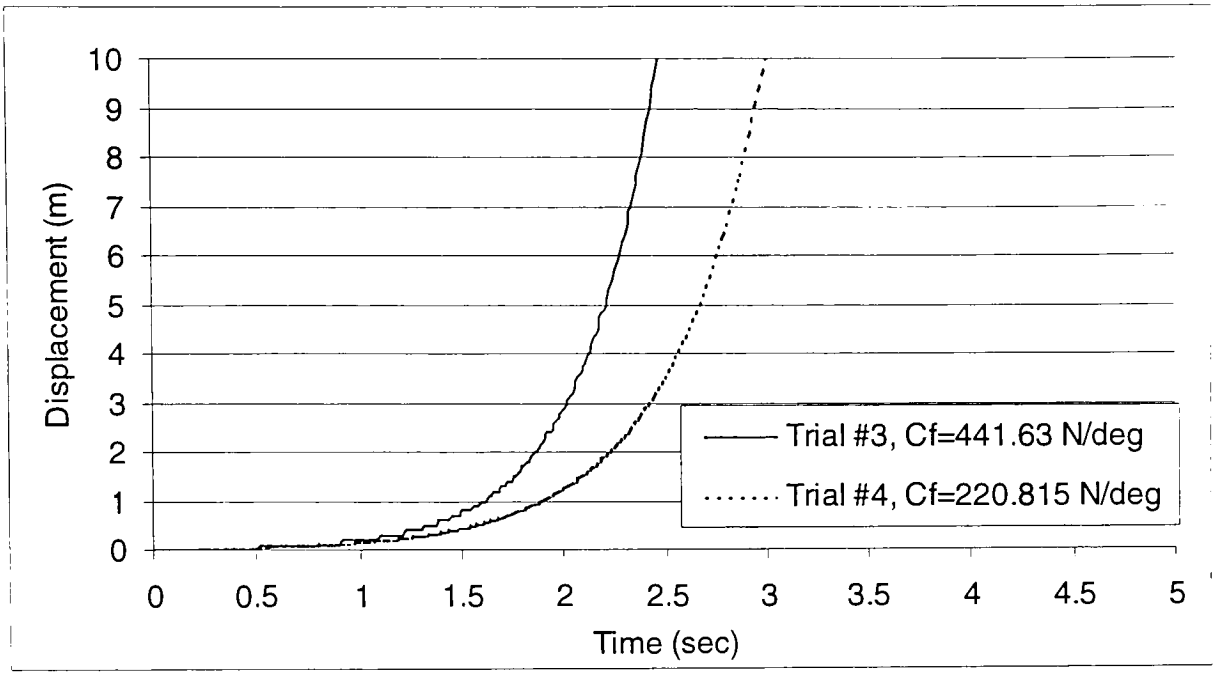

Figure 4.7: Linear Lateral Displacement Response for Main Gear 0.5 m in Front of CG, Main Gear Only

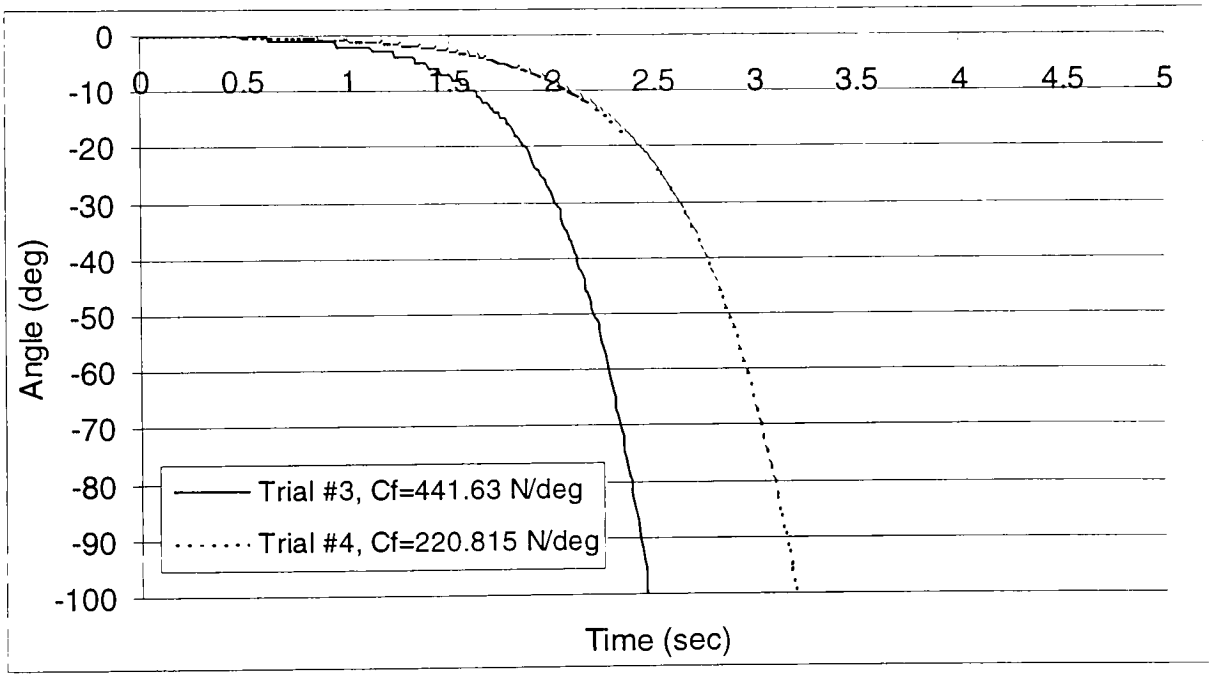

Figure 4.8: Linear Angular Rotation Response for Main Gear 0.5 m in Front of CG, Main Gear Only

Table 4.4 also includes other parameters, besides the steady state value, that are useful in stability analyses. These are the time constant, settling time, rise time, and peak overshoot. The time constant tells us how fast the system approaches a new steady state condition after being disturbed. If the time constant is small, the system will respond very rapidly; if the time constant is large, the system will respond very slowly. It is found by taking the negative of the reciprocal of the eigenvalues. The time constant for Trial #1 is 0.411 seconds while for Trial #2 it is 0.822 seconds. Therefore, the aircraft is responding twice as slow when it is taking off or landing as compared to when it is actually cruising down the runway. The settling time, the time it takes the response to stay within a specified tolerance band of 5% of the final value, is approximately 1.23 seconds for Trial #1 and 2.46 seconds for Trial #2. The rise time is the time required for the response to rise from 10% to 90% of the final value. For Trial #1 the rise time is 0.907 seconds and for Trial #2 it is 1.81 seconds. The peak overshoot is a measure of the oscillations about the final output. Since there are no oscillations, the peak overshoot is 0%. It is desirable to have a system that responds rapidly with minimum overshoot. Thus, there are trade-offs for each configuration.

The results of the main gear simulation are important to the designers of aircraft. What we have learned, and what has been known by pilots for years, is that placing the main landing gear in front of the CG makes the aircraft inherently unstable. That is why the tricycle gear configuration, where the main landing gear is behind the CG, is preferred over the taildragger configuration.

4.5.7 Simulation of Main Landing Gear & Vertical Tail Only

Further development of the model can be achieved by modifying Eq. (4.31) to allow for the vertical tail force as follows:

$$\begin{aligned} -C_f\left(\frac{v+ar}{u}\right) - \left(\frac{1}{2}\rho u^2 A_p C_{L\gamma}\right)\left(\frac{v-br}{u}\right) &= m(\dot{v}+ur) \\ -a*C_f\left(\frac{v+ar}{u}\right) + b*\left(\frac{1}{2}\rho u^2 A_p C_{L\gamma}\right)\left(\frac{v-br}{u}\right) &= I_{zz}\dot{r} \end{aligned} \tag{4.34}$$

Simulation is performed just as in Section 4.5.6. The state derivatives for this model are

$$\begin{aligned} \dot{v} &= \frac{-F_{y\_front-tire} - F_{y\_tail}}{m} - ur \\ \dot{r} &= \frac{-a*F_{y\_front-tire} + b*F_{y\_tail}}{I_{zz}} \end{aligned} \tag{4.35}$$

As you can see from the state derivatives in Eq. (4.35), the response of the aircraft is not only a function of the distance from the main gear to the CG, a, as in the previous section, but it also depends on the distance from the aerodynamic center of the vertical tail to the CG, b. Therefore, for the following simulations, the location of the CG is varied between its forward and aft limits, which directly affects the distance from the CG to the vertical tail as shown in Figures 4.1 through 4.4. The main gear is also varied to simulate a taildragger and a tricycle gear aircraft, as in Figures 4.2 and 4.4, respectively. Also, as in the previous section, two values of cornering stiffness are used to simulate an aircraft that is completely on the runway and one that is in the process of taking off or landing. Table 4.5 shows the configurations that are used for this simulation.

Table 4.5: Main Landing Gear & Vertical Tail Simulation Configurations

Trial #	CG Location (inches)	Distance From Main Gear to CG, *a* (m)	Vertical Tail Position, *b* (m)	Main Gear Cornering Stiffness, C_f (one tire) (N/deg)
5	13.6	-0.5	3.92176	441.630
6	13.6	-0.5	3.92176	220.815
7	16.8	-0.5	3.84048	441.630
8	16.8	-0.5	3.84048	220.815
9	13.6	0	3.92176	441.630
10	13.6	0	3.92176	220.815
11	16.8	0	3.84048	441.630
12	16.8	0	3.84048	220.815
13	13.6	0.5	3.92176	441.630
14	13.6	0.5	3.92176	220.815
15	16.8	0.5	3.84048	441.630
16	16.8	0.5	3.84048	220.815

The numerical results of the simulation of these configurations are summarized in Table 4.6 and shown graphically in Figures 4.9 through 4.20. Figures 4.9 through 4.12 simulate the tricycle gear configuration. The main landing gear is located behind the CG at a distance of 0.5m, or *a* is –0.5m. Figures 4.9 and 4.10 represent the scenario when the CG is at its forward limit. This is an underdamped response, as shown by the oscillations and the imaginary eigenvalues listed in Table 4.6. As you can see, the aircraft reaches steady state values for both the lateral displacement and angular rotation. However, the steady state values increase as the cornering stiffness decreases. Consequently, the time constant, settling time, rise time, and peak overshoot all increase.

Figures 4.11 and 4.12 show the same responses for the case when the CG is at its aft limit. As you can see, the response almost exactly matches that of the forward CG limit. A closer look at the data shows that the steady state values for this configuration are actually less than those for the forward CG limit. The difference is approximately

2%. Because the steady state values are less, the time constants, settling times, and rise times are all faster than in the previous configuration. This would suggest that it is favorable to move the CG to its aft limit when the main gear is behind the CG. The peak overshoot, on the other hand, increases when the CG is aft instead of forward. So depending on the type of response desired, the CG location can be modified to accommodate the designer's interests.

When the cornering stiffness is halved to simulate a load change due to the wheels leaving the runway during take-off or just touching the runway during landing, the stability of the aircraft decreases. The steady state values, time constants, settling times, rise times, and peak overshoots all increase due to the decreased lateral force generated by the main gear.

Figures 4.13 through 4.16 show the results of the main gear being positioned right at the CG. Again, these responses are underdamped, and both the lateral displacement and angular response reach steady state values regardless of the CG location or the cornering stiffness. All of the parameters listed in Table 4.6 show the same trends as when the main gear is behind the CG. Also, the same conclusion can be made about decreasing the cornering stiffness in that it decreases the stability of the aircraft. The major difference between placing the main gear at the CG as opposed to behind it is that the steady state values of displacement more than double when the CG is at the main gear, but the steady state values of the rotation actually decrease. This is due to the elimination of the moment created by the main gear. Moving the main gear to the CG did have other positive effects. The time constant and settling time increased, and the

peak overshoot decreased. In exchange for the decreased overshoot, the rise time increased. Thus, if the designer and pilot can live with an increase in lateral displacement and increased time in getting there, it is beneficial to move the main gear closer to the CG.

Figures 4.17 through 4.20 simulate the conditions that represent a taildragger aircraft. In these configurations, the main landing gear is 0.5m in front of the CG. As with the previous simulations, the CG is varied between its forward and aft limits and the cornering stiffness of the main gear is reduced to simulate take-off and landing conditions. These figures show the aircraft to be unstable. All of the responses, regardless of CG location or cornering stiffness, increase exponentially with time. Figures 4.17 and 4.19 show that the aircraft is sliding in the positive y-direction, while Figures 4.18 and 4.20 show that the aircraft is rotating in a counterclockwise manner. This agrees with what is known about the stability of taildragger aircraft while on the runway. The CG is realigning itself to be in front of the main gear. The location of the CG determines the rate of the lateral displacement and angular rotation. The response is slower when the CG is at its forward limit, as seen when comparing Figures 4.17 and 4.18 to Figures 4.19 and 4.20. This is because the CG has less distance to travel to get in front of the main gear as compared to when it is at its aft limit.

Furthermore, this is the first simulation for which the cornering stiffness has had a significant effect on the response of the aircraft. In the previous configurations, the cornering stiffness only slightly affected the steady state values of the lateral displacement and angular rotation. However, when the main gear is in front of the CG, the reduced

cornering stiffness greatly reduces the displacement and yaw. Figure 4.17 shows that the displacement for the full-static condition is approximately 10m at 4 seconds, whereas the half-static condition shows a displacement of approximately 2m at 5 seconds. The same is true for the rotation of the aircraft. Figure 4.18 shows that is takes the full-static condition approximately 2 seconds to rotate –10 degrees, as compared to the half-static condition that takes 5 seconds for the same rotation. These results show that a taildragger aircraft flies better in the air than it drives on the runway. That is why it is often said that such a plane has to be flown on the ground.

Table 4.6: Results of Linear Simulation of Main Gear & Vertical Tail Only

Trial #	Eigenvalues	Steady State Displacement (m)	Steady State Angle (deg)	Time Constant (sec)	Settling Time (sec)	Rise Time (sec)	Peak Overshoot (%)
5	-1.6868 ± 4.0996i	0.0043	0.1948	0.0279	2.2531	0.0365	281
6	-1.0135 ± 3.2999i	0.0060	0.1968	0.0390	4.5638	0.0497	295
7	-1.6747 ± 4.0877i	0.0042	0.1952	0.0274	2.2661	0.0357	290
8	-1.0014 ± 3.2865i	0.0059	0.1972	0.0386	4.5314	0.0495	302
9	-1.5574 ± 1.7867i	0.0105	0.1535	0.0728	2.8585	0.0982	135
10	-0.9488 ± 1.9998i	0.0120	0.1760	0.0805	4.3865	0.1060	178
11	-1.5453 ± 1.7562i	0.0103	0.1543	0.0713	2.9064	0.0958	141
12	-0.9367 ± 1.9763	0.0118	0.1766	0.0788	4.4850	0.1039	185
13	-5.0356, 1.6621	N/A	N/A	N/A	N/A	N/A	N/A
14	-2.7804, 0.7533	N/A	N/A	N/A	N/A	N/A	N/A
15	-5.0403, 1.6909	N/A	N/A	N/A	N/A	N/A	N/A
16	-2.7951, 0.7922	N/A	N/A	N/A	N/A	N/A	N/A

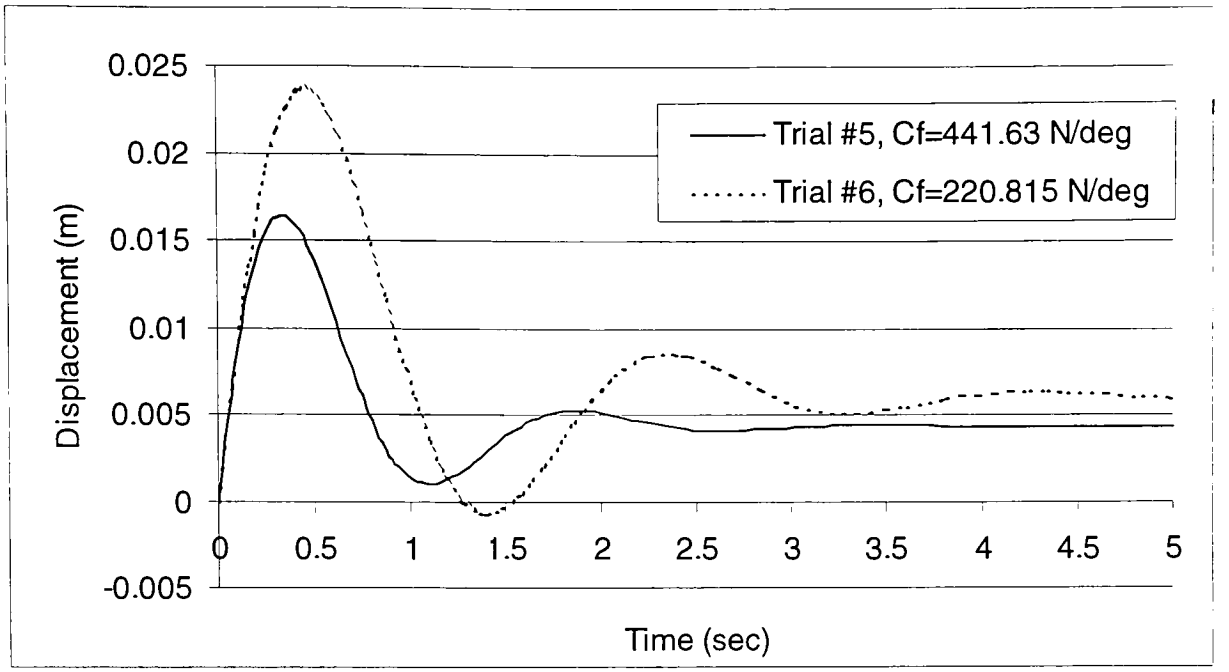

Figure 4.9: Linear Lateral Displacement Response for Main Gear Position –0.5 m & Forward CG Limit, Main Gear & Vertical Tail Only

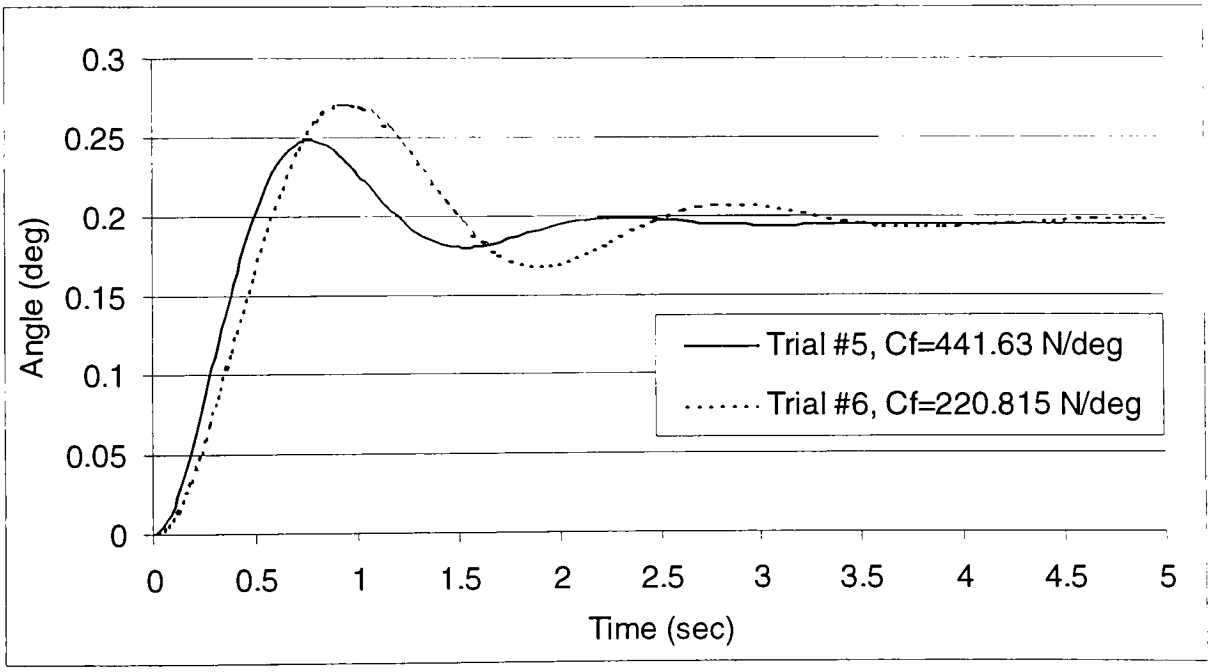

Figure 4.10: Linear Angular Rotation Response for Main Gear Position –0.5 m & Forward CG Limit, Main Gear & Vertical Tail Only

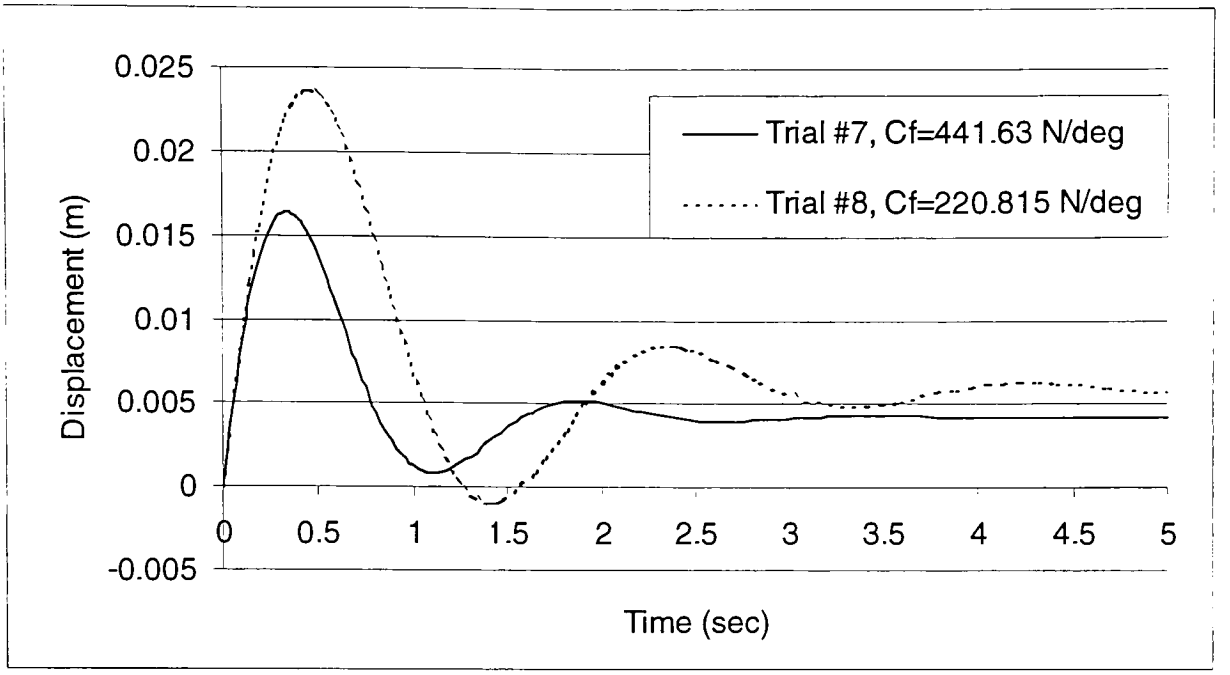

Figure 4.11: Linear Lateral Displacement Response for Main Gear Position –0.5 m & Aft CG Limit, Main Gear & Vertical Tail Only

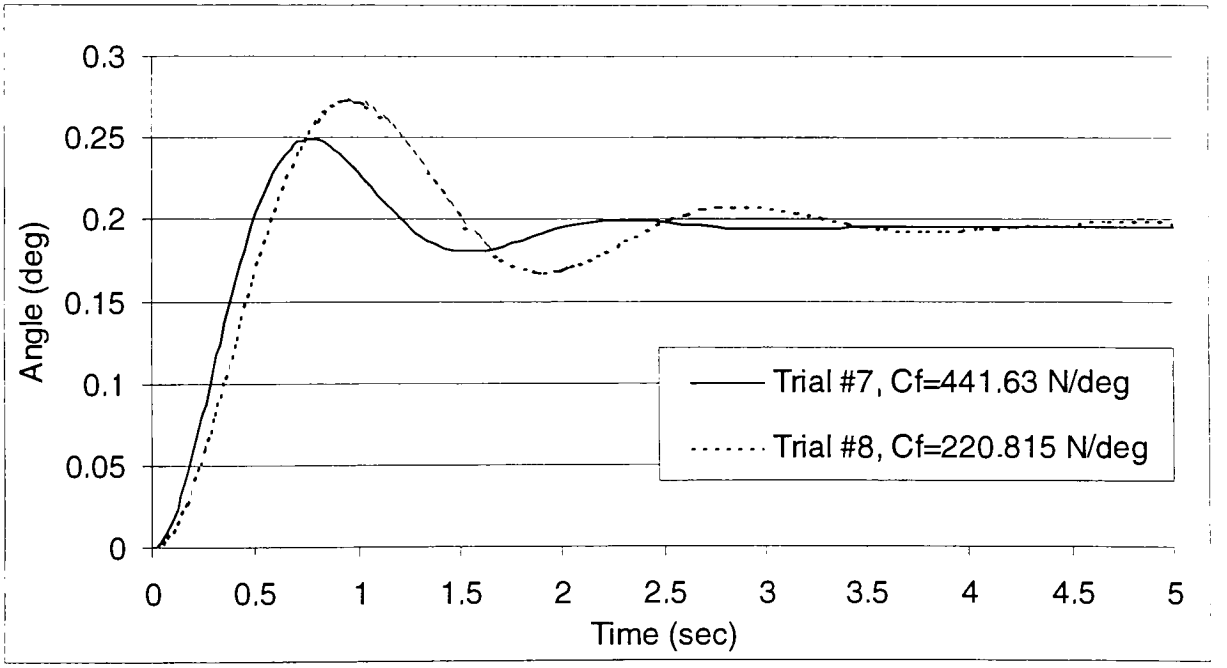

Figure 4.12: Linear Angular Rotation Response for Main Gear Position –0.5 m & Aft CG Limit, Main Gear & Vertical Tail Only

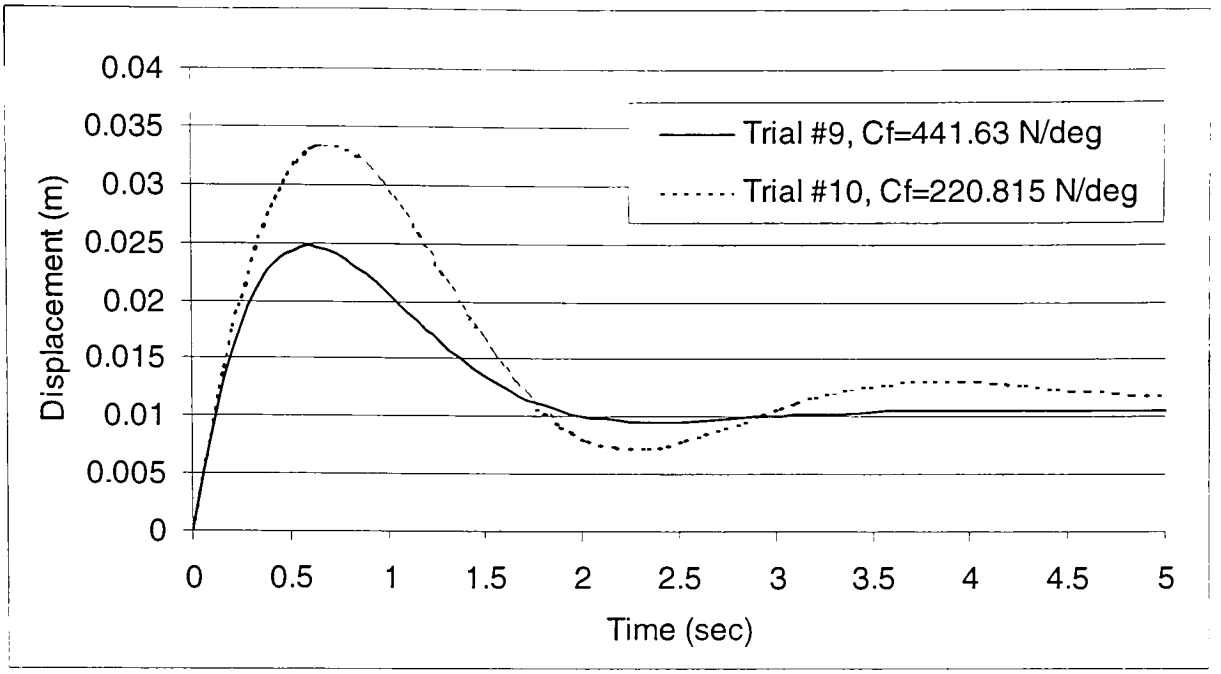

Figure 4.13: Linear Lateral Displacement Response for Main Gear Position at CG & Forward CG Limit, Main Gear & Vertical Tail Only

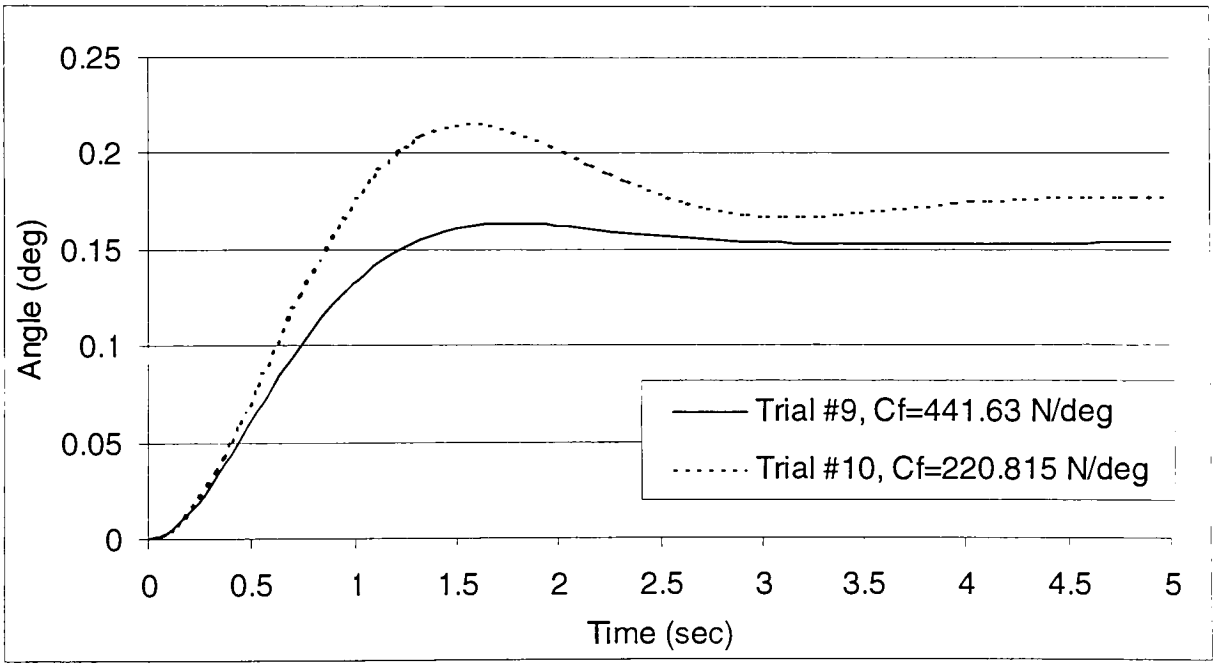

Figure 4.14: Linear Angular Rotation Response for Main Gear Position at CG & Forward CG Limit, Main Gear & Vertical Tail Only

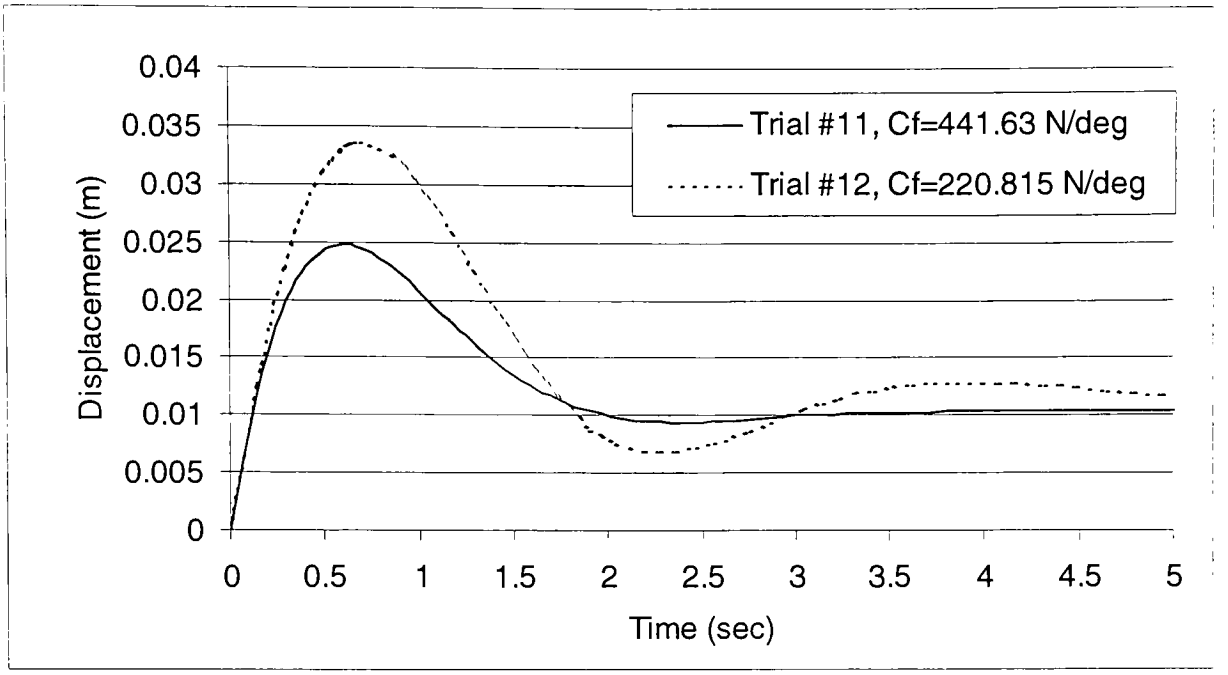

Figure 4.15: Linear Lateral Displacement Response for Main Gear Position at CG & Aft CG Limit, Main Gear & Vertical Tail Only

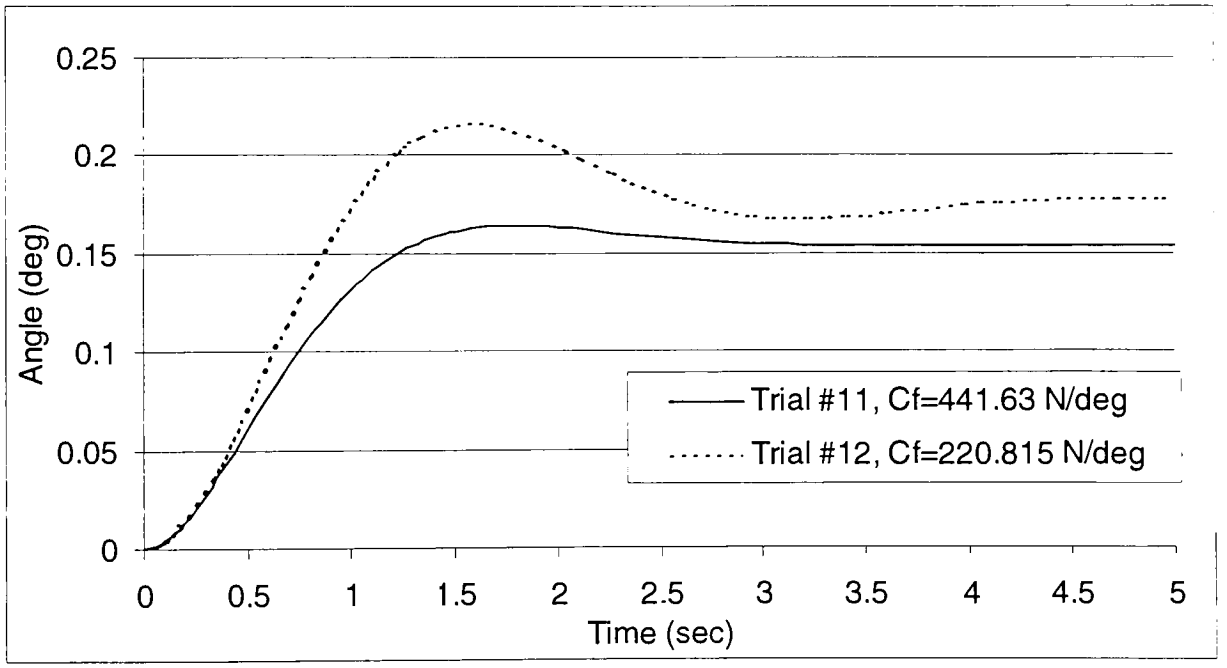

Figure 4.16: Linear Angular Rotation Response for Main Gear Position at CG & Aft CG Limit, Main Gear & Vertical Tail Only

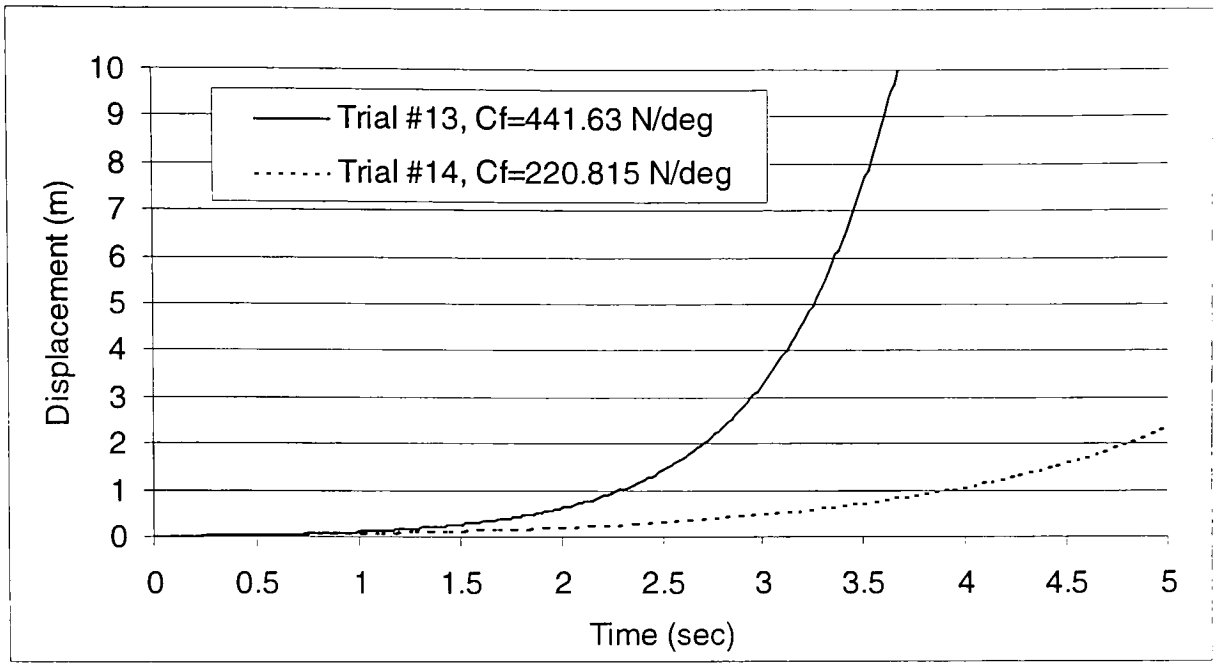

Figure 4.17: Linear Lateral Displacement Response for Main Gear Position 0.5 m in Front of CG & Forward CG Limit, Main Gear & Vertical Tail Only

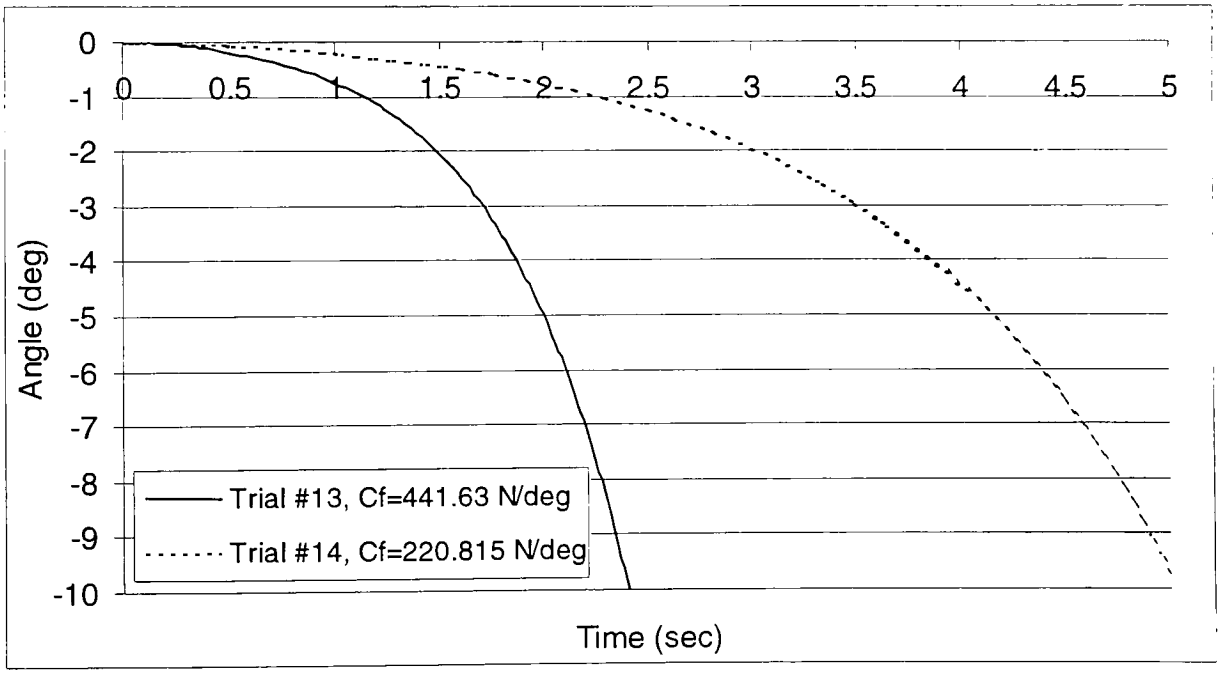

Figure 4.18: Linear Angular Rotation Response for Main Gear Position 0.5 m in Front of CG &Forward CG Limit, Main Gear & Vertical Tail Only

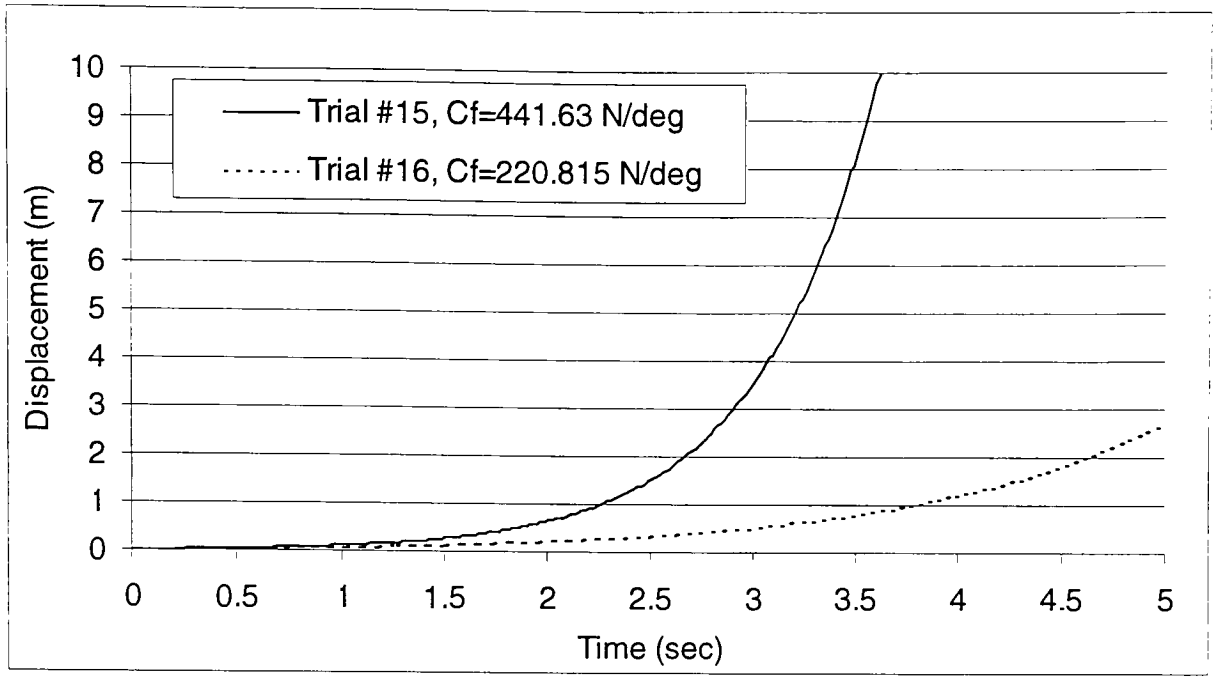

Figure 4.19: Linear Lateral Displacement Response for Main Gear Position 0.5 m in Front of CG &Aft CG Limit, Main Gear & Vertical Tail Only

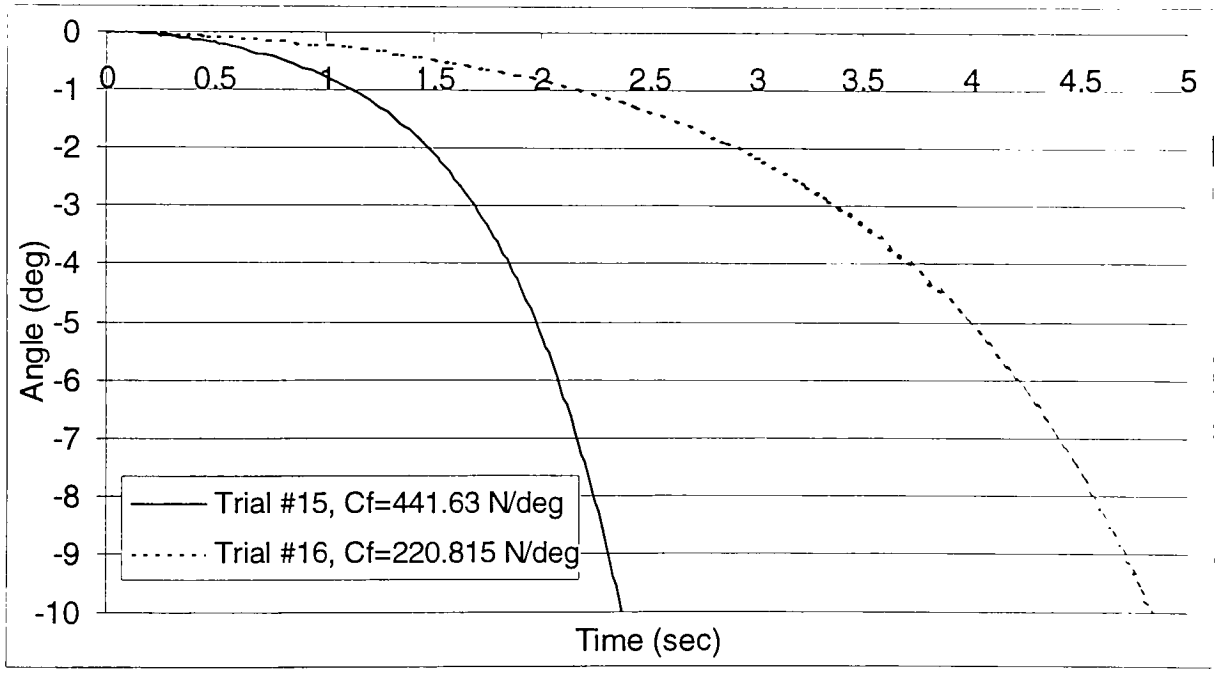

Figure 4.20: Linear Angular Rotation Response for Main Gear Position 0.5 m in Front of CG &Aft CG Limit, Main Gear & Vertical Tail Only

As with the main gear simulation, it is helpful to examine the frequency and damping of this system which includes the vertical tail. Figures 4.21 and 4.22 show how the frequency and damping ratio compare for different CG locations and main gear cornering stiffnesses as a function of the main gear location. Notice that there is no data for a positive main gear location because all of those simulations were unstable. Figure 4.21 shows that the frequency of the system decreases as the main gear is moved closer to the CG, just as in the main gear simulation. There is relatively no difference in frequency when the CG is at its forward limit as compared to its aft limit. The interesting feature of this plot is that the frequencies are lower when the cornering stiffness is decreased. However, this is only true up to a main gear location of approximately –0.06 meters. From this point on, as the main gear gets closer to the CG, the frequency is lower for the higher cornering stiffness value.

The damping ratio is shown in Figure 4.22. As the main gear is moved closer to the CG, the damping ratio increases meaning the aircraft will become more stable. Again, there is very little difference in the damping ratio when the CG is moved from the forward limit to the aft limit. The damping ratio does, however, decrease when the cornering stiffness is decreased. Thus, the aircraft is more stable on the ground than when taking off or landing.

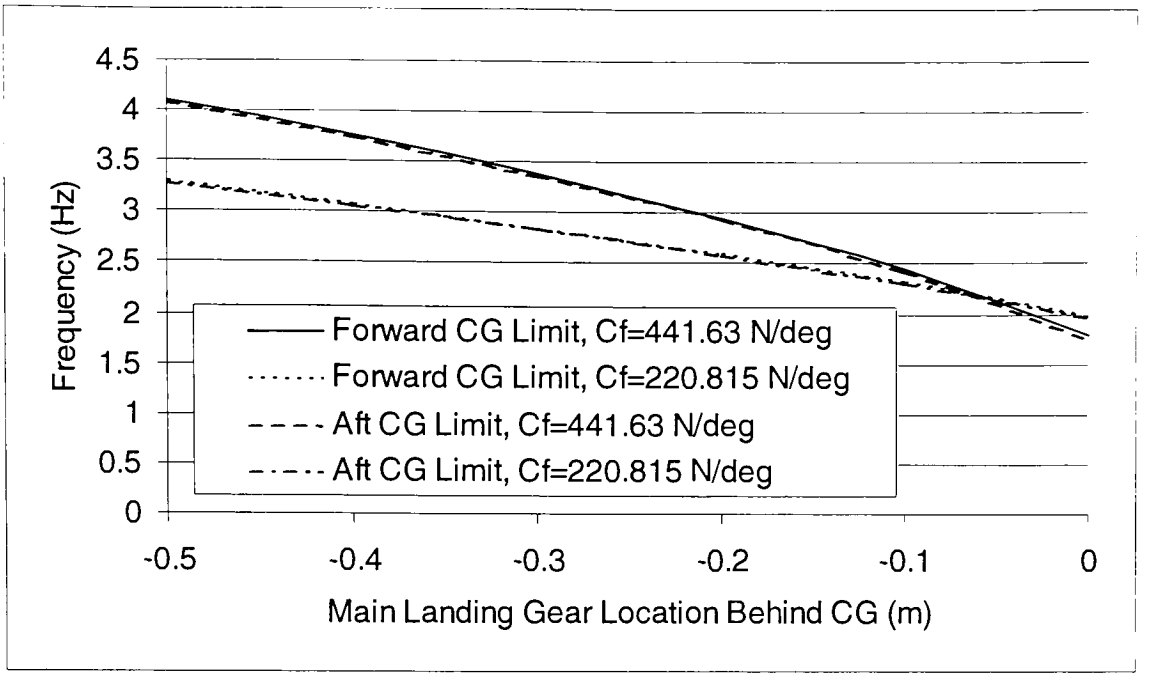

Figure 4.21: Frequency versus Main Gear Location, Main Gear & Vertical Tail Only

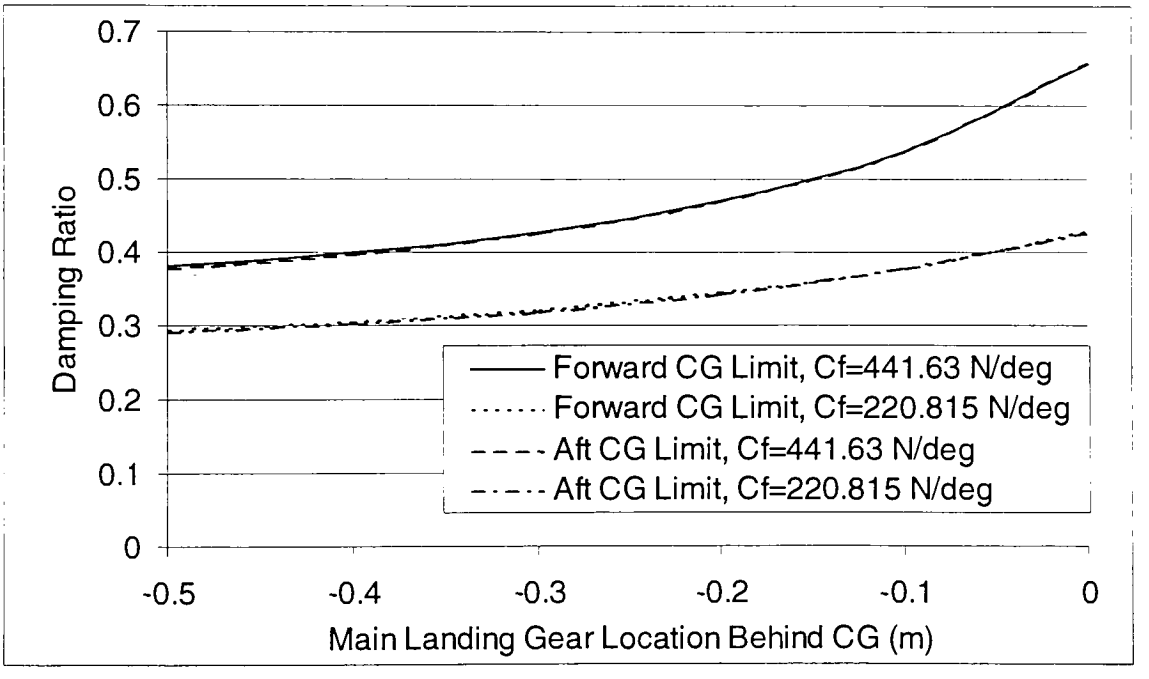

Figure 4.22: Damping Ratio versus Main Gear Location, Main Gear & Vertical Tail Only

4.5.8 Simulation of the Main Landing Gear, Vertical Tail, & Tail Wheel

The final component to be added on to the model to complete it fully is the tail wheel. The differential equations for the complete model were developed in Section 4.5.5 and are repeated here for convenience.

$$\begin{aligned} -C_f\left(\frac{v+ar}{u}\right) + F_{y\_disturbance} - \left(\frac{1}{2}\rho u^2 A_p C_{L\gamma} + C_{f-tail}\right)\left(\frac{v-br}{u}\right) &= m(\dot{v}+ur) \\ -a*C_f\left(\frac{v+ar}{u}\right) - b*F_{y\_disturbance} + b*\left(\frac{1}{2}\rho u^2 A_p C_{L\gamma} + C_{f-tail}\right)\left(\frac{v-br}{u}\right) &= I_{zz}\dot{r} \end{aligned} \tag{4.31}$$

Simulation for this model is performed in the same manner as the previous simulations. The state derivatives are found by solving Eq. (4.31) for $\dot{v}$ and $\dot{r}$ and resubstituting Eqs. (4.24), (4.26), (4.28), (4.29), and (4.30):

$$\begin{aligned} \dot{v} &= \frac{-F_{y\_front-tire} + F_{y\_disturbance} - F_{y\_tail} - F_{y\_tail-wheel}}{m} - ur \\ \dot{r} &= \frac{-a*F_{y\_front-tire} - b*F_{y\_disturbance} + b*(F_{y\_tail} + F_{y\_tail-wheel})}{I_{zz}} \end{aligned} \tag{4.36}$$

In performing this simulation, the location of the CG and the main landing gear were set at their default locations of 15.2 inches and 0.6401 meters, respectively. The only variables in this section are the main gear cornering stiffness and the tail wheel cornering stiffness. The cornering stiffnesses of the main gear are the same as those used in the previous section which correspond to the aircraft at full-static load and half-static loads. Full-static is when the aircraft is completely on the runway and the full cornering stiffness of the tires is used. Half-static is when the aircraft is taking off or landing and lift is being generated to get the main gear off the runway, so the cornering stiffness is halved. In a similar manner, the tail wheel cornering stiffness is varied to simulate

conditions of 2x, 1x, and 0.5x the static load on the tail wheel. These configurations will help us to better understand how the down force on the tail wheel affects stability. The tail wheel cornering stiffness is found by using the default fraction of weight on the tail wheel in conjunction with Figure 3.8. Then the value of the cornering stiffness is found for two-times this load and half of this load. The parameters used for simulation in this section are given in Table 4.7.

Table 4.7: Main Gear & Tail Wheel Cornering Stiffness for Simulating Main Gear, Vertical Tail, & Tail Wheel

Trial #	**Main Gear Cornering Stiffness, C_f (one tire) (N/deg)**	**Tail Wheel Cornering Stiffness, C_f (N/deg)**
17	441.630	145
18	441.630	112
19	441.630	70
20	220.815	145
21	220.815	112
22	220.815	70

The numerical results of the simulations are summarized in Table 4.8 while Figures 4.23 through 4.26 show the graphical results. Figure 4.23, the lateral displacement response, shows that the cornering stiffness of the tail wheel significantly influences the stability of the aircraft when the main gear is completely on the runway. As the tail wheel stiffness decreases, the steady state values of the displacement increase. The steady state value of the rotation angle, on the other hand, is positive when the tail wheel cornering stiffness is at its highest, and then decreases and becomes negative as the tail wheel cornering stiffness is decreased. Also, the time constant, settling time and rise time all increase as the tail wheel cornering stiffness is decreased. The peak overshoot,

on the other hand, decreases. It is important to note that Trial #19 in Figure 4.23 is stable. The steady state value of the displacement is more than 10 times greater than the other trials. You can see in Table 4.8 that the time constant is extraordinarily high as compared to the other trials. Thus, in order to compare the results on the same graph, the upper limit was set at a value that showed all three results. Consequently, Trial #19 looks as though it is unstable, when in actuality, it is overdamped.

When the cornering stiffness is halved to simulate take-off or landing conditions, as in Figures 4.25 and 4.26, the aircraft is still stable for both the displacement and yaw responses regardless of the tail wheel cornering stiffness. However, as the tail wheel cornering stiffness is decreased, the steady state values for the lateral displacement increase. The angular rotation, on the other hand, sees a reduction in steady state values as the tail wheel cornering stiffness is decreased. The time constant, settling time, and rise time all show the same increasing trend as in Figures 4.23 and 4.24, just as the peak overshoot decreases as in these figures.

Table 4.8: Results of Linear Simulation of Main Gear, Vertical Tail & Tail Wheel

Trial #	Eigenvalues	Steady State Displacement (m)	Steady State Angle (deg)	Time Constant (sec)	Settling Time (sec)	Rise Time (sec)	Peak Overshoot (%)
17	$-3.24 \pm 1.98i$	0.025	0.058	0.216	0.487	0.388	3
18	-2.56, -3.26	0.036	-0.003	0.391	1.10	0.802	0
19	-4.84, -0.118	0.394	-1.97	8.49	25.2	18.7	0
20	$-2.53 \pm 3.47i$	0.018	0.148	0.133	1.01	0.192	29
21	$-2.19 \pm 2.92i$	0.021	0.141	0.153	1.19	0.223	28
22	$-1.76 \pm 1.92i$	0.030	0.115	0.229	1.68	0.350	20

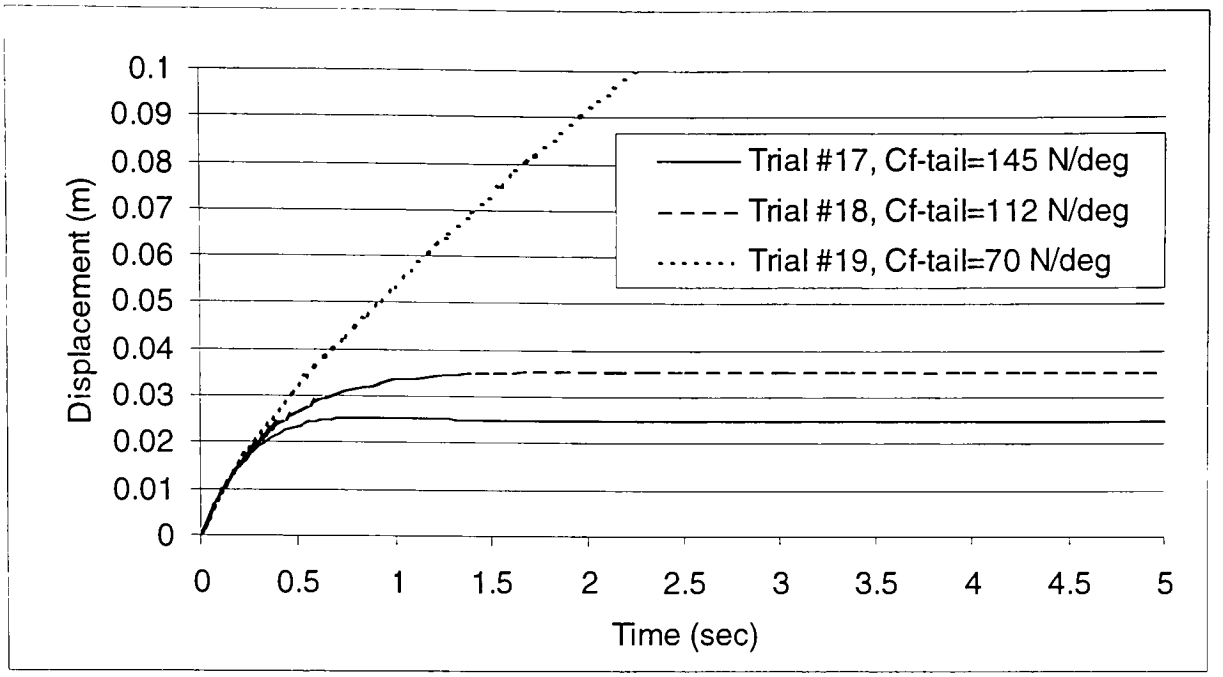

Figure 4.23: Linear Lateral Displacement Response with Main Gear at Full-Static Load, Main Gear, Vertical Tail & Tail Wheel

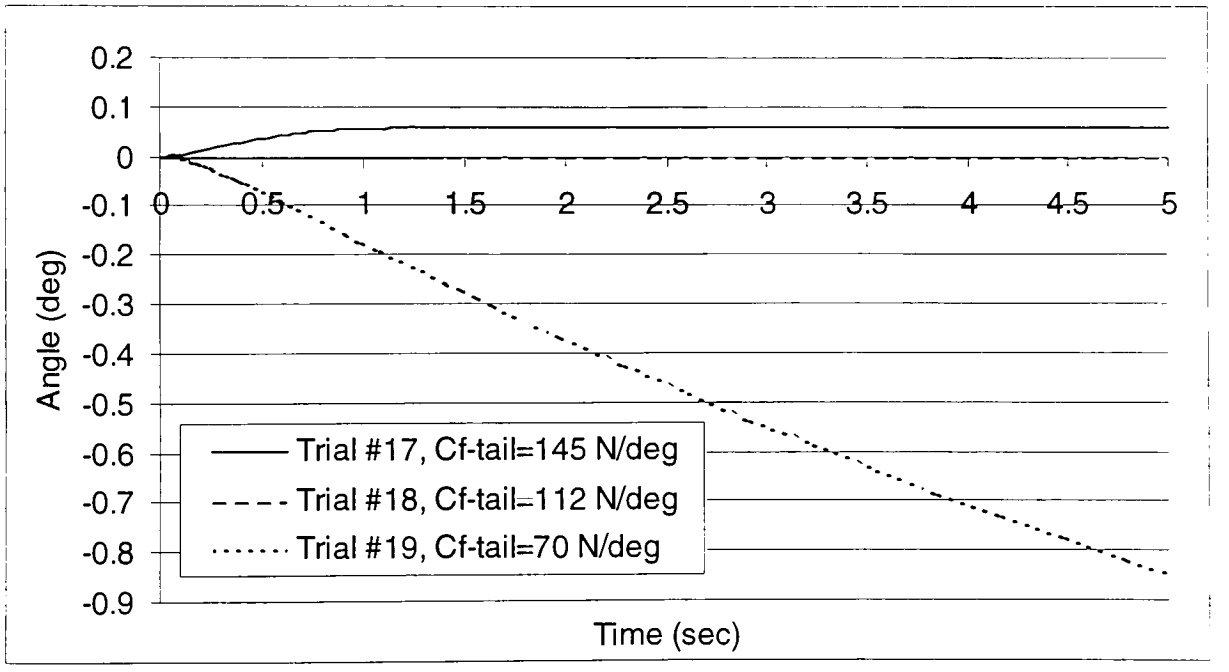

Figure 4.24: Linear Angular Rotation Response with Main Gear at Full-Static Load, Main Gear, Vertical Tail & Tail Wheel

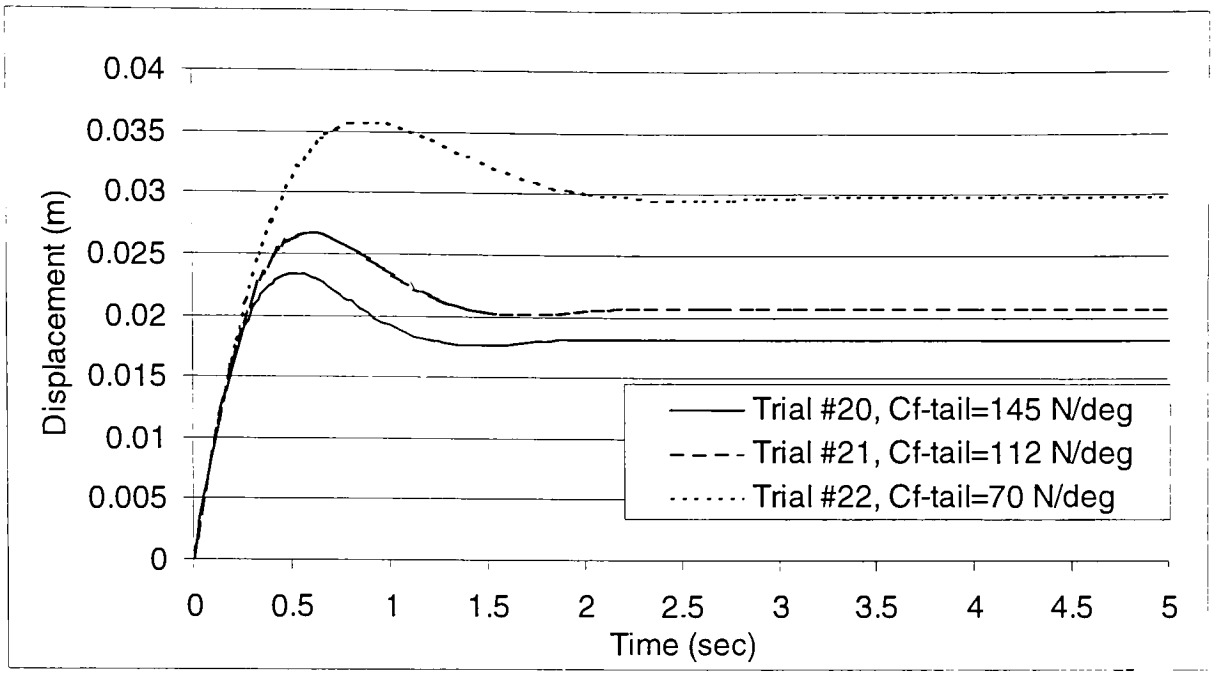

Figure 4.25: Linear Lateral Displacement Response with Main Gear at Half-Static Load, Main Gear, Vertical Tail & Tail Wheel

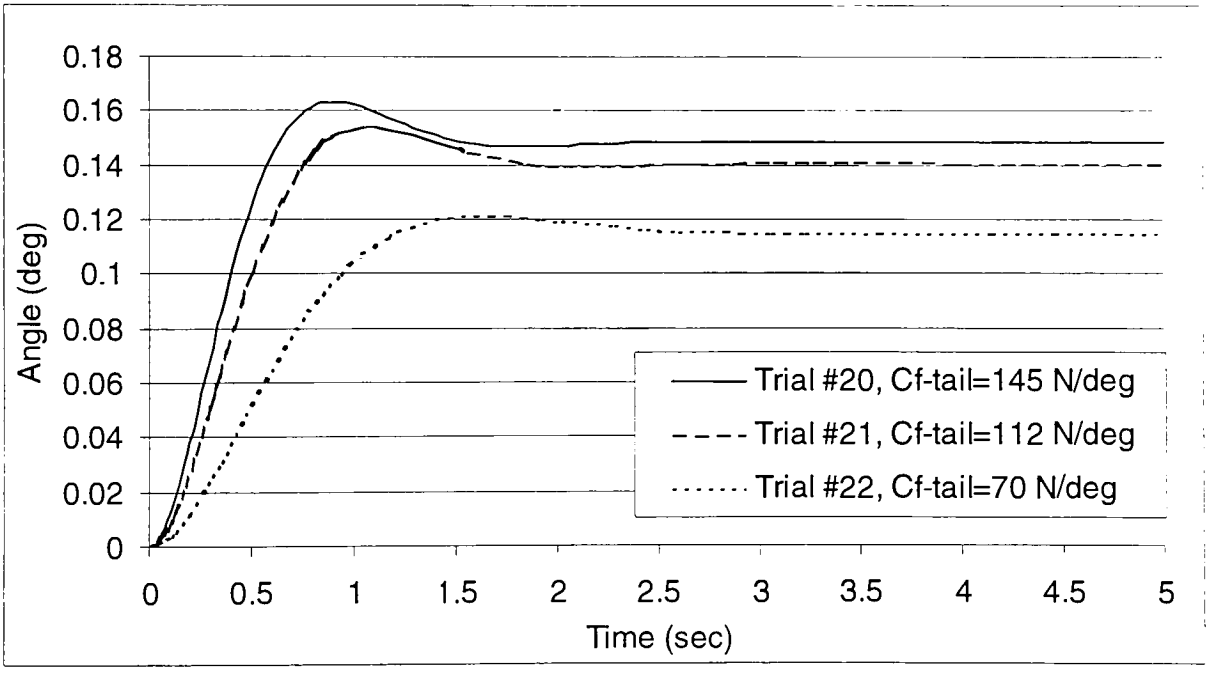

Figure 4.26: Linear Angular Rotation Response with Main Gear at Half-Static Load, Main Gear, Vertical Tail & Tail Wheel

The frequency and damping ratio were also plotted for this set of simulations, this time as a function of the tail wheel cornering stiffness. The results are shown in Figures 4.27 and 4.28. The frequency plot shows that for each main gear cornering stiffness, the frequency decreases as the tail wheel cornering stiffness decreases. However, at any tail wheel cornering stiffness, the system shows a lower frequency for the main gear at its full-static load, $C_f = 441.63$ N/deg.

The damping ratio results shown in Figure 4.28 concur with the frequency results. As the tail wheel cornering stiffness is decreased, the damping ratio increases. Also, the damping ratios are higher for the case when the main gear is at full-static load as compared to half-static.

The results of this simulation provide the designer and the pilot with the down force necessary on the tail wheel in order to get the best frequency and damping ratio. However, as we have seen, there are several trade-offs to be considered when deciding the location of the main landing gear and the stiffness of the tail wheel. Although the frequency and damping ratio may improve, the steady state value, time constant, settling time, and rise time may worsen.

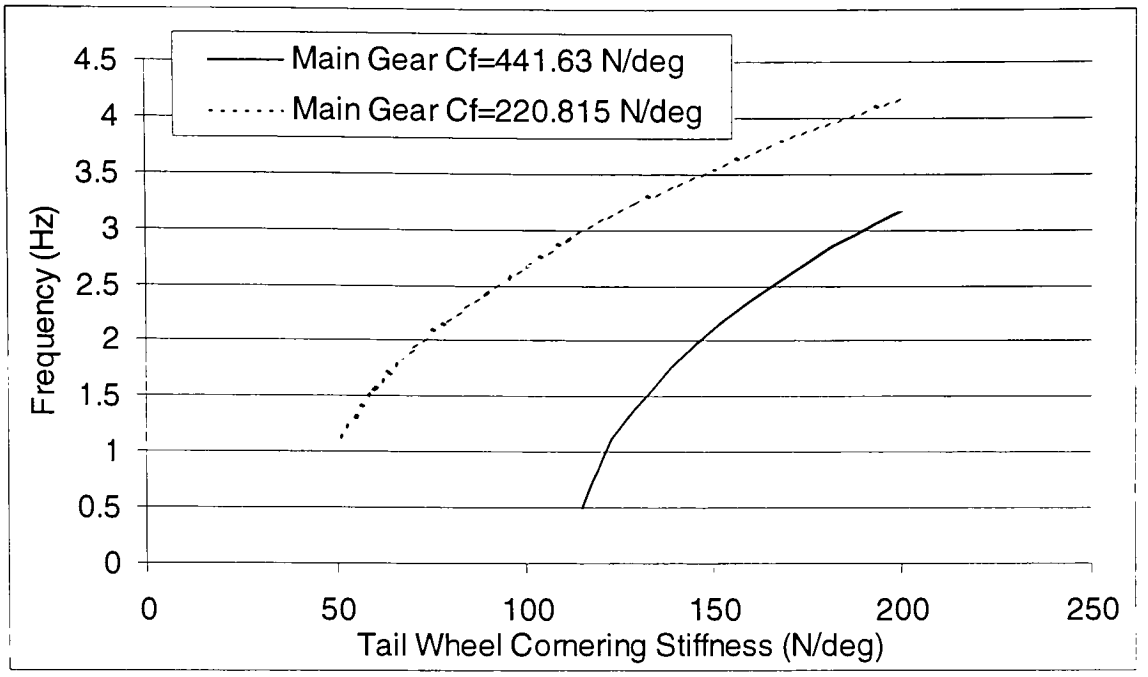

Figure 4.27: Frequency versus Tail Wheel Cornering Stiffness, Main Gear, Vertical Tail & Tail Wheel

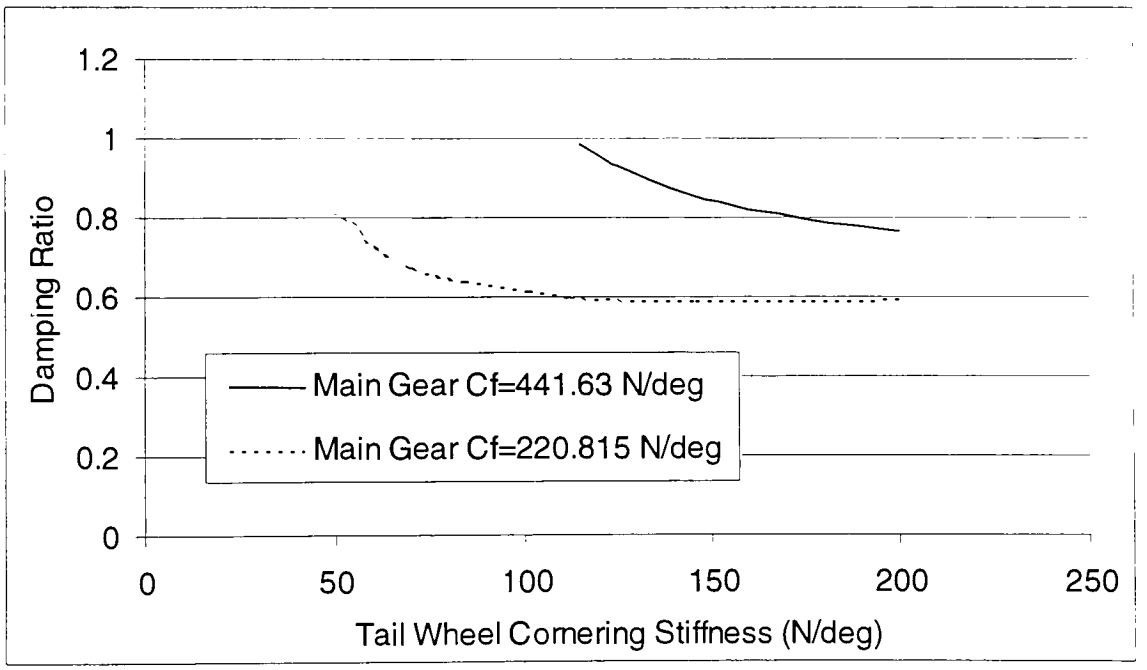

Figure 4.28: Damping Ratio versus Tail Wheel Cornering Stiffness, Main Gear, Vertical Tail & Tail Wheel

4.6 Non-Linear Model

Development of a non-linear model becomes necessary as tire slip angles increase to a point where the linear model can no longer accurately predict the tire lateral forces. Chapter 3 discusses the technique that was used to model the behavior of a tire at high slip angles. This method, called tire data non-dimensionalization developed by Hugo Radt, is discussed in detail in Section 3.4. The equations and results of Section 3.4 are put to use in simulating the two degree-of-freedom non-linear system.

4.6.1 Non-Linear Model Equations

The general equations of motion for the system have already been derived in Sections 4.3 and are repeated here for convenience.

$$\begin{aligned} -F_{y\_front-tire} + F_{y\_disturbance} - F_{y\_tail} - F_{y\_tail-wheel} &= m(\dot{v} + ur) \\ -a * F_{y\_front-tire} - b * F_{y\_disturbance} + b * (F_{y\_tail} + F_{y\_tail-wheel}) &= I_{zz}\dot{r} \end{aligned} \tag{4.9}$$

The difference between the linear and non-linear models is in the development of the slip angles. Expressions for the general tire slip angles and the tail incidence angle have already been derived in Section 4.4 and are shown here again.

$$\alpha = atan\left(\frac{v + ar}{u}\right) \tag{4.14}$$

$$\gamma = atan\left(\frac{v - br}{u}\right) \tag{4.19}$$

The tire lateral force is given by the following expressions as described in Section 3.4 and repeated here for convenience. From these equations the tire lateral force, $F_{y\_front\text{-}tire}$, can be calculated based upon the vertical load, F_z, and the tire slip angle, α.

$$C_c = B_3 + C_3 F_z \tag{3.3}$$

$$\mu_y = B_5 + C_5 F_z \tag{3.5}$$

$$\overline{\alpha} = \frac{C_c tan(\alpha)}{\mu_y} \tag{3.6}$$

$$\overline{F}_y = D_1 sin(\overline{\theta}) \tag{3.8}$$

$$\overline{\theta} = C_1 atan(B_1 \overline{\psi}) \tag{3.9}$$

$$\overline{\psi} = (1 - E_1)\overline{\alpha} + \frac{E_1 atan(B_1 \overline{\alpha})}{B_1} \tag{3.10}$$

$$F_y = \overline{F}_y \mu_y F_z \tag{3.11}$$

4.6.2 Simulation of Main Landing Gear Only

In order to simulate the model without the effects of the vertical tail and tail wheel, Eq. (4.9) should be modified as follows

$$\begin{aligned} -F_{y\_front-tire} &= m(\dot{v} + ur) \\ -a * F_{y\_front-tire} &= I_{zz}\dot{r} \end{aligned} \tag{4.37}$$

Simulation of the non-linear model uses the same tools as the linear model. The files used to perform the simulation are also listed in Appendix A and are very similar to

those used in the linear model. The MATLAB script file *DOF2NLSIM.m,* listed in Appendix A.9, implements the simulation much like the file *DOF2LSIM.m* implemented the linear simulation. The files *DOF2CONT.m*, *DOF2PARA.m*, and *DOF2DEPA.m* are again used in the non-linear simulation to input the controls and the dependent and independent parameters that are going to be used. The built-in MATLAB function *ODE23* is again used to perform integration on the differential equations of motion, which are contained in the script file *DOF2NLDE.m*. At each time step the *ODE23* function refers to the file *DOF2NLDE.m* which calculates the state derivatives $\dot{v}$ and $\dot{r}$ based upon the instantaneous values of the state variables v and r. *DOF2NLDE.m* can be found in Appendix A.10. The state derivatives are found by solving Eq. (4.37) for $\dot{v}$ and $\dot{r}$:

$$\begin{aligned} \dot{v} &= \frac{-2F_{y\_front-tire}}{m} - ur \\ \dot{r} &= \frac{-2a * F_{y\_front-tire}}{I_{zz}} \end{aligned} \tag{4.38}$$

The most significant difference between the non-linear and linear model simulations is in the calculation of the tire lateral forces. The MATLAB script file NLTIRE.m that is listed in Appendix A.3 calculates the tire lateral forces. This file uses the tire vertical load and slip angle as inputs and returns the tire lateral force. Note that with the non-linear tire model the lateral force, $F_{y\_front-tire}$, is only for one tire, while for the simplified linear model it is for two tires. Thus, here they are multiplied by the factor of two in Eq. (4.38). *DOF2NLDE.m* calls *NLTIRE.m* at each time step.

For comparison purposes, the non-linear model is simulated using the same configurations as in the linear model. For the main gear only simulation, those configurations are listed in Table 4.3 in Section 4.5.6. The results of the non-linear simulations performed in this section are listed in Table 4.9 and shown graphically in Figures 4.29 through 4.32. The linear simulation results are included in these plots for comparison. Notice that only the configurations for Trial #1 and #3 are used, which correspond to an aircraft with full-static loading. In these configurations, the aircraft is fully on the runway and has not started to take-off or begin landing. Simulation of an aircraft taking off or landing is not performed in this section. For the linear model, simulation of a take-off was done by using only half of the cornering stiffness. Non-linear modeling of a take-off becomes much more complex because the cornering stiffness is no longer a constant as in the linear model. Thus, to ease the analysis, simulation is done as if the aircraft is not generating any lift and it is still fully on the runway. As you will see, this provides enough data to draw reasonable conclusions about the use of a linear model.

Figure 4.29 shows the lateral displacement response when the main landing gear is at the CG. As you can see, the response is overdamped and the system reaches steady state. The difference in steady state values for the linear and non-linear model is approximately 2%. As expected, the angular rotation, shown in Figure 4.30, is zero due to the absence of a moment arm for the tire lateral force.

When the main landing gear is moved in front of the CG, the aircraft becomes unstable as we saw in the linear simulation. As a result, the magnitude of the

displacement and rotation both increase with time. This can be seen in Figures 4.31 and 4.32, respectively. In comparison, the linear model is more unstable than the non-linear model. The exponential rise is greater in the linear model. This is due to the linear model overestimating the tire lateral forces. Thus, the aircraft displaces faster and shows a faster yaw rate.

Table 4.9: Results of Non-Linear Simulation of Main Gear Only

Trial #	Steady State Displacement (m)	Steady State Angle (deg)	Time Constant (sec)	Settling Time (sec)	Rise Time (sec)	Peak Overshoot (%)
1	0.042	0.000	0.417	1.25	0.917	0.0000
3	N/A	N/A	N/A	N/A	N/A	N/A

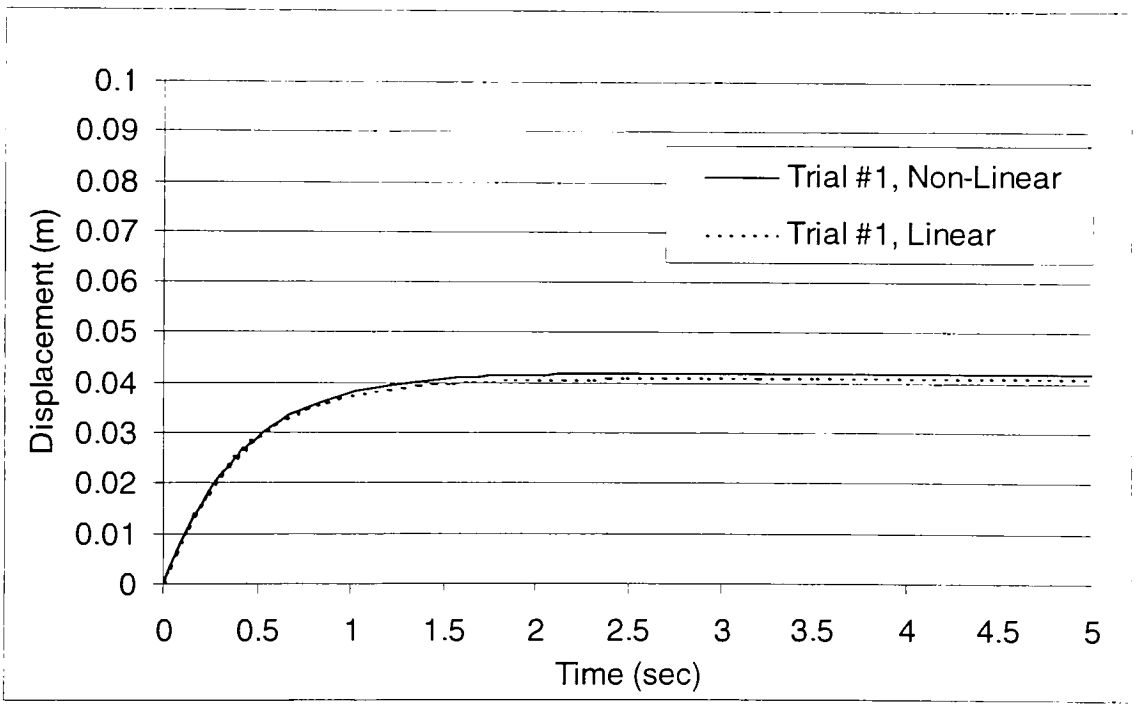

Figure 4.29: Non-Linear Lateral Displacement Response for Main Gear at CG, Main Gear Only

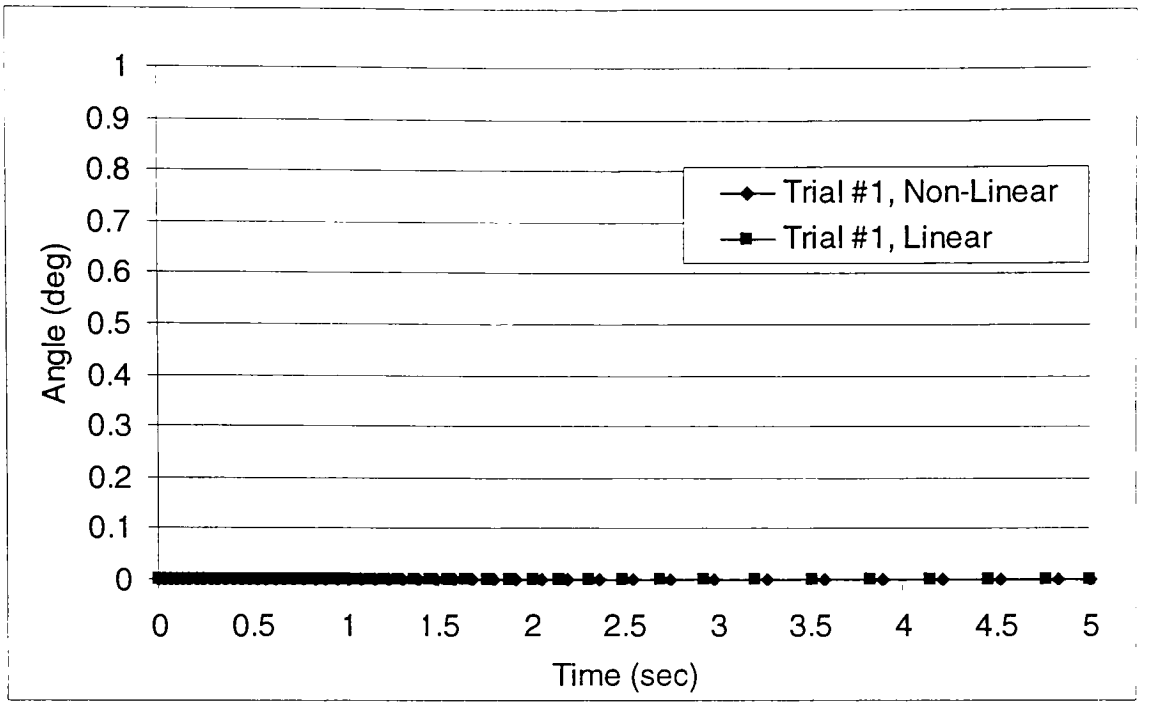

Figure 4.30: Non-Linear Angular Rotation Response for Main Gear at CG, Main Gear Only

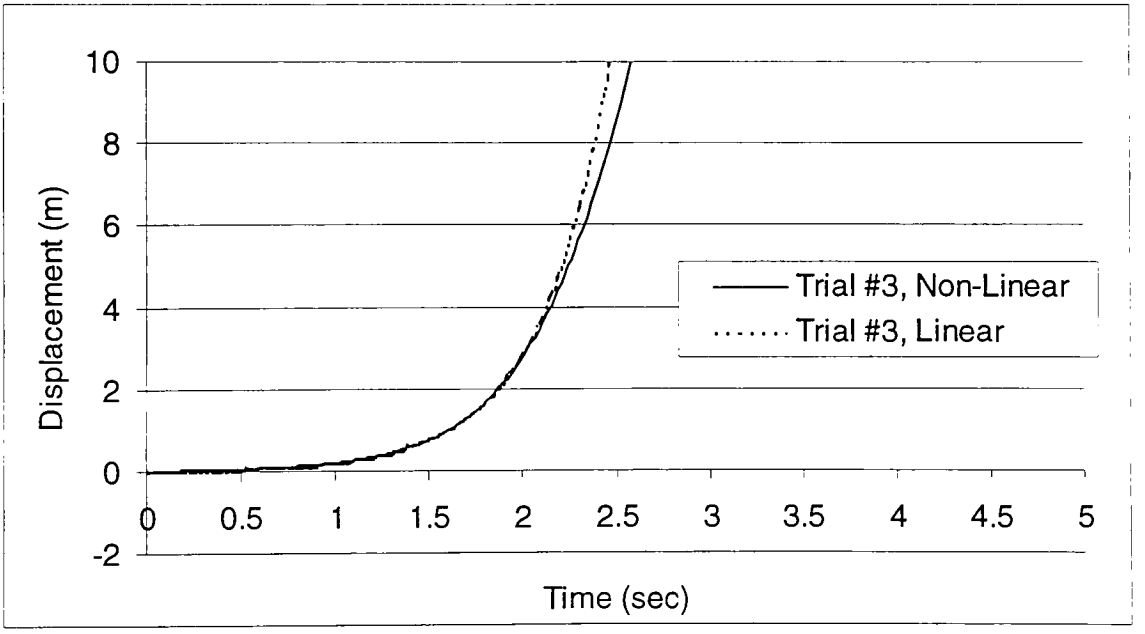

Figure 4.31: Non-Linear Lateral Displacement Response for Main Gear 0.5 m in Front of CG, Main Gear Only

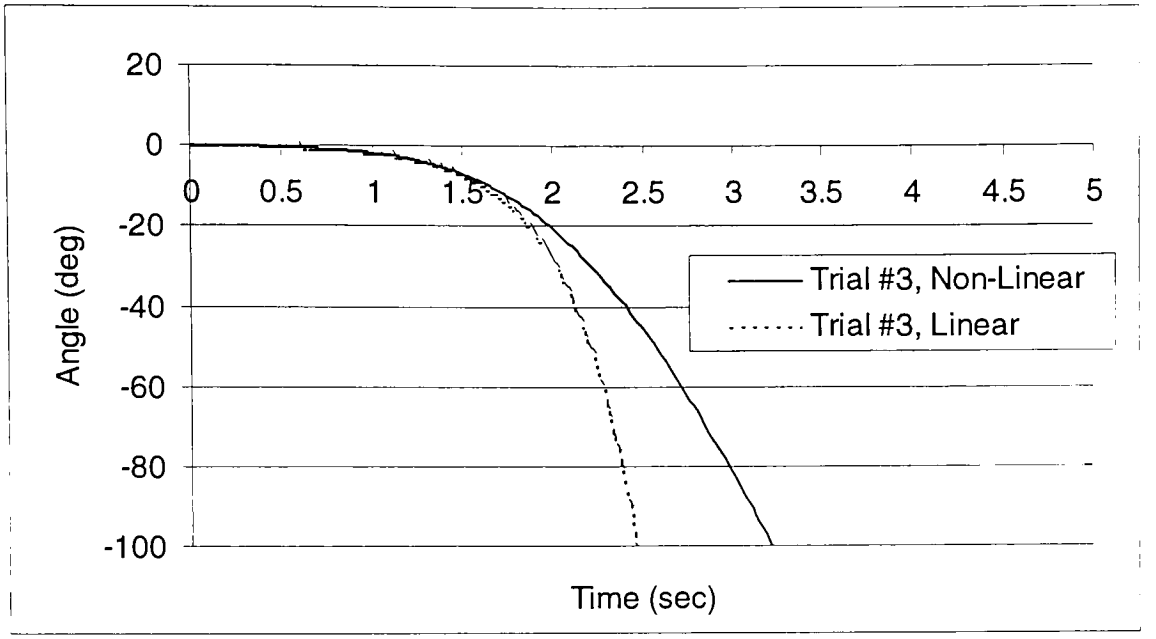

Figure 4.32: Non-Linear Angular Rotation Response for Main Gear 0.5 m in Front of CG, Main Gear Only

4.6.3 Simulation of Main Landing Gear & Vertical Tail Only

The previous section allowed us to develop a better understanding of the effects of the location of the main landing gear. Those results can be put to use in this section where the vertical tail component is added into the model. The equations of motion should then be modified to be:

$$\begin{aligned} -F_{y\_front-tire} - F_{y\_tail} &= m(\dot{v} + ur) \\ -a * F_{y\_front-tire} + b * F_{y\_tail} &= I_{zz}\dot{r} \end{aligned} \tag{4.39}$$

Simulation for this model is performed in the same manner as the previous simulations. The state derivatives are found by solving Eq. (4.39) for $\dot{v}$ and $\dot{r}$:

$$\dot{v} = \frac{-F_{y\_front-tire} - F_{y\_tail}}{m} - ur$$
$$\dot{r} = \frac{-a * F_{y\_front-tire} + b * F_{y\_tail}}{I_{zz}} \tag{4.40}$$

The configurations used to perform the analysis with the addition of the vertical tail are the same as those used in the linear model. They can be found in Table 4.5 in Section 4.5.7.

The results of the non-linear simulation are shown numerically in Table 4.10 and graphically in Figures 4.33 through 4.38. The linear simulation results are also plotted for comparison. When the aircraft is stable, as in Figures 4.33 through 4.36, the linear model accurately predicts the behavior. In fact, the difference in steady state values is less than 1%. When the system is unstable, as in Figures 4.37 and 4.38, the linear results predict a faster response for the aircraft in both displacement and rotation.

Table 4.10: Results of Non-Linear Simulation of Main Gear & Vertical Tail Only

Trial #	Steady State Displacement (m)	Steady State Angle (deg)	Time Constant (sec)	Settling Time (sec)	Rise Time (sec)	Peak Overshoot (%)
5	0.004	0.195	0.029	2.87	0.038	277
7	0.004	0.195	0.028	2.27	0.037	286
9	0.011	0.154	0.074	2.96	0.099	135
11	0.010	0.155	0.072	2.95	0.094	140
13	N/A	N/A	N/A	N/A	N/A	N/A
15	N/A	N/A	N/A	N/A	N/A	N/A

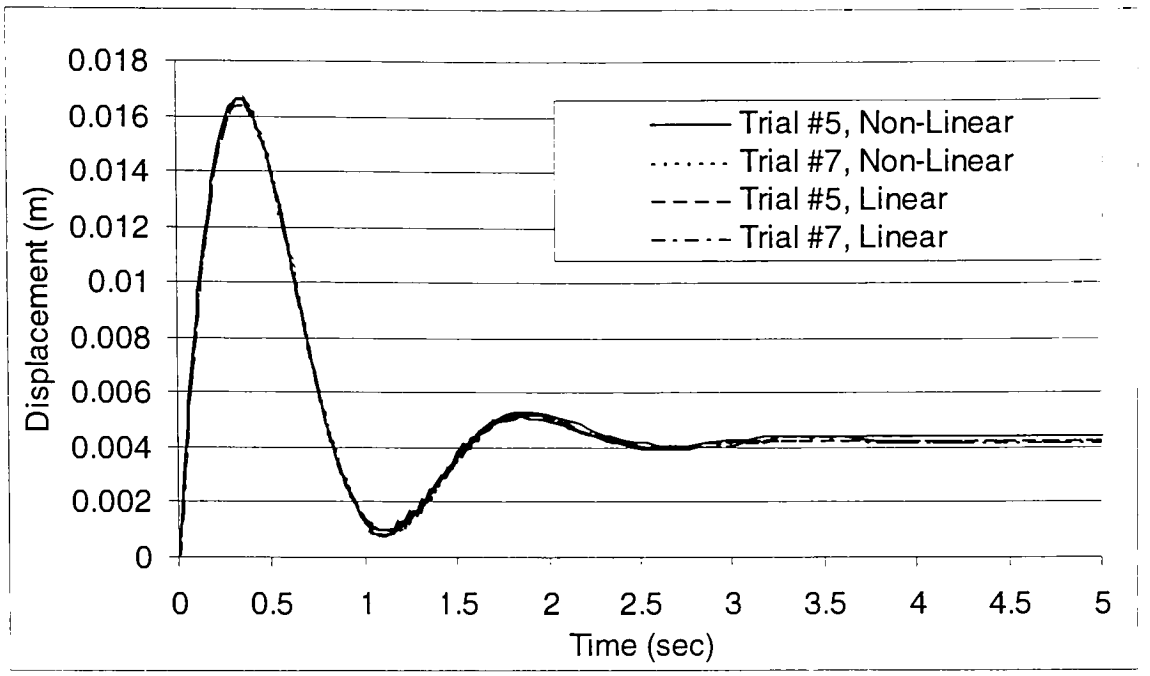

Figure 4.33: Non-Linear Lateral Displacement Response for Main Gear Position –0.5 m, Main Gear & Vertical Tail Only

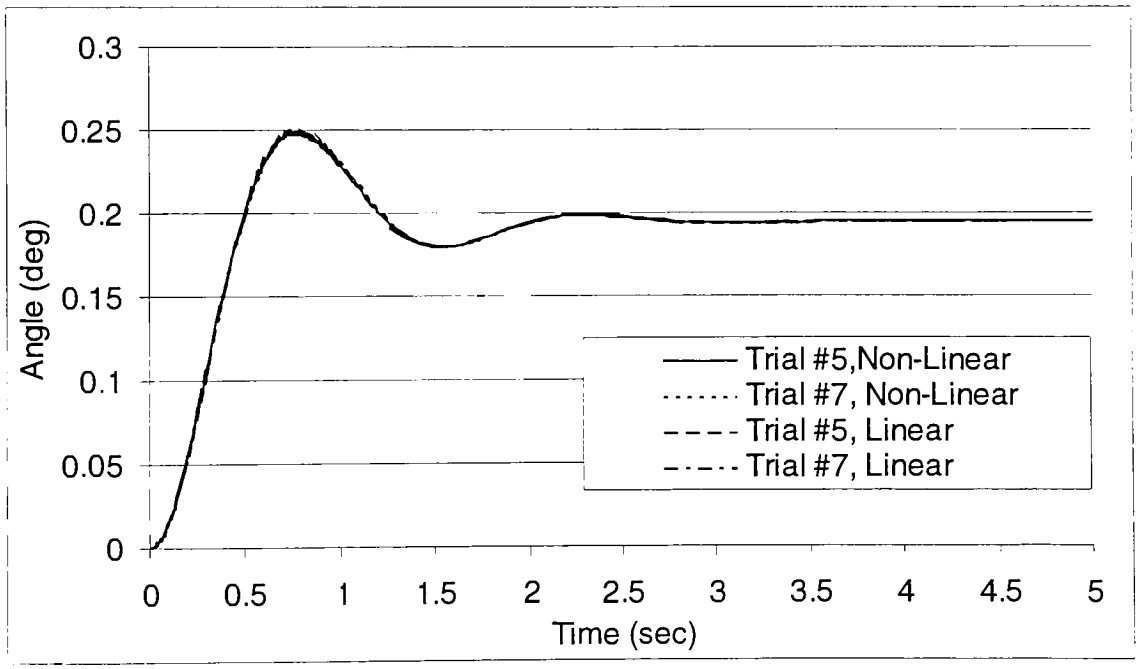

Figure 4.34: Non-Linear Angular Rotation Response for Main Gear Position –0.5 m, Main Gear & Vertical Tail Only

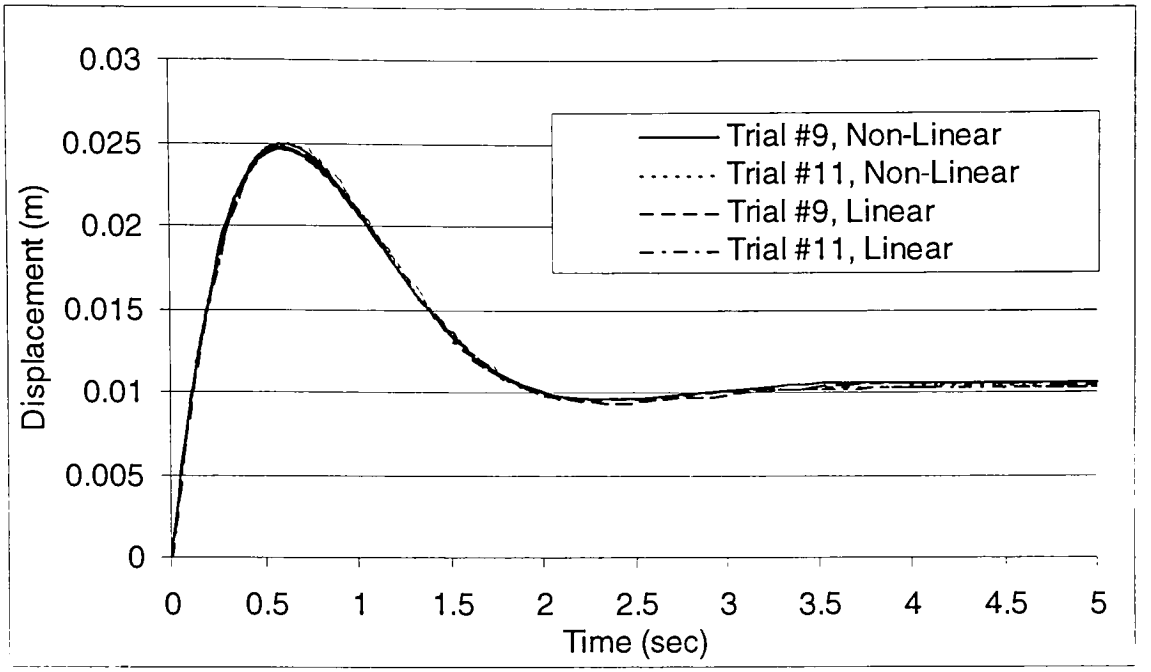

Figure 4.35: Non-Linear Lateral Displacement Response for Main Gear Position 0 m, Main Gear & Vertical Tail Only

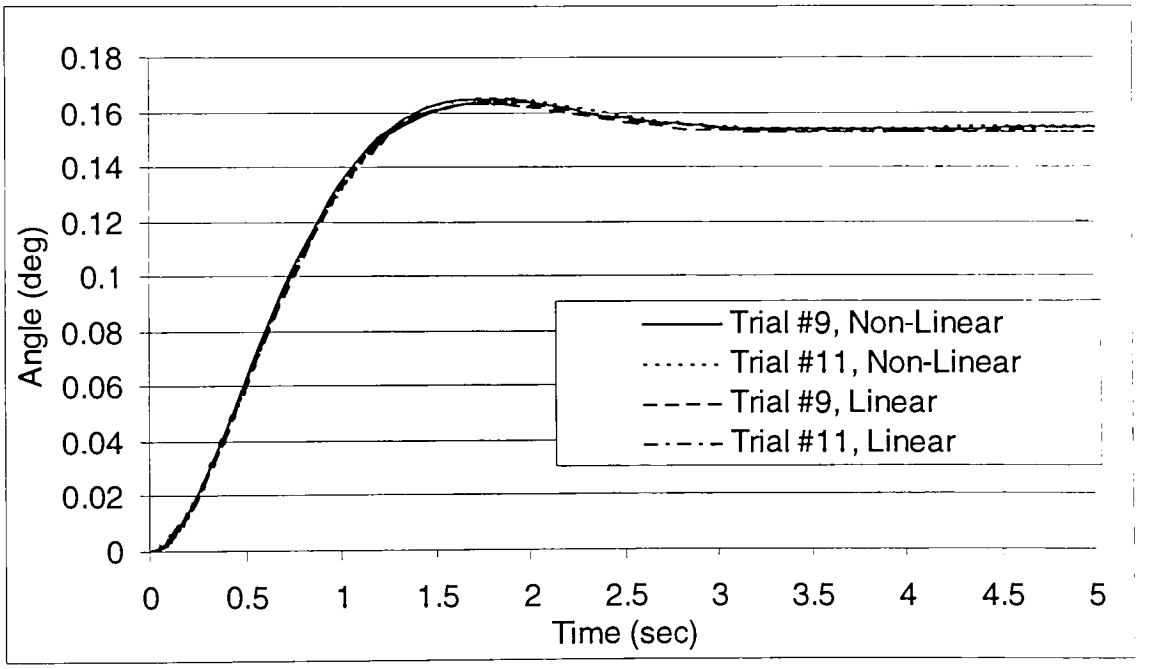

Figure 4.36: Non-Linear Angular Rotation Response for Main Gear Position 0 m, Main Gear & Vertical Tail Only

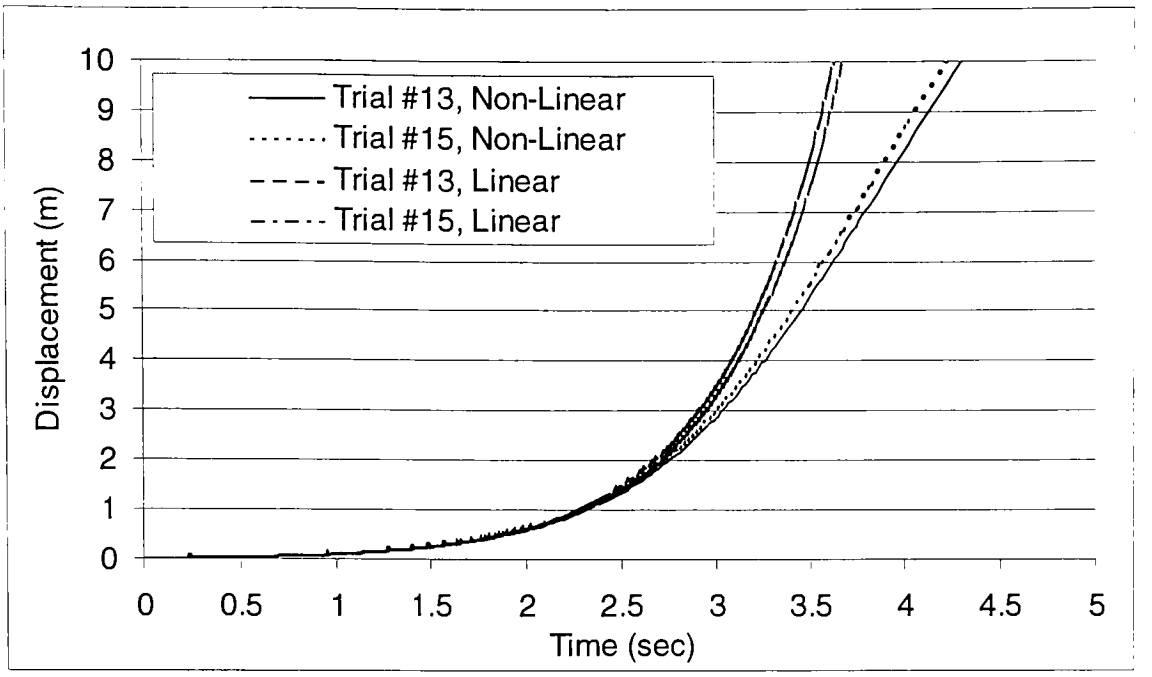

Figure 4.37: Non-Linear Lateral Displacement Response for Main Gear Position 0.5 m, Main Gear & Vertical Tail Only

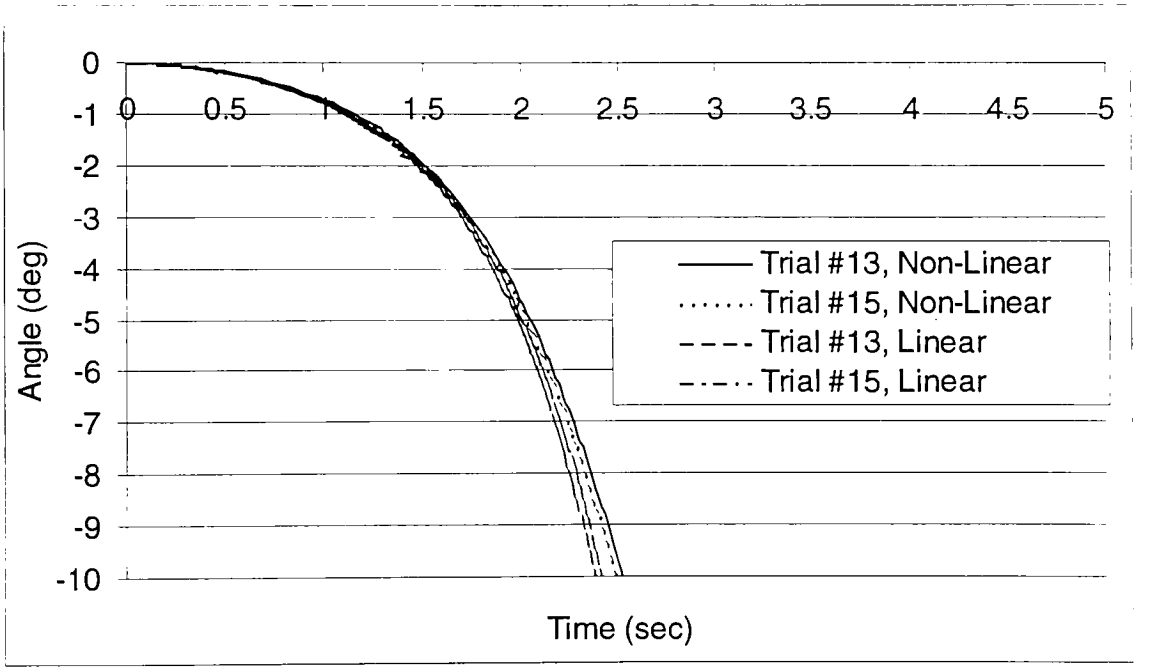

Figure 4.38: Non-Linear Angular Rotation Response for Main Gear Position 0.5 m, Main Gear & Vertical Tail Only

4.6.4 Simulation of Main Landing Gear, Vertical Tail, & Tail Wheel

With the effects of the main landing gear and vertical tail better understood, the tail wheel component can now be added in to complete the non-linear model. The equations of motion for the complete model have already been developed and are repeated here for convenience:

$$\begin{aligned} -F_{y\_front-tire} + F_{y\_disturbance} - F_{y\_tail} - F_{y\_tail-wheel} &= m(\dot{v} + ur) \\ -a * F_{y\_front-tire} - b * F_{y\_disturbance} + b * (F_{y\_tail} + F_{y\_tail-wheel}) &= I_{zz}\dot{r} \end{aligned} \tag{4.9}$$

Simulation for this model is performed in the same manner as the previous simulations. The state derivatives are found by solving Eq. (4.9) for $\dot{v}$ and $\dot{r}$:

$$\begin{aligned} \dot{v} &= \frac{-F_{y\_front-tire} + F_{y\_disturbance} - F_{y\_tail} - F_{y\_tail-wheel}}{m} - ur \\ \dot{r} &= \frac{-a * F_{y\_front-tire} - b * F_{y\_disturbance} + b * (F_{y\_tail} + F_{y\_tail-wheel})}{I_{zz}} \end{aligned} \tag{4.41}$$

For comparison purposes, the same configurations were used for the complete non-linear model as those that were used for the complete linear model. Those configurations are listed in Table 4.7 in Section 4.5.8. The generalized non-linear form of all angles is used for this simulation as well as the non-linear tire model described in Chapter 3.

The results of the non-linear model are listed in Table 4.11 and shown graphically in Figures 4.39 and 4.40. In this case, the linear model was not as accurate in predicting the response as the non-linear model. For example, the difference in steady state displacement for Trial #17 is 67%. The difference in steady state angle for the same trial is over 70%. On the other hand, Trial #18 and #19 do not show drastic differences

between the linear and non-linear results. The steady state values have approximately a 10% error in these cases.

Table 4.11: Results of Non-Linear Simulation of Main Gear, Vertical Tail, & Tail Wheel

Trial #	Steady State Displacement (m)	Steady State Angle (deg)	Time Constant (sec)	Settling Time (sec)	Rise Time (sec)	Peak Overshoot (%)
17	0.0234	0.0758	0.1970	0.9421	0.3387	6
18	0.0323	0.0308	0.2991	0.7729	0.5935	N/A
19	0.2736	-1.2803	5.5305	17.2026	12.7399	N/A

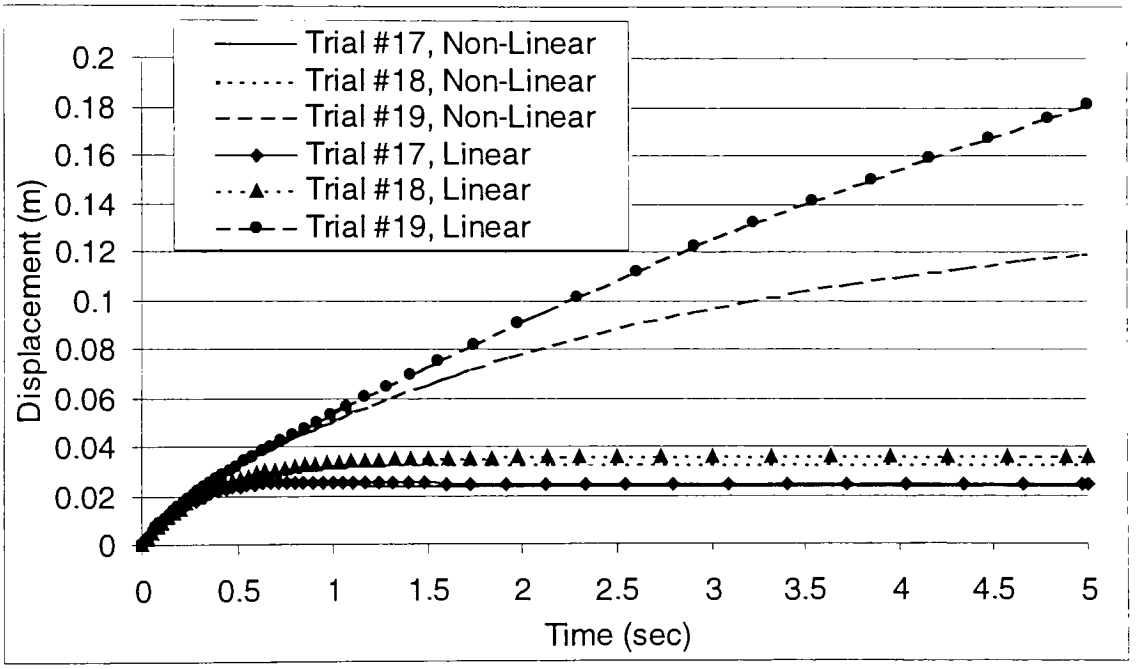

Figure 4.39: Non-Linear Lateral Displacement Response with Main Gear at Full-Static Load, Main Gear, Vertical Tail & Tail Wheel

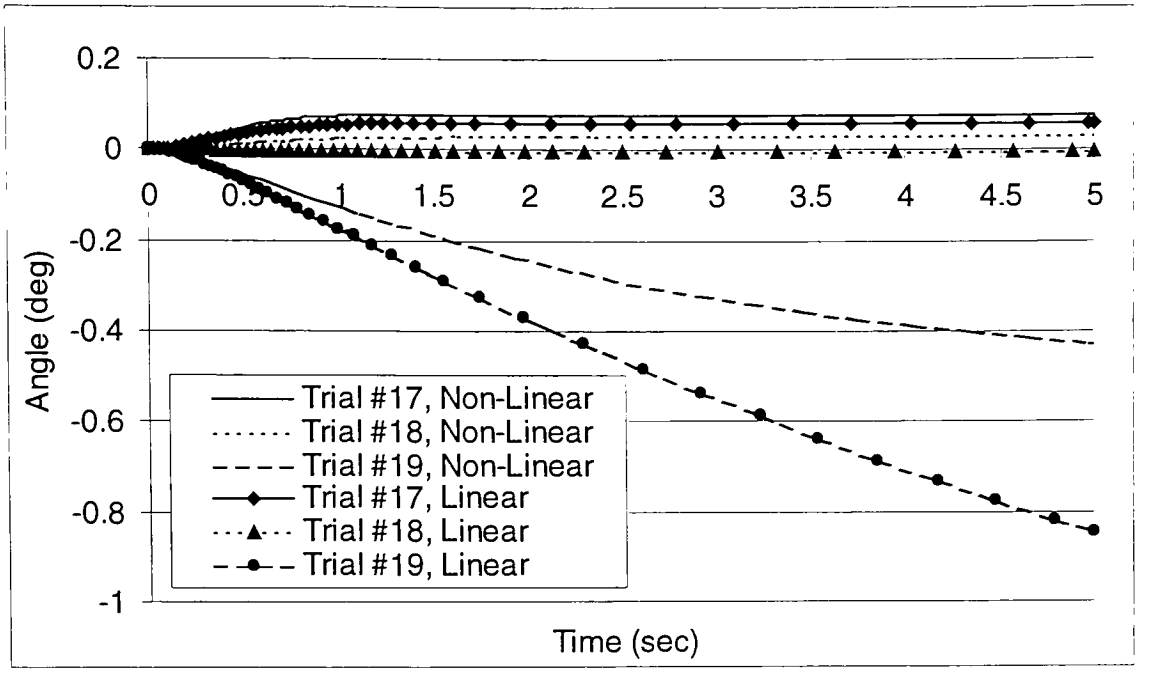

Figure 4.40: Non-Linear Angular Rotation Response with Main Gear at Full-Static Load, Main Gear, Vertical Tail & Tail Wheel

4.7 Summary

The exact location of the roots was found using digital computer solution. However, if we were only interested in knowing whether the system was stable, unstable, marginally stable, or limitedly stable we could use the Routh-Hurwitz criterion. This is an alternative method used to determine how many roots, if any, are located in the right-half s plane or on the imaginary axis. The Routh-Hurwitz criterion can also be used to determine relationships among system parameters necessary for stability. The major disadvantage of this criterion is that is does not specifically locate the roots of the characteristic equation. Consequently, we know only the absolute stability of the system and nothing about the degree of stability or the nature of the transient response.[29]

As we have seen through numerous simulations, the linear model has proved to be a very good approximation of the non-linear model. Both Chapter 3 and this chapter have described the major difference between these two models. The most significant factor was the calculation of the lateral force of the main gear. The non-linear model's purpose was to predict this lateral force at high slip angles. As it turns out, for stable configurations, the front tire slip angle was very small. Thus, the linear model was capable of predicting this force just as well. Perhaps higher speeds would have caused this angle to increase to a point where the non-linear model was necessary. However, the 100km/hr speed used is very representative of a landing aircraft.

When the system was unstable, the front tire slip angles were large enough so that use of a non-linear model was justified. Figure 4.41 is an example of the slip angle over the time period for one of the unstable configurations used in the non-linear model. As you can see, the magnitude of the angle increases dramatically over the time period. Notice that the maximum angle is only 0.21°. This may not seem like a large enough angle to warrant use of a non-linear model. However, keep in mind that the aircraft never goes through any large radius turns while on the runway as a car would on the road. Therefore, the front tires will not experience large slip angles. Thus, for an aircraft, these are high slip angles and linear model does not accurately predict the tire lateral forces. Consequently, the linear model overestimated the response.

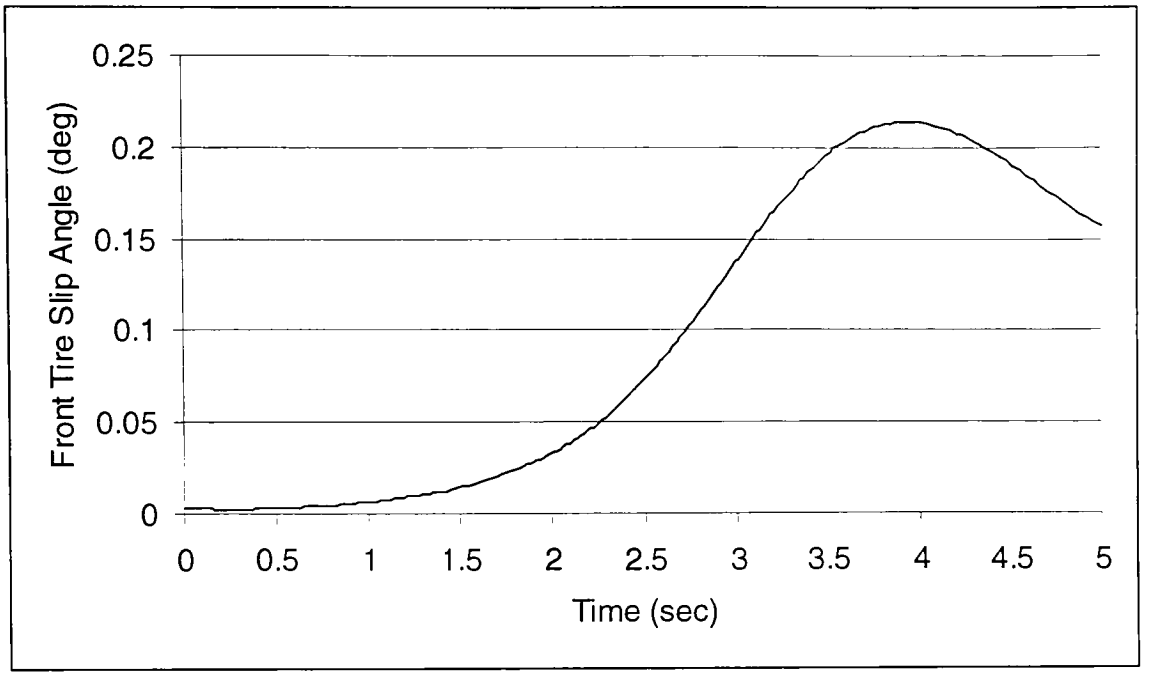

Figure 4.41: Front Tire Slip Angle Result from Non-Linear Model

Finally, it is sometimes helpful to see certain results from a different point of view. Figure 4.42 puts the lateral displacement of the aircraft into perspective. The response is still in the aircraft coordinate system. This data was taken from stable configurations for the non-linear simulations to show what happens as the airplane travels down the runway at 100 km/hr. The responses may look like as if the airplane is out of control. However, notice the units are in meters. At most, the maximum displacement of the airplane is less than 2 inches. These responses will probably not even be noticed by the pilot.

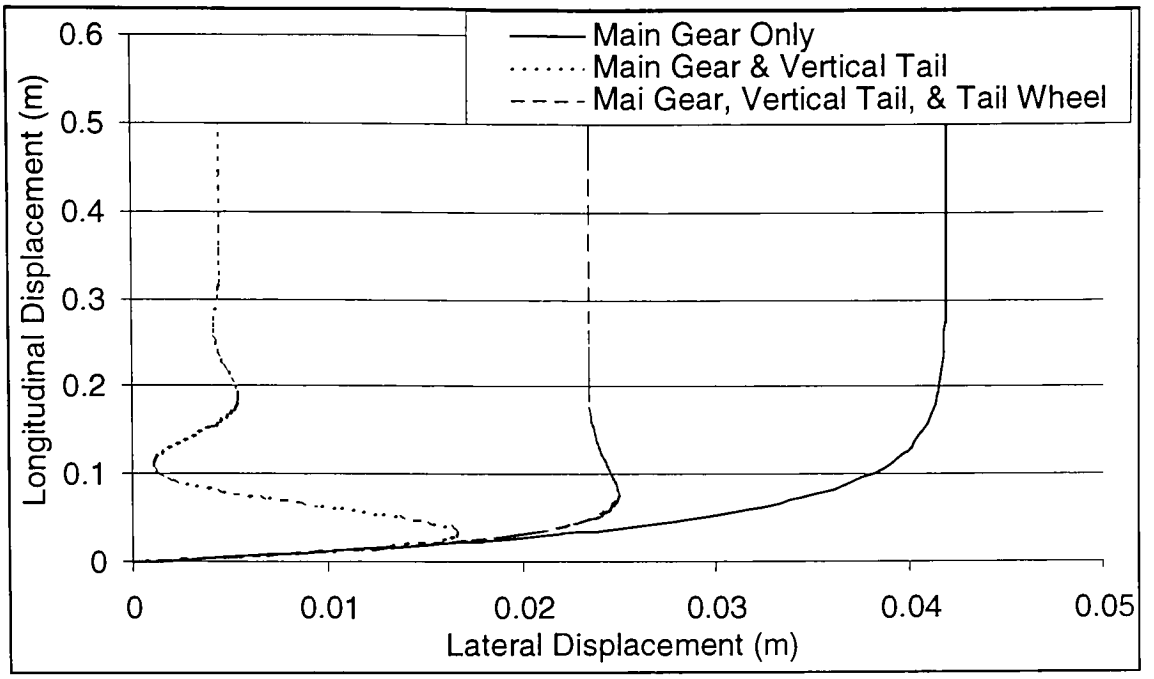

Figure 4.42: Lateral Displacement versus Forward Motion

5 Conclusion

An understanding of flight stability and control played an important role in the ultimate success of the earliest aircraft designs. In later years the design of automatic controls was widespread across the aviation industry. Today, both military and civilian aircraft rely heavily on automatic control systems to provide artificial stabilization and autopilots to aid pilots in navigating and landing their aircraft in adverse weather conditions. Unfortunately, controls have not yet been developed that will land a taildragger aircraft in the hands off condition. Most likely they will never be developed. There are very few taildraggers being flown today. The issue over their stability has driven most pilots towards tricycle gear aircraft. However, it is my understanding that taildraggers are more fun to fly. If the results of this study are put to use then we will be taking away the thrill of flying and landing a taildragger.

The goal of this thesis was to present a well developed model that would allow the basic elements of aircraft ground stability to be analyzed in hopes of improving the performance of the aircraft. Mathematical modeling of the system proved to be a useful tool for understanding the effects of the interaction between the tires, the runway, and the vertical tail. There is a great deal of literature available on both flight stability and vehicle dynamics. Together with the appropriate tire model, these topics can be brought together to produce an accurate description of aircraft ground stability.

In Chapter 3 the tire model used in this thesis was described in detail. The model for the main landing gear was developed for both the linear and non-linear scenario. The tire data nondimensionalization technique proved to be an accurate method of fitting a

curve to tire data. This allowed the tire lateral force to be predicted as a non-linear function of both the vertical load and slip angle.

The tail wheel model was developed using empirical data provided by the manufacturer of the tire. This data was used in conjunction with *MICROSOFT EXCEL* and the *TRENDLINE* function to produce a fourth order polynomial that fit the data perfectly. The tail wheel only used a linear model.

In Chapter 4 the equations of motion were developed for the two degree-of-freedom bicycle model. These equations were then broken down into components and an analysis was done by using *MATLAB* to perform simulation on the system. The differential equations of motion were integrated over a time period using the *ODE23* function. After each components results were verified, the system was developed into a linear and non-linear model. Several different configurations of landing gear and CG location were used to describe the lateral displacement and angular rotation response. The responses were simulated for an aircraft that was completely on the runway as well as an aircraft that had just started to take-off or land. These responses were compared for the linear and non-linear model. It turned out that the front tire slip angle remained small for stable configurations, so the linear model was just as accurate as the non-linear model in these cases. When the aircraft was inherently unstable, the tire slip angle was sufficiently large enough to warrant the use of a non-linear model.

In conclusion, the results of this study should be helpful to aircraft designers and pilots when deciding what configuration an aircraft should have. This thesis has also brought to light the issues surrounding aircraft ground stability and lateral dynamics.

References

1. *The New Encyclopedia Britannica.* Chicago, IL: Esposito. Volume 28, 1994, p. 802.

2. Nelson, Robert C. *Flight Stability and Automatic Control.* Boston, MA: McGraw-Hill, 1998.

3. Roskam, Jan. *Airplane Flight Dynamics and Automatic Flight Controls.* Lawrence, KA: DARcorporation, 1995.

4. Abzug, Malcom J. *Airplane Stability and Control: A History of the Technologies That Made Aviation Possible.* Cambridge: Cambridge University Press, 1997.

5. Babister, A.W. *Aircraft Dynamic Stability and Response.* Oxford: Pergaman Press, 1986.

6. Etkin, Bernard. *Dynamics of Flight: Stability and Control.* New York, NY: John Wiley & Sons, Inc., 1996.

7. Hacker, Tiberiu. *Flight Stability and Control.* New York, NY: American Elsevia Publishing Co., 1970.

8. Russel, J.B. *Performance and Stability of Aircraft.* New York, NY: John Wiley & Sons, Inc., 1996.

9. Schmidt, Louis V. *Introduction to Aircraft Flight Dynamics.* Reston, VA, American Institute of Aeronautics and Astronautics, 1998.

10. Lanchester, F. William. "Some Reflections Peculiar to the Design of an Automobile." *Proceedings of the Institution of Mechanical Engineers*, Vol. 2, 1908, P. 187-257.

11. Olley, Maurice. "Suspension and Handling." Detroit, MI: Chevrolet Engineering Center, 1937.

12. Olley, Maurice. "Notes on Suspensions." Detroit, MI: Chevrolet Engineering Center, 1961.

13. Olley, Maurice. "Suspension Notes II." Detroit, MI: Chevrolet Engineering Center, 1966.

14. Milliken, William F. and Doug L. Milliken. *Race Car Vehicle Dynamics.* Warrendale, PA: SAE, 1995.

15. Society of Automotive Engineers. *Car Suspension Systems and Vehicle Dynamics.* Warrendale, PA: SAE, 1991.

16. Wong, Jo Yung. *Theory of Ground Vehicles.* New York, NY: John Wiley & Sons, Inc., 1993.

17. Ellis, John R. *Vehicle Dynamics.* London: Business Books, 1969.

18. Gillespie, Thomas D. *Fundamentals of Vehicle Dynamics.* Warrendale, PA: SAE, 1992.

19. Kiefer, Joseph R. *Modeling of Road Vehicle Lateral Dynamics, Thesis.* Rochester, NY: Rochester Institute of Technology, 1996.

20. Mola, Simone. *Fundamentals of Vehicle Dynamics.* Detroit, MI: General Motors Institute, 1969.

21. Nordeen, Donald L. *Analysis of Tire Lateral Force and Interpretation of Experimental Tire Data.* New York, NY: SAE, 1967.

22. Society of Automotive Engineers. "Vehicle Dynamics Terminology." SAE J670e, 1976.

23. Radt, Hugo S. and D.A. Glemming. "Normalization of Tire Force and Moment Data." *Tire Science and Technology*, Vol. 21, No. 2, Apr.-June 1993.

24. Radt, Hugo S. "An Efficient Method for Treating Race Tire Force-Moment Data." SAE Paper No. 942536, Dec. 1994.

25. Bakker, Egbert, Lars Nyborg, and Hans B. Pacejka. "Tyre Modelling for Use in Vehicle Dynamics Studies." SAE Paper No. 870421, 1987.

26. Meriam, J.L. and L.G. Kraige. *Engineering Mechanics: Dynamics.* New York, NY: John Wiley & Sons, Inc., 1992.

27. Meirovitch, Leonard. *Analytical Methods in Vibrations.* New York, NY: Macmillan Publishing Co., Inc., 1967.

28. MATLAB *Reference Guide.* The MathWorks, Inc., 1994.

29. Hale, Francis J. *Introduction to Control System Analysis and Design.* Englewood Cliffs, NJ: Prentice-Hall, Inc., 1973.

Appendix A MATLAB Script Files

A.1 MAGICFIT.m

```
% MagicFit    Curve Fitting of Tire Data to Magic Formula
%
%       Finds parameters for Magic Formula curve fit of tire lateral force,
%       longitudinal force, or aligning moment versus slip angle data read from file
%       TireSlip.dat
%
% Created 12/17/97
% Howard Brott

% Initialization
clear all;
clc;

% Load data from file
load TireSlip.dat
t = TireSlip(:,1);
y = TireSlip(:,2);

% Find curve fit parameters
x0 = [0.7407 1.35 1.00 -0.51];
x = leastsq('MagicError', x0, [], [], t, y)

% Construct fit function
t1 = linspace(0, max(t), 10);
psi = (1-x(4))*t1 + x(4)/x(1)*atan(x(1)*t1);
theta = x(2)*atan(x(1)*psi);
F = x(3)*sin(theta);

% Plot data and fit function
plot(t1, F, t, y, 'o')
title(['Tire Data Magic Formula Fit (B=' num2str(x(1)) ', C=' num2str(x(2))...
        ', D=' num2str(x(3)) ', E=' num2str(x(4)) ')'])
xlabel('t')
ylabel('y')
grid
```

A.2 MAGICERROR.m

```
function e = MAGICERROR(x, t, y)
% MagicError Error in Magic Formula Curve Fit
%
% e = MagicError(x, t, y)
%
%       Calculates vectors of errors of Magic Formula Curve Fit given parameters
%       x and data (t, y)
%
%       Inputs:
%               x                       Vector of curve fit parameters
%                       x(1)    B
%                       x(2)    C
%                       x(3)    D
%                       x(4)    E
%               t                       Vector of independent data
%               y                       Vector of dependent data
%       Outputs:
%               e                       Vector of errors between data and fit function
%
% Created 12/17/97
% Howard Brott

psi = (1-x(4))*t + x(4)/x(1)*atan(x(1)*t);
theta = x(2)*atan(x(1)*psi);
F = x(3)*sin(theta);

e = y-f;
```

A.3 NLTIRE.m

```
function Fy = NLTire(Fz, alpha)
% NLTire              Non-Linear Tire Model Lateral Force
%
% Fy = NLTire(Fz, alpha)
%
%       Calculates tire lateral force from inputs of tire vertical load and slip
%       angle. Based on Radt's tire data nondimensionalization model and the
%       Magic Formula Model.  Focre is for one tire.  Called by the function
%       DOF2NLDE.m.
%
%       Inputs:
%               alpha                   Tire slip angle (rad)
%               Fz                      Tire vertical load (N)
%       Outputs:
%               Fy                      Tire lateral force (N)
%
% Created 1/13/98
% Howard W. Brott Jr.

global B1 C1 D1 E1 B3 C3 B5 C5;

% Normalization Parameters
Cc = B3 + C3*Fz;                % N/deg/N     Cornering coefficient
mu = B5 + C5*Fz;                % N/N         Friction coefficient

% Normalized Slip Angle
alphaN = Cc.*tan(alpha)./mu*180/pi;

% Normalized Lateral Force
psiFN = (1-E1)*alphaN + E1/B1*atan(B1*alphaN);
thetaFN = C1*atan(B1*psiFN);
FyN = D1*sin(thetaFN);

% Lateral Force
Fy = -FyN.*mu.*Fz;
```

A.4 DOF2CONT.m

```
% DOF2Control                2 DOF Model Execution Control
%
%       Controls execution of 2 DOF model.  Sets control input type(step)
%       Sets simulation parameters
%
% Created 1/12/98
% Howard W. Brott Jr

% Control Input Type
step=1;                 %Step Steer

input = 1;              %select which control input to use

% Simulation Parameters
t0 = 0.0;               % s     Initial time for steer input
tf = 4;         % s     Final time for simulation
tol = 1e-5;             %       Simulation accuracy (default = 1e-3)
```

A.5 DOF2PARA.m

```
% DOF2Para          2 DOF Model Independent Parameters and Simulation Control
%
%       Sets independent vehicle, tire, and disturbance parameters
%       for 2 DOF model.
%
% Created 1/11/98
% Howard W. Brott Jr.

% Initialization
clear all;
clc;
global m Izz L a b f rho Ap Cl_gamma Fy_disturbance Cf_tail u Cf Fz t0 tf input;
global B1 C1 D1 E1 B3 C3 B5 C5;

% Constants
g = 9.81;           % m/s^2           Acceleration due to gravity
rho = 1.225;        % kg/m^3      Density of air

% Aircraft Independent Parameters
m = 748.43;         % kg          Gross vehicle mass
Izz = 1760;         % kg-m^2      Yaw inertia
f = 1;              %               Fraction of weight on front axle
L = 4.7752;         % m           Wheelbase
u = 100;            % km/hr             Vehicle forward speed
Ap = 0.6929;        % m^2         Area of vertical tail
Cl_gamma = 0.1;             % (0.1) 1/deg         Coefficient of lift on tail

% Disturbance Inputs
Fy_disturbance = 0; % N           Aerodynamic side force

% linear Tire Model Parameters
Cf = -441.63;       % N/deg             front cornering stiffness (one tire)
Cf_tail = 0;        % N/deg             tail wheel cornering stiffness (one tire)

% Non-Linear Tire Model Parameters
%       Normalized Lateral Force Magic Formula Parameters
B1 = 0.7947;
C1 = 0.1901;
D1 = 6.1197;
E1 = 1.0637;

%       Cornering Coefficient Parameters
```

```
B3 = 0.2117;
C3 = -2.2918e-5;

%       Friction Coefficient Parameters
B5 = .7221;
C5 = -8.81055e-5;

% Unit Conversions
u = u*1000/3600;                    % m/s  Vehicle forward speed
Cf = Cf*180/pi*2;                % N/rad      Front tire cornering stiffness (two tires)
Cf_tail = Cf_tail*180/pi;           % N/rad Tail wheel cornering stiffness (one tire)
Cl_gamma = Cl_gamma*180/pi;      %1/rad Coefficient of lift on tail
```

A.6 DOF2DEPA.m

```
% DOF2DePa          2 DOF Model Dependent Parameter Calculation
%
%       Calculate values of dependent parameters for 2 DOF model
%
% Created 1/11/96
% Howard W. Brott Jr.

% Dependent Parameters
a = (1-f)*L;          % m       Distance from front tire to CG
b = f*L;              % m       Distance from rear tire to CG
V = u;                % m/s     Vehicle speed
Fz = m*g*f/2;         % N       Front tire normal load (one tire)
```

A.7 DOF2LSIM.m

```
%DOF2LSim  Simulation of Linear 2 DOF Model Response to Control and Disturbance
%                    Inputs
%
%     Performs simulation of linear 2 DOF model response to control and
%     disturbance inputs. Determines yaw speed, lateral speed, sideslip angle,
%     front and rear tire slip angles, front and rear tire lateral forces, and
%     lateral acceleration. Plots these responses versus time. Reads data from
%     DOF2Param, DOF2DependParam.
%
% Created 1/12/98
% Howard W. Brott Jr.

DOF2Para;                          % Set independent parameters
DOF2Cont;                          % Set execution control parameters
DOF2DePa;                          % Calculate dependent parameters

% Perform Simulation
[t,x] = ODE23('DOF2LDE', t0, tf, [0.1 0 0 0]', tol);
v = x(:,1);
r = x(:,2);
y = x(:,3);
theta = x(:,4)*180/pi;

% Vehicle, tire, & tail Angles
beta = (v/u);                      % rad      Vehicle sideslip angle
alpha = ((v+a*r)/u);               % rad      Front tires slip angle
gamma = ((v-b*r)/u);               % rad      tail incidence angle

% External Forces and Moments
Fy_fronttire = Cf*alpha;                    % N   Front tires lateral force
Fy_tail = ((1/2)*rho*u^2*Ap*Cl_gamma)*gamma; % N   Vertical tail force
Fy_tailwheel = Cf_tail*gamma;

% State Derivatives
vdot = (-Fy_fronttire+Fy_disturbance-Fy_tail-Fy_tailwheel)/m-u*r;
rdot = (-a*Fy_fronttire-b*Fy_disturbance+b*(Fy_tail+Fy_tailwheel))/Izz;

% Lateral Acceleration
ay = vdot + u*r;                   % m/s^2          Lateral Acceleration

% Do Plots
subplot(2,1,1)
```

```
plot(t,y)
grid
title('Linear Lateral Displacement (y)')
xlabel('Time (s)')
ylabel('Displacement (m)')

figure
subplot(2,1,2)
plot(t,theta)
grid
title('Linear Angular Displacement (Theta)')
xlabel('Time (s)')
ylabel('Displacement (deg)')

figure
plot(t,v)
grid
title('Linear Lateral Speed (v)')
xlabel('Time (s)')
ylabel('Speed (m/s)')

figure
plot(t,r*180/pi)
grid
title('Linear Yaw Speed (r)')
xlabel('Time (s)')
ylabel('Speed (deg/s)')

figure
plot(t,beta*180/pi)
grid
title('Linear Vehicle Sideslip Angle (beta)')
xlabel('Time (s)')
ylabel('Slip Angle (deg)')

figure
plot(t,alpha*180/pi)
grid
title('Linear Front Tire Slip Angle (alpha)')
xlabel('Time (s)')
ylabel('Slip Angle (deg)')

figure
plot(t,ay/g)
```

```
grid
title('Linear Lateral Acceleration')
xlabel('Time (s)')
ylabel('Acceleration (g)')
```

A.8 DOF2LDE.m

```
function xdot = DOF2LDE(t,x)
% DOF2LDE          Linear Differential Equations for 2 DOF Model
%
% xdot = DOF2LDE(t,x)
%
%       Determines derivatives of lateral speed and yaw speed given time and
%       state vector.  Linea tire and linear slip angles.  Used with ode23
%       for simulation.
%
%       Inputs:
%               t               Time (s)
%               x(1)=v          Lateral speed (m/s)
%               x(2)=r          Yaw speed (rad/s)
%       Outputs:
%               xdot(1)         Derivative of lateral speed (m/s^2)
%               xdot(2)         Derivative of yaw speed (rad/s^2)
%
% Created 1/12/98
% Howard W. Brott Jr.

global m Izz L a b Cf Cl_gamma rho Ap u Fy_disturbance Cf_tail

xdot=[(1/m)*(-((x(1)+a*x(2))/u)*Cf+Fy_disturbance-((x(1)-
b*x(2))/u)*(Cl_gamma*(1/2)*rho*u^2*Ap+Cf_tail))-x(2)*u
(1/Izz)*(-((x(1)+a*x(2))/u)*Cf*a-b*Fy_disturbance+((x(1)-
b*x(2))/u)*(Cl_gamma*(1/2)*rho*u^2*Ap+Cf_tail)*b)
x(1)
x(2)];
```

A.9 DOF2NLSI.m

```
%DOF2NLSi  Simulation of Non-Linear 2 DOF Model Response to Control and
Disturbance
%                       Inputs
%
%       Performs simulation of non-linear 2 DOF model response to control and
%       disturbance inputs. Determines yaw speed, lateral speed, sideslip angle,
%       front and rear tire slip angles, front and rear tire lateral forces, and
%       lateral acceleration. Plots these responses versus time. Reads data from
%       DOF2Param, DOF2DependParam.
%
% Created 1/12/98
% Howard W. Brott Jr.

DOF2Para;                       % Set independent parameters
DOF2Cont;                       % Set execution control parameters
DOF2DePa;                       % Calculate dependent parameters

% Perform Simulation
[t,x] = ode23('DOF2NLDE',0,tf,[0.1 0 0 0]',tol);
v = x(:,1);
r = x(:,2);
y = x(:,3);
theta = x(:,4)*180/pi;

% Vehicle and tire Slip Angles
beta = atan(v/u);               % rad       Vehicle sideslip angle
alpha = atan((v+a*r)/u);        % rad       Front tires slip angle
gamma = atan((v-b*r)/u);        % rad       Rear tires slip angle

% External Forces and Moments
Fy_fronttire = NLTire(Fz, alpha);   % N       Front tire lateral force (one tire)
Fy_tail = ((1/2)*rho*u^2*Ap*Cl_gamma)*gamma; % N    Vertical tail force
Fy_tailwheel = Cf_tail*gamma;

% State Derivatives
vdot = (-2*Fy_fronttire+Fy_disturbance-Fy_tail-Fy_tailwheel)/m-u*r;
rdot = (-2*a*Fy_fronttire-b*Fy_disturbance+b*(Fy_tail+Fy_tailwheel))/Izz;

% Lateral Acceleration
ay = vdot + u*r;                % m/s^2             Lateral Acceleration

% Do Plots
```

```
subplot(2,1,1)
plot(t,y)
grid
title('Non-Linear Lateral Displacement (y)')
xlabel('Time (s)')
ylabel('Displacement (m)')

figure
subplot(2,1,2)
plot(t,theta)
grid
title('Non-Linear Angular Displacement (Theta)')
xlabel('Time (s)')
ylabel('Displacement (deg)')

figure
plot(t,v)
grid
title('Non-Linear Lateral Speed (v)')
xlabel('Time (s)')
ylabel('Speed (m/s)')

figure
plot(t,r*180/pi)
grid
title('Non-Linear Yaw Speed (r)')
xlabel('Time (s)')
ylabel('Speed (deg/s)')

figure
plot(t,beta*180/pi)
grid
title('Non-Linear Vehicle Sideslip Angle (beta)')
xlabel('Time (s)')
ylabel('Slip Angle (deg)')

figure
plot(t,alpha*180/pi)
grid
title('Non-Linear Front Tire Slip Angle (alpha)')
xlabel('Time (s)')
ylabel('Slip Angle (deg)')

figure
```

```
plot(t,ay/g)
grid
title('Non-Linear Lateral Acceleration')
xlabel('Time (s)')
ylabel('Acceleration (g)')
```

A.10 DOF2NLDE.m

```
function xdot = DOF2NLDE(t,x)
% DOF2NLDE                Non-Linear Differential Equations for 2 DOF Model
%
% xdot = DOF2NLDE(t,x)
%
%       Determines derivatives of lateral speed and yaw speed given time and
%       state vector. Non-linear tire and non-linear slip angles. Used with ode23
%       for simulation.
%
%       Inputs:
%               t               Time (s)
%               x(1)            Lateral speed (m/s)
%               x(2)            Yaw speed (rad/s)
%       Outputs:
%               xdot(1)         Derivative of lateral speed (m/s^2)
%               xdot(2)         Derivative of yaw speed (rad/s^2)
%
% Created 1/12/98
% Howard W. Brott Jr.

global m Izz L a b Fz Cf Cl_gamma rho Ap u Fy_disturbance Cf_tail

alpha = atan((x(1)+a*x(2))/u);
Fy_fronttire = NLTire(Fz, alpha);

xdot=[(1/m)*(-2*Fy_fronttire+Fy_disturbance-((x(1)-
b*x(2))/u)*(Cl_gamma*(1/2)*rho*u^2*Ap+Cf_tail))-x(2)*u
(1/Izz)*(-2*Fy_fronttire*a-b*Fy_disturbance+((x(1)-
b*x(2))/u)*(Cl_gamma*(1/2)*rho*u^2*Ap+Cf_tail)*b)
x(1)
x(2)];
```